Inhibiting Carbon Dioxide Hydrate Formation using Deep Eutectic Solvents

By

Themba Luyanda Ngcobo

Btech Chemical Engineering

Mangosuthu University of Technology, uMlazi

A thesis submitted in full fulfilment of the Degree of Master of Engineering (M. Eng.) for the Faculty of Engineering and Built Environment and the Department of Chemical Engineering.

Supervisor: Prof Suresh Ramsuroop

Co-Supervisors: Prof Kaniki Tumba

Dr Madison Lasich

2023

Dedication

To my family and friends, thank you for being the rock upon which I have been able to lean. When I decided to further my education, I was aware of your support behind me. When I had the urge to give up, you gave me words of encouragement. Furthermore, when I needed to go further, you gave me financial support. It is impossible for me to adequately express my appreciation to everyone in the family for having been there for me through good and bad times. I salute you, guys!

Declaration

I, the undersigned Themba Luyanda Ngcobo hereby declare that,

i. The research presented in this dissertation is entirely my own original work, apart from passages that expressly state otherwise
ii. This dissertation has not been presented to any other academic institution for the purpose of receiving a degree or passing any kind of examination.
iii. This dissertation does not include any data, pictures, graphs, or other information that belongs to other people unless such information is specifically acknowledged as having been specifically sourced from other people.
iv. This dissertation does not include the writing of any other individuals; the only exceptions to this rule are any passages that expressly acknowledge that they are derived from the work of other researchers. The following protocols have been adhered to whenever it has been necessary to cite information obtained from other sources: a) the words of the original authors have been paraphrased, but the information that can be attributed to them in general has been referenced.

    b) whenever the words of the original authors have been used verbatim, their writing has been enclosed in quotation marks and referenced.
v. dissertation does not include any text, graphics, or tables that have been copied and pasted from the internet. The only exception to this rule is if the source of the material has been specifically acknowledged, and the source has been described in detail in both the thesis section and the reference section.

Mr Themba Luyanda Ngcobo Department of Chemical Engineering, Durban University of Technology. 2023

This thesis is submitted after examination and approval of the following supervisors

Prof. Suresh Ramsuroop, Department of Chemical Engineering, Durban University of Technology. 2023

Prof. Kaniki Tumba, Department of Chemical Engineering, Mangosuthu University of Technology. 2023

Dr. Madison Lasich, Department of Chemical Engineering, Mangosuthu University of Technology. 2023

Acknowledgments

- Prof. Suresh Ramsuroop, Prof. Kaniki Tumba and Dr Madison Lasich are to be commended for providing me with the opportunity to conduct this project under their supervision and guidance. I also thank them for their invaluable contribution to my research, thereby ensuring that I do not stray from the core of my investigation.

- I am grateful to Dr Nkululeko Nkosi, the Thermodynamics Researcher at MUT. He helped to build and set up the equipment used for this study.

Abstract

The formation of gas hydrates in pipelines during gas and petroleum extraction processes can result in multiphase systems including gas hydrates. These will form as solids in the presence of water and gas under thermodynamically favourable temperature and pressure conditions. Gas hydrates raise safety concerns, hinder process performance, and impact on financial resources as they block pipelines. The formation of gas hydrates can be efficiently prevented by using certain substances referred to as inhibitors. However, most inhibitors are expensive, potentially dangerous, and damaging to the environment. Hence, there is need to investigate environmentally friendly alternatives to mitigate gas hydrates.

The objective of this study was to examine the efficiency of green additives referred to as deep eutectic solvents (DES) in inhibiting carbon dioxide gas hydrate formation. Deep eutectic solvents consisting of Tetrapropylammonium bromide + glycerol (DES-1), Tetramethylammonium chloride + glycerol (DES-2), and Tetramethylammonium chloride + ethylene glycol (DES-3) on carbon dioxide hydrates is investigated. These solvents are worth studying because their synthesis, purification, and environmental friendliness offer economic advantages.

Molecular Dynamics (MD) simulations were used to theoretically determine the conditions that promote or inhibit the formation and stability of cardon dioxide hydrates in the presence of the selected inhibitors. The conditions investigated include temperature, pressure, and inhibitor concentration. The use of rigorous computational methods for preliminary screening significantly reduces the cost and the duration of experiments. MD simulation results were further validated using experimental gas hydrate equilibrium data. Results obtained in the present study indicated that the various DES solutions have both inhibiting and promoting effects. It was also found that low concentrations promoted hydrate dissociation, whereas high concentration greater than 0,20 stabilised hydrate formation. Pressure and temperature also impacted on the concentration of the DES solutions that inhibited or promoted hydrate formation. The concentration of the DES solutions shifted the hydrate curve to inhibit or promote hydrate formation.

Preface

The work presented in this dissertation was conducted in the Department Chemical Engineering Research Laboratory at Mangosuthu University of Technology. The work was supervised by Professor S. Ramsuroop and co-supervised by Prof Kaniki Tumba and Dr Madison Lasich.

This dissertation is submitted in full fulfilment of the Master of Engineering in Chemical Engineering degree requirements. The results presented in this dissertation have not been previously submitted to any tertiary institution as part of a degree program, except where the work of others is clearly cited in the text.

Table of Contents

Declaration i

Aknowledgement iii

Abstract iv

Preface v

Table of Content vi

List of Table xi

List of Figures xii

Nomeclature xv

Chapter 1 1

1 Introduction 1

1.1 Background Information and Motivation 1

1.2 Problem statement 2

1.3 Scope of the study 3

1.4 Aim 3

1.5 Structure of the structure of the thesis 4

Chapter 2 5

2 Literature Review 5

2.1 The Definition of Clathrate Hydrates and Their Initial Discovery 5

2.2 Conditions necessary for hydrates formation 5

2.3 Hydrate formation kinetics 6

2.3.1 Process of hydrate fromation 7

2.3.1.1 The formation of hydrate nuclei 7

2.3.1.2 Hydrate growth 7

2.3.2 Hydrate dissociation 9

2.3.2.1 Physical Inhibition 10

2.3.2.2 Chemical Inhibition 14

2.4 Gas hydrate equilibrium models 19

2.4.1 Method based on gas gravity 19

2.4.2 The distribution coefficient method (K_{vsi} – value) 20

2.4.3 The sour gas chart technique 20

2.4.4 Empirical Correlations 21

2.4.4.1 Makogon Correlation 21

2.4.4.2 Towler and Makogon correlation 22

2.4.5 Computational Method 22

2.4.5.1 The Van der Waals Platteew model 22

2.4.5.2 Parrish and Prausnitz 22

2.4.5.3 The Klauda and Sandler model 23

2.5 Methods and equipment for measuring hydrate equilibria 24

2.5.1 Methods for hydrates 24

2.5.1.1 Method of searching using visual isothermal method 24

2.5.1.2 Isobaric Method 24

2.5.1.3 Isochoric method 26

2.5.2 Experimental Equipments 27

2.5.2.1 Hydrate equilibrium cell 28

2.5.2.2 Quartz crystal microbalance 28

2.5.2.3 High pressure differential scanning calorimeter 29

2.5.2.4 Rocking cell 30

2.5.2.5 Variable volume cell 31

Chapter 3 32

3 Deep eutectic solvents (DESs) 32

3.1 History and Definition 32

3.2 Properties of deep eutectic solvents 35
3.3 The DES's physicochemical characteristics 36
3.3.1 Freezing point 37
3.3.2 Density 37
3.3.3 Viscosity 37
3.3.4 Conductivity 37
3.4 The Law of Polarity 38
3.5 Possible applications of DESs in the industrial sector 38
3.6 Molecular dynamic simulation 39
3.6.1 Methods for Temperature Control in Dynamic Simulation 43
3.6.1.1 Thermostat 43
3.6.1.2 Barostat 45
Chapter 4 47
4 Experimental apparatus and procedure 47
4.1 Chemicals 48
4.1.1 DESs 48
4.1.2 The procedure for DES synthesis 48
4.1.3 Experimental apparatus 49
4.1.3.1 The equilibrium cell 51
4.1.3.2 Agitation device 53
4.1.3.3 The enclosure for the equipment cell 53
4.1.3.4 Liquid bath 54
4.1.3.5 Temperature controller 53
4.1.3.6 Pressure controller 54
4.1.3.7 Data acquisition system 54
4.1.4 The preparation of the isochoric cell 55

4.1.4.1 The process of isochoric cleaning 55

4.1.4.2 Leak test 56

4.1.5 Calibration of measuring devices 56

4.1.5.1 Calibration of temperature probes 56

4.1.5.2 Calibration of pressure probes 58

4.2 Experimental procedure 59

4.2.1 Sample preparation 59

4.2.2 Hydrate dissociation dissociation measurements 60

4.2.3 Shutdown procedure 61

4.3 Simulation Method 61

Chapter 5 67

5 Results and discussion 67

5.1 Chemical used in this study 67

5.2 Experimental measurements of gas hydrates dissociation conditions 68

5.3 Purity of Chemicals 68

5.4 FTIR 69

5.5 Test systems 70

5.6 Experimental results 72

5.6.1 CO_2 + H_2O + DES-1 (Tetrapropylammonium Bromide TPABr + Glycerol) 72

5.6.2 CO_2 + H_2O + DES-2 (Tetramethylammonium chloride TMACl + Glycerol) 74

5.6.3 CO_2 + H_2O + DES-3 (Tetramethylammonium chloride TMACl + Ethylene Glycol) 76

5.7 MD simulation results 83

5.7.1 Radial distribution function 83

6 Conclusion and Recommendations 88

6.1 Conclusion 88

6.2 Recommendations 88

References 90

List of Tables

Table 2-1: Experimental hydrates reported in the literature 16

Table 3-1: General formula of DES types (Smith *et al*., 2014) 33

Table 3-2: Considerations to be made when choosing a "green" solvent (Plechkova and Seddon, 2008) 36

Table 4-1: Salts and their formulas used in this study 48

Table 4-2: HBDs and their formulas used in this study 48

Table 5-1: Solvents and Densities used in this study 67

Table 5-2: Hydrate phase equilibria measured in this study 68

Table 5-3: Suppliers and purity of all Organic salts and HBDs used in this study. 68

Table 5-4: Purity and supplier of the gas used in hydrate phase equilibrium measurements. 68

Table 5-5: Experimental results and literature data for the CO_2 + water system 71

Table 5-6: Hydrate equilibrium data for the CO_2 + H_2O + DES-1 system 73

Table 5-7: Hydrate phase equilibrium data for the CO_2 + H_2O + DES-2 system 75

Table 5-8: Hydrate phase equilibrium data for the CO_2 + H_2O + DES-3 system 76

Table 5-9: Hydrate phase equilibrium data of aqueous AILs compared to DES for CO_2 hydrates at different concentrations 79

Table 5-10: Challenges for different classes of Inhibitors/ promoters for gas hydrates 82

Table of Figures

Figure 2-1: The H_2O molecule forms a cage around the gas molecule (Giavarini,2011). 6

Figure 2-2: Common hydrate unit ice structure. The arrows indicate cages of a particular type of structure (Sloan, 2008). 7

Figure 2-3: Pressure-temperature phase diagram for a binary system at a specific composition (Sloan and Koh, 2008) 8

Figure 2-4: Pressure-temperature phase diagram for a binary system of water + gas (–). The phase behaviour of the unary system of water (---) and gas (-.-.-) is included as a reference, as well as the triple point of water (▲), the critical point of the gas (●) (Mooijer-van den Heuvel, 2004) 9

Figure 2-5: Pipeline rapture due to heat (Carrol, 2014).....11

Figure 2-6: Represents flow chart for dehydration system unit (Carrol, 2014).....13

Figure 2-7: Represents process flow diagram of the refrigeration plant unit (Carrol, 2014). 13

Figure 2-8: Shows various types of chemical hydrate inhibitors.....14

Figure 2-9: Basic structure of amino acids 16

Figure 2-10: Displays a chart for predicting three-phase conditions based on the gas gravity (Sloan, 2007).....19

Figure 2-11: Baillie-Wichert chart for sour gas hydrate formation conditions estimation (Carroll, 2014).....21

Figure 2-12: Schematic diagram of the non-visual isothermal pressure search procedure (Makogon and Sloan, 1994).....25

Figure 2-13: Shows the isochoric method's primary cooling and heating curves for the generation and dissociation of simple hydrates (Sloan and Koh, 2008).....26

Figure 2-14: Static hydrate equilibrium cell design by Deaton and Frost, 1946 (Sloan and Koh, 2008). 28

Figure 2-15: (1) The schematic diagram of the QCM, (2) the QCM mounted with high pressure (Sloan and Koh, 2008). 29

Figure 2-16: Schematic diagram for high-pressure differential scanning calorimeter (Deschamps and Dalmazzone, 2003).....30

Figure 2-17: Rocking cell for hydrate equilibrium apparatus (Sloan and Koh, 2008). 31

Figure 2-18: Schematic diagram of Transparent variable volume cell used by Ngema et al. (2014). 31

Figure 3-1: Schematic representation of the two components phase diagram 33

Figure 4-1: Schematic diagram of the apparatus developed in this study. 50

Figure 4-2: A photograph of the experimental setup 50

Figure 4-3: Schematic diagram of the equilibrium cell used in this study 52

Figure 4-4: photograph of equilibrium cell used in this study 52

Figure 4-5: The picture shows the top view of the equilibrium cell with magnetic stirrer inside, the picture on sideview of the cell 51

Figure 4-6: The picture shows the top flange of the cell 53

Figure 4-7: Calibration of temperature probe (TP1) and on the right is the deviation from the standard pressure 57

Figure 4-8: Calibration of temperature probe (TP2) and at the right is the deviation from the standard temperature 57

Figure 4-9: Calibration of pressure probe (PP1) and on the right is the deviation from the standard pressure 58

Figure 4-10: Calibration of pressure probe (PP2) and at the bottom is the deviation from the standard pressure 58

Figure 4-11: The stages involved in the molecular dynamic simulation of the dissociation of CO2 gas hydrate 66

Figure 5-1: FTIR spectrum for DESs, with its HBD and HBA 69

Figure 5-2: Experimental hydrate dissociation conditions and comparison with literature data for the carbon dioxide + water system; (●) Khan et al. 2017 (▲) Mannar et al. 2017; (◊) Bavoh et al. 2017. (■) This work 71

Figure 5-3: Hydrate equilibrium data of the (CO_2 + DES-1 + H_2O) system with symbols representing experimental dissociation conditions; Pure water (■); 0,05 (+); 0,15 (▲) and 0,20 (●) 73

Figure 5-4: Hydrate equilibrium data of the (CO_2 + DES-2+ H_2O) system with symbols representing experimental dissociation conditions; Pure water (■); 0,05 (+); 0,15 (▲) and 0,20 (●)……75

Figure 5-5: Hydrate equilibrium data of the (CO_2 + DES-3 + H_2O) System symbols representing experimental dissociation conditions; 0 (■) and 0,05 (+)……77

Figure 5-6: Average suppression temperature (ΔŦ) of carbon dioxide gas hydrates in the presence of 10 wt% aqueous solutions 80

Figure 5-6: RDFs of DES-1 at defferent temperature and pressure 84

Figure 5-7: RDFs of DES-2 at different temperature and pressure 86

Figure 5-6: RDFs of DES-3 at different temperature and pressure 87

Nomenclature

Latin symbols

N_A	Avogadro's Constant
b	Bond length
q	Charges of particles
Z	Compressibility factor
F	Force
f	Fugacity
G	Gravity
m	Mass
M_w	Molecular weight
y	Mole fraction in aqueous phase
x	Mole fraction in gaseous phase
n	Number of moles
P	Pressure
t	Simulation time
w_r	Spherical core cell potential function
r	The distance from the cavity centre to the guest molecules
z	The coordination number of the cavity
R^0	The free cavity radius

R	Universal gas constant

Greek letters

θ	Angle between two covalent bonds
μ	Chemical potential
σ	Distance between molecules
α	Interaction between water and gas molecule
τ	Relaxation time
ζ	The friction coefficient

Superscript

i	Coefficient for repulsive
j	Coefficient for attractive
0	Initial position
H	Solid phase
β	Unoccupied hydrate phase

Abbreviation

NPT	Constant pressure, constant volume
NVT	Constant temperature, constant volume
DES	Deep eutectic solvent
MSD	Mean square displacement

MD	Molecular dynamic
RDF	Radial distribution function

Chapter 1

1 Introduction

1.1 Background Information and Motivation

Clathrate hydrates are solids that have the appearance of ice and are composed of water (the host molecules) and gas (guest molecule). Hydrates will form in the presence of water and gas under thermodynamically favourable temperature and pressure conditions. (Sloan et al., 2008). The formation of gas hydrates is quite unwanted in flow assurance processes, and it can have adverse economic effects and raises concerns about safety in transportation, and processing, in oil and gas industry (Naijibi et al., 2013). When hydrates form production is reduced and eventually halted because of the obstruction in the pipeline. The removal of gas hydrates can be an expensive and risky process. Insulation, water removal (also known as dehydration), gas phase modification, and chemical treatment are the preventative measures that can be taken to avoid the formation of gas hydrate. The use of chemical as additives inhibitors that are injected into the line will be the option that offers the highest degree of reliability. The thermodynamic inhibitor is the one that has the greatest demand. In the presence of a thermodynamic hydrate inhibitor (THI), the curve for hydrate formation is shifted by lowering the temperature while simultaneously raising the pressure (Wu et al., 2007). Inhibitors of low dose, also known as hydrate inhibitors, are an alternative type of inhibitor that can be employed to solve economic and safety concerns (Kelland et al., 1995).

It has come to light that gas hydrates, which may be found in both the subsea and the permafrost regions, have the potential to serve as a source of energy. On the other hand, the production of natural gas hydrates in oil and gas pipelines is never taken into consideration. This is due to the fact that the formation of hydrates in pipes has led to blockage and has disrupted the flow assurance of natural gas (Kim et al., 2011). In extreme situations, environmental catastrophes may also arise as a result of blockages, notwithstanding the fact that they produce economic losses. Several strategies, such as isobaric thermal heating, the extraction of water, the reduction of pressure, and the injection of chemical inhibitors, have been developed and put into practice in attempts to forestall the occurrence of this event. However, the first three approaches are not only impractical but also prohibitively expensive. Because of this, a significant amount of work has been put into the study and development of chemical inhibitors over the past few years to regulate the growth of hydrate.

1.2 Problem statement

The formation of gas hydrates during the processing of oil and gas is something that should be avoided at all costs. The production of gas hydrates in pipelines can sometimes result in multiphase systems, which can raise safety concerns, hinder process performance, and cause a loss of financial resources. Through the manipulation of thermodynamic parameters, it is possible to forestall the development of gas hydrates. For instance, the development of gas hydrates can be efficiently stopped by using certain substances referred to as inhibitors. On the other hand, the vast majority of inhibitors are expensive, potentially dangerous, and damaging to the environment.

Current approaches for gas hydrate inhibition in gas exploration rely on some compounds that are harmful to the environment as well as processes that need a significant amount of energy. As a result of this, other inhibitors will be studied as potential alternatives for compounds such as methanol, glycols, and electrolytes that are currently being utilized. Thermodynamic hydrate inhibitors (THIs) can cause substantial environmental damage. Because of kinetic and hydrate nucleation parameters, it may not be possible to make accurate predictions regarding the probability distribution of Low dosage hydrate inhibitors (LDHI). Conventionally inhibitors, in general, have a detrimental impact on the environment and cause harm. This is due to the toxicity of such chemical inhibitors, which poses significant environmental risks.

Ionic liquids (ILs) or room temperature ionic liquids (RTILs) are molten ionic salts composed of a poorly co-ordinating sizeable organic cation combined with an organic or inorganic anion, which leads to low melting temperature (lower than 373 K). The main characteristics of most ionic liquids include high thermal stability, negligible vapour pressure, non-flammability, and high solvating capacity for organic, inorganic, and organometallic compounds.

Because of this, research into the development of inhibitors that are less harmful to people and the environment is required. In many different procedures, deep eutectic solvents are recognized as a safe alternative to traditional solvents. (Nkosi et al. 2018a). The eco -friendly of the DES can be evaluated by the following properties .

- higher biodegradability and biocompatibility as ‘green‘ solvent;
- high chemical and thermal stability;
- negligible vapour pressure; • non-flammability;

- low toxicity;
- wide liquid range;
- chemical compatibility with water.

1.3 Scope of the study

The goal of this project is to determine whether certain deep eutectic solvents can inhibit the formation of carbon dioxide hydrates in a manner that is both friendly to the environment and economical. Molecular simulation tool, specifically Material studio, were utilized as a simulation tool for the purpose of determining probable DES inhibitors and circumstances for the purpose of subsequent experimental verification.

The use of computational methods for preliminary screening helps to cut down significantly on the requirement for prolonged and pricey experimental effort. The method of trial and error is not the best choice because it takes a lot of time and money to conduct experiments to find the correct solvent that can inhibit the formation of hydrate, and it is also sometimes impossible to find a solvent that has the potential to inhibit the formation of hydrate. To forecast the formation of gas hydrates in systems that contain water, carbon dioxide, and deep eutectic solvents, molecular simulation tools were evaluated as potential predictive tools.

In the research that has been done, there has been no exploration into the use of deep eutectic solvents as carbon dioxide gas hydrate inhibitors. The following DESs used by Nkosi and co researchers (2018a; 2018b; 2018c) during their investigation on limiting activity coefficient measurements were selected for experimentation on the basis of their availability and the fact that ammonium-based ionic liquids are promising inhibitors:

1. Tetramethylammonium chloride in combination with glycerol
2. Tetramethylammonium chloride in combination with ethylene glycol
3. Tetrapropylammonium bromide in combination with glycerol

The isochoric pressure search approach, which was described by Mohammadi et al., 2005, was utilized to acquire the data pertaining to the dissociation of gas hydrates.

1.4 Aim

The aim of the present study is to assess selected deep eutectic solvent as carbon dioxide hydrate inhibitors. Its objectives are as follows:

- To establish the effect of deep eutectic solvent concentration on carbon dioxide hydrate dissociation conditions.
- To compare the performance of deep eutectic solvents with that of currently used inhibitors.
- To Evaluate material studio as a simulation tool for carbon dioxide, hydrate inhibition by deep eutectic solvents.

1.5 Structure of the structure of the thesis

This study consists of six different chapters. The Introduction, the Motivation, and the Aim of the Study are Presented in the First Chapter. Chapter 2 is centred on the review of the literature that is pertinent to this study. This review includes the history of gas hydrates, the structures of gas hydrates, the dynamics of hydrates, experimental methods and equipment utilized for gas hydrate research, etc. Molecular dynamics simulation, in particular their implementation in the Materials Studio computer program, and deep eutectic solvents are discussed in Chapter 3. The details of the set-up and methodological technique that were utilized in this investigation are discussed in Chapter 4. The findings of the study and a discussion of those findings are presented in Chapter 5. Both the conclusion and the recommendation are presented.

Chapter 2

2. Literature Review

The reviews of the important literature pertaining to gas hydrates are presented in this chapter. It is divided into five sections, each of which is discussed in the following order: In section 2.1, the definition of gas hydrates as well as background information is discussed, including the conditions under which they originate and the structures of gas hydrates. In section 2.2, a review is given on the kinetics of hydrates, including both the formation and the dissociation of hydrates. The calculation of phase equilibrium data is covered in Section 2.3 after a discussion of the various methods and equipment utilized for hydrates. These include gas hydrate equilibrium methods, and the fundamentals of Thermodynamics which are necessary for comprehending the conditions of gas hydrate equilibria that have been mentioned in all the experimental work.

2.1 The Definition of Clathrate Hydrates and Their Initial Discovery

Clathrate Hydrates are solids that have the consistency of ice and are created when water and the hydrate guest molecule are present. The water molecules surround the guest molecule and confine it within their cavities. The presence of weak Van der Waals interactions between gas molecules and water molecules is necessary for the formation of the gas hydrate structure (Sloan et al., 2008).

When Sir Humphrey Davy was undertaking experiments on chlorine and water combinations in the year 1810, he noticed the production of crystals at temperatures that were higher than the water's freezing point. This led him to the discovery and documentation of gas hydrates. The study of hydrates began as a matter of scientific interest in the 19^{th} century, beginning with Hammerschmidt in 1934. He was the first person to discover that hydrates were the cause of blocked flow lines in oil and gas production.

2.2 Conditions necessary for hydrates formation

There are three conditions that need to be met before hydration may develop (Carroll, 2020).

1. Suitable temperature and pressure conditions.

2. Hydrate former must be present e.g. CH_4, CO_2. The size of the gas molecule must be exactly right so that it can squeeze into a particular kind of hydrate.
3. There must be a satisfactory quantity of water present.

The structural makeup of gas hydrates

Figure 2-1 depicts the structure of a gas hydrate that is being formed. This structure is based on the classification of the gas molecule and occurs when Van der Waal force allows gas molecules to become trapped within cavities formed by water molecules.

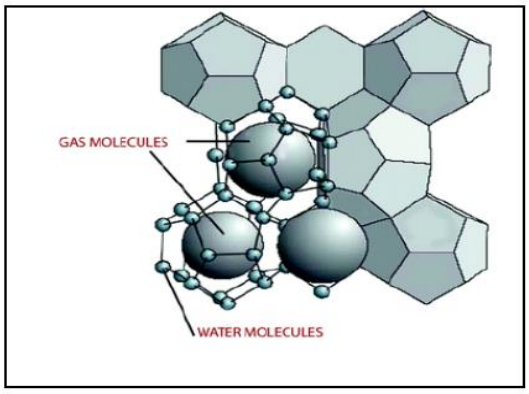

Figure 2-1: The H_2O molecule forms a cage around the gas molecule (Giavarini,2011).

Currently, three different possibilities for the arrangements are discussed in detail. They are capable of properly arranging themselves following the chemical composition of the guest as well as the molecules of water. Figures 2-2 depict each of the three distinct structures that are produced because of this formation. Classen (1951) proposed two different structures, both of which are cubic solids: the structure I and the structure II. Stackelberg and Muller (1951) used x-ray analysis to validate Classen's hypothesis and demonstrate that it was accurate. 1987 was the year that Ripmeester and his colleagues made the discovery that led to the designation of structure H. This structure is in the form of a hexagon.

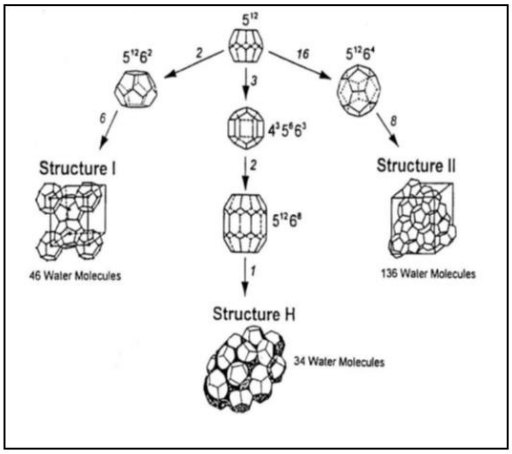

Figure 2-2: Common hydrate unit ice structure. The arrows indicate cages of a particular type of structure (Sloan, 2008).

Structure I is made up of 46 water molecules, and it has two smaller cavities in the shape of a pentagonal dodecahedron (5^{12}), and six larger cavities in the shape of tetrahedrons ($5^{12}6^2$). Structure II is made up of 136 water molecules and has 8 larger cavities that are shaped like a tetrakaidecahedron and 16 smaller cavities that are shaped like a pentagonal dodecahedron (5^{12}). ($5^{12}6^4$). Structure H is made up of 34 water molecules, and it has 3 small cavities in the shape of a dodecahedron (5^{12}), 2 medium cavities in the shape of an irregular dodecahedron ($4^35^66^3$), and one large cavity in the shape of an icosahedron ($5^{12}6^8$). (Sloan et al., 2008; Carroll, 2014).

For hydrates to form, it is necessary for the gas molecule to fulfil the following requirements: (Jeffrey, 1984).

a) The hydrogen bonds that exist between gas molecules ought to be moderate or weak.

b) In order to trap a gas molecule, the molecule's size must be between 0.35 and 0.9 nanometres; it is difficult to trap molecules that are smaller than this.

2.3 Hydrate formation kinetics

According to Yin and co-workers (2018), the gas hydrates formation process is like crystallization. The processes involved are the following: Gas hydrate formation (nucleation, hydrate growth) and gas hydrate dissociation.

2.3.1 Process of gas hydrate formation

2.3.1.1 The formation of hydrate nuclei

The process involves the formation of nuclei and their subsequent growth to the required size. During this process, water molecules gather to form clusters around gas molecules, which results in the formation of hydrate unit cells. This is an early stage of development, and the clusters will keep merging until they reach the size required to be considered critical. When the clusters of hydrates reach the necessary size, they become stable and begin to form hydrates(Bishnoi et al., 1996). The amount of energy needed for this process is negligible. It is decided by the temperature and pressure (Ke et al., 2019).

2.3.1.2 Hydrate growth

The formation of a solid mass is caused by the formation of hydrate as well as the joining together of crystals. Under conditions of equilibrium, the factor area, mixing, and the general water and gas composition of the background all play a significant role in the growth of hydrates (Ke et al., 2019). According to Sloan et al. (2008) and Ou et al. (2016), the combination of factors that have been considered for the growth of hydrates is the kinetics of crystal growth at the hydrate surface, mass transfer of the components, and heat transfer of the hydrate formation away from the growing crystal surface. These are the factors that have been considered for the growth of hydrates.

Systems containing gas hydrates are classified as binary or ternary if they have two or three components. A binary system consists of water and one guest molecule; a ternary system consists of water, one guest molecule, and an additive such as a promoter/inhibitor. All of the systems evaluated in this work have multiple components (water, carbon dioxide, and salt/s). The gas hydrate structure is made up of only water and CO_2, with the salts staying in the liquid solution. Only binary systems (former/gas and water) will be covered in this section.

According to the Gibbs phase rule, for a binary system, F_{max} is 3. Full representation of the phase behaviour cannot be achieved in a two-dimensional P-T plane and must be projected onto a third axis that shows the dependency of composition on the equilibrium conditions, i.e., P, T, and x. Due to this increased complexity, the phase behaviour is often presented in a planar cross-section of the equilibrium conditions at a fixed value of one of the variables. Figure 2-3 demonstrates a P-T phase diagram for a binary system at a specified composition.

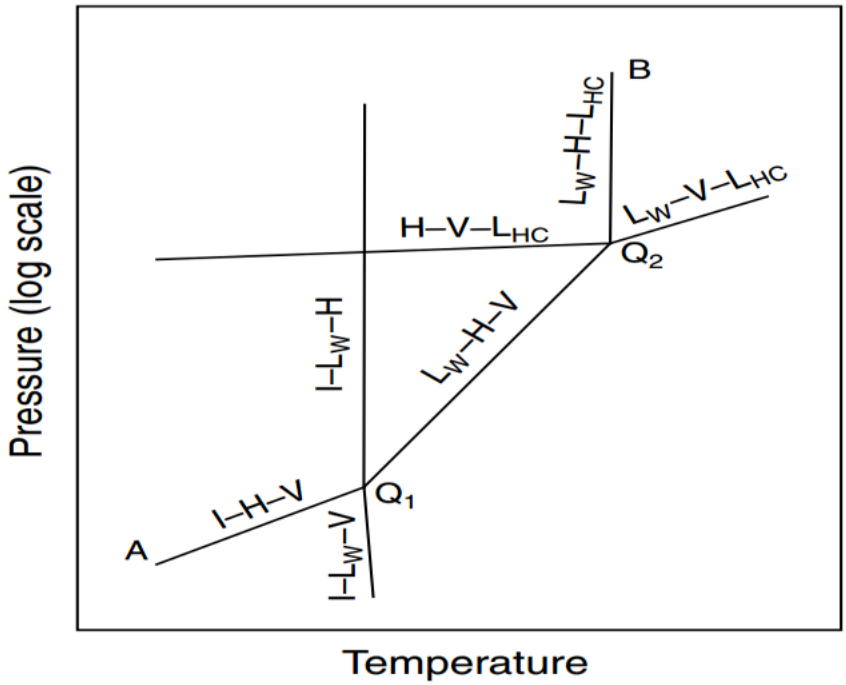

Figure 2-3: Pressure-temperature phase diagram for a binary system at a specific composition (Sloan and Koh, 2008).

The phases that occur in a binary system of gas hydrates are: ice (I), liquid water (L_w), vapour (V), hydrate (H), and liquefied guest (LHC). Two-phase regions are bound by three-phase equilibrium curves (I-H-V, L_w-H-V etc.). Four three-phase equilibrium curves intersect at a quadruple point, i.e., the point where four phases coexist in equilibrium (Q_1 and Q_2) in Figure 2-3..

Two variations of the phase diagram presented in Figure 2-4 are encountered. The distinction between the phase diagrams is related to the critical temperature (T_c) of the gas, and its proximity (lower or higher) to the triple point of water (T_{tr},H_2O). Gases with T_c lower, or close to T_{tr},H_2O, are referred to as gas-like, while gases with T_c above T_{tr},H_2O , are referred to as liquid-like. The triple point temperature of water is 273.16 K. The former used in this study, carbon dioxide, has a critical temperature of 304.25 K, appreciably above the triple point of water. The systems investigated in this study exhibits a liquid-like behaviour in the hydrate formation region. The P-T diagram for such systems (guest molecule with high critical temperature) is shown in Figure 2-4.

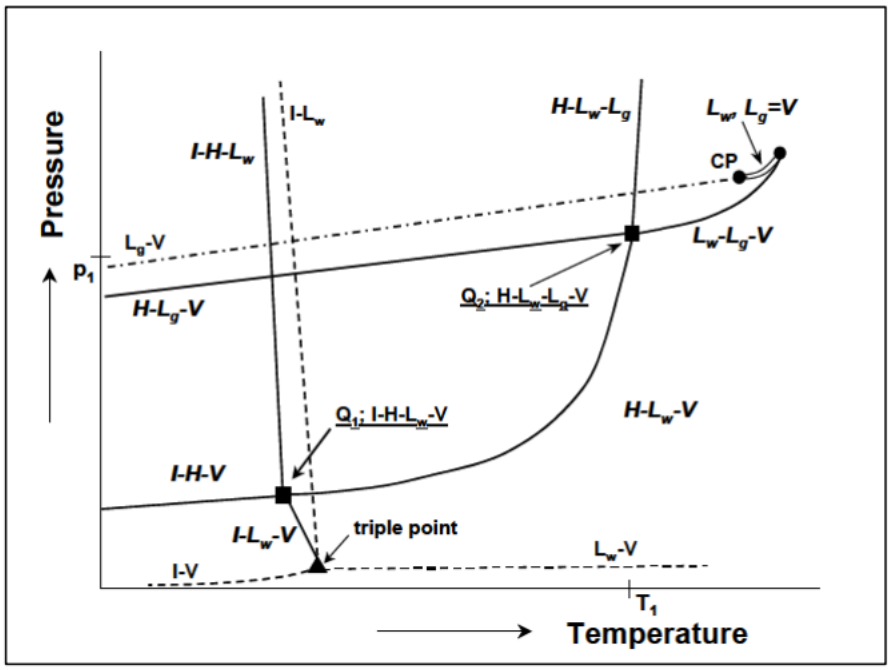

Figure 2-4: Pressure-temperature phase diagram for a binary system of water + gas (–). The phase behaviour of the unary system of water (---) and gas (-.-.-) is included as a reference, as well as the triple point of water (▲), the critical point of the gas (●) (Mooijer-van den Heuvel, 2004).

The H-L_g-V equilibrium curve in Figure 2-4 proceeds to higher temperatures and intersects with the H-Lw-V curve at a quadruple point (Q_2). The four phases that coexist at Q_2 are H-L_w-L_g-V. The equilibrium curves that intersect at Q2 are H-L_w-V, H-L_g-V, H-L_w-Lg and L_w-Lg-V. The I-H-V equilibrium line at conditions below Q1, the H-L_w-V equilibrium line between Q1 and Q_2 as well as the H-L_w-L_g equilibrium line at conditions above Q2 bind the hydrate region. Hydrates are able to form at conditions of lower temperature or higher pressure to the left of this region enclosed by the three lines. To the right no hydrate formation is possible. Due to the fact that the H-L_w-L_g equilibrium curve is so steep, the temperature of Q_2 is often taken as the maximum temperature for gas hydrate existence (Mooijer-van den Heuvel, 2004). The L_w-L_g-V equilibrium curve continues to higher temperatures above Q_2 and terminates at the critical end point.

2.3.2 Hydrate dissociation

Yin and colleagues (2018) stated that previous research had shown that heat transfer is an important factor in the process of hydrate dissociation. Heat handles controlling the dissociation process between the water molecule and the Van der Waals forces that exist

between the host and guest molecules (Hong et al., 2003). Physical and chemical inhibition are the types of methods that are used to either inhibit or prompt the dissociation of gas hydrate.

2.3.2.1 Physical inhibition

Altering the system's physical properties to avoid the formation of gas hydrates is one way to achieve physical inhibition. Some of the physical criteria that must be met are the process of heating the pipeline, a reduction in pressure, and the elimination of water.

a) Heating the pipeline

Conditions must be distinct from those that lead to the production of hydrates to avoid the formation of gas hydrates (high temperature and low pressure). To avoid the formation of gas hydrate, a heater that uses trace heating is utilized. This keeps heat from being lost to the surrounding area.

A heater can be used to keep a gas or fluid at a desired temperature. The heat is only applied to one section of the pipeline, even though the gas needs to be kept heated along the entire pipeline. This is the downside of this method. The usage of trace heating is yet another form of heating that may be used. Along the length of the pipeline, the heat is consistently injected. Due to the Joule-Thomson phenomenon, having a trace heating system on the valves is highly crucial because valves normally freeze.

Insulation is yet another approach that can be used in the process of heating the pipeline. The insulated pipeline has a lower rate of heat loss compared to pipes that are not insulated. By insulating a pipe for short transit pipelines, the system conditions can be moved to the hydrate-free zone, which will prevent the formation of hydrates. When transit takes place along a lengthy pipeline, the cost of insulating the pipeline might become rather high.

It is not possible to determine the position of the gas hydrate once it has formed if the pipe carrying the gas is buried underground, but it is possible if the line is above ground. Valves and fittings are significant components for subterranean pipelines, and they will continue to be so. When it comes to the surface pipeline, an infrared temperature gun can be used to take temperature readings. This is important because the location of the temperature reading that is the lowest could be an indicator of the formation of gas hydrate.

The inefficient technique of eliminating gas hydrate by heating it

It is a common misconception that removing gas hydrate is an effortless process. However, this is not the case. Figure 2-5 shows a pipeline that ruptured because of the heat used to remove gas hydrate (Carrol, 2020). Only the side of the pipe on which the heat is applied will melt, and as a result, the pipe will become overly pressurized when heat is placed in the middle of the pipe. The pipe could explode at any moment.

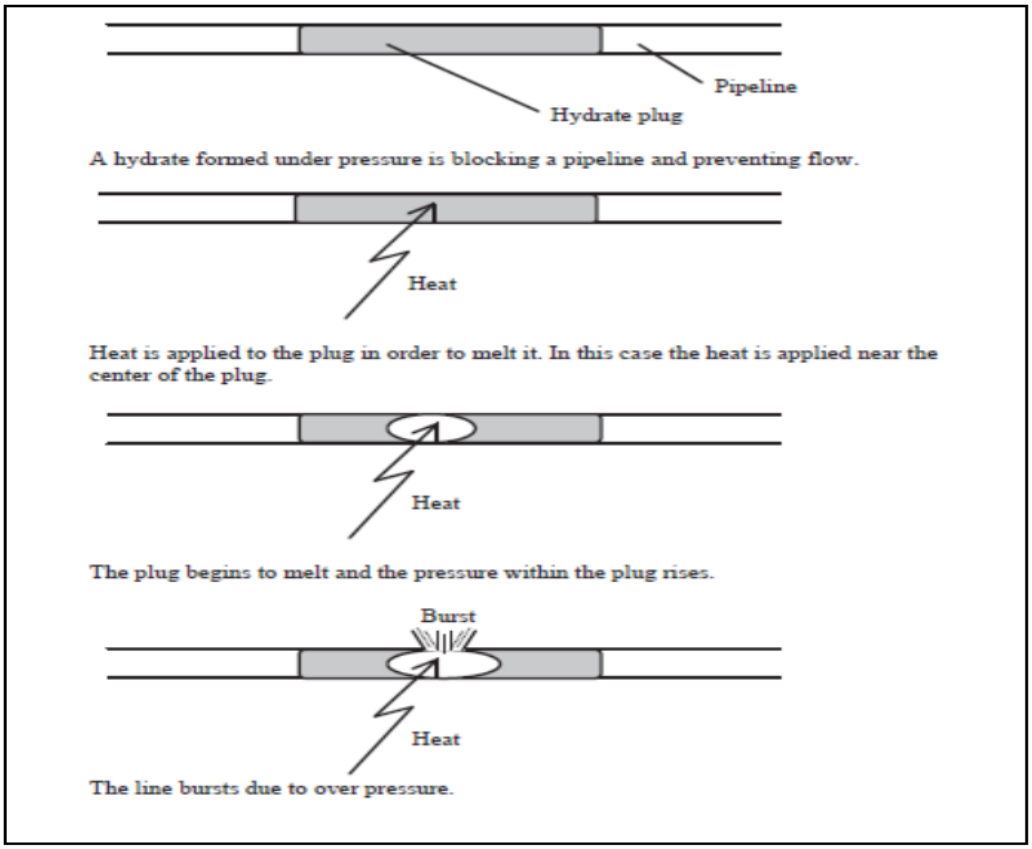

Figure 2-5: Pipeline rapture due to heat (Carrol, 2020).

b) ***Water removal***

The removal of water can be accomplished by reducing the total amount of water present in the system in such a way that it prevents the formation of condensate. The process of dehydration can be accomplished using hygroscopic solutions (glycols), molecular sieves, and refrigeration (Carrol, 2014).

Glycol dehydration

The use of a liquid desiccant system is the most common and well-known method of dehydration. Method by which the gas is made to come into contact with the solvent. The result is a dry gas, which is produced when the water vapor in the gas is absorbed by the solvent. To successfully remove water vapor from the atmosphere, solvents need to adhere to a set of fundamental requirements. (Carrol, 2020).

Glycols

Glycols are consistent with the ideas outlined earlier. It is important to note that glycols will break down at higher temperatures; as a result, this will become a limiting element in the procedures. Most acceptable glycols are Monoethylene glycol, triethylene glycol diethylene glycol, and tetraethylene glycol. Because it possesses the necessary properties as well as the advantages that other glycols lack, triethylene glycol is the glycol that is utilized the most in the process of dehydrating gases. In comparison to DEG, TEG has a low water content and a low dew point (depression). TEG was a more expensive option than DEG. TEG is easier to work with because its viscosity is lower than that of TREG. It's important to note that TREG has a low vapor pressure, so keep that in mind. TEG was more affordable than TREG.

Molecular sieves

In the cryogenic process, molecular sieves play a significant role (very dry gas is needed). The wet gas is introduced into the bed of absorbency, where it undergoes the process of adsorption, which results in the production of dry gas. To get rid of most of the water, the glycol dehydration unit is utilized. After that, the gas is put through the molecular sieve unit, which results in the production of dry gas. This is done to cut on the quantity of sieves that are needed to remove the water from the gas. The process schematic for a two-bed adsorption unit is shown in Figure 2-6. After reaching its water-holding ability, the bed undergoes a process of

regeneration. For the bed to be regenerated, the hot gas must first be removed from the bed, and then the water must be added.

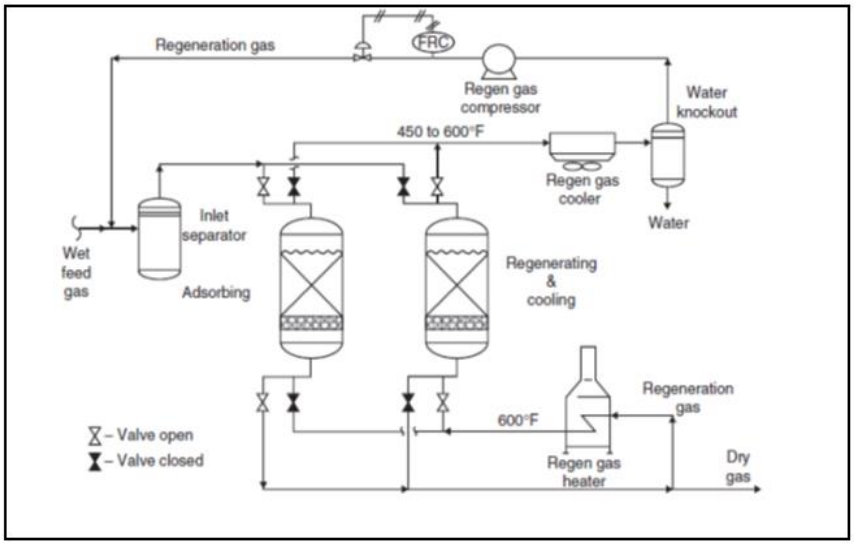

Figure 2-6: Flow chart for dehydration system unit (Carrol, 2020).

c) Refrigeration

The process of lowering the temperature of the gas is known as refrigeration. To separate the heavier hydrocarbons from the gas, the gas is cooled. The process of refrigeration involves the removal of water in the form of cold gases, which contain less water overall. After that, the cold gas is combined with ethylene glycol to prevent the formation of gas hydrates. The process of refrigeration is depicted in the flow diagram that can be found in figure 2-7

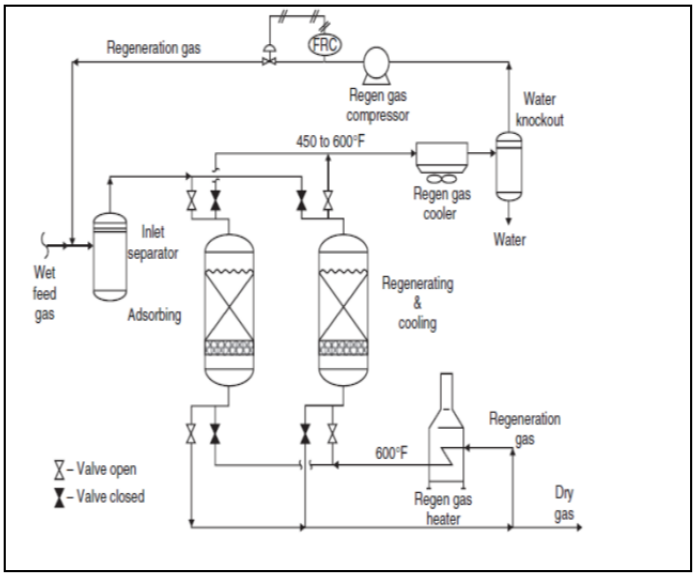

Figure 2-7: Represents process flow diagram of the refrigeration plant unit (Carrol, 2020).

2.3.2.2 Chemical Inhibition

To prevent gas hydrates from forming, chemical inhibition requires the utilization of additives, alcohols, glycols, and solvents. The main types of chemical hydrates are outlined in Figure 2-8.

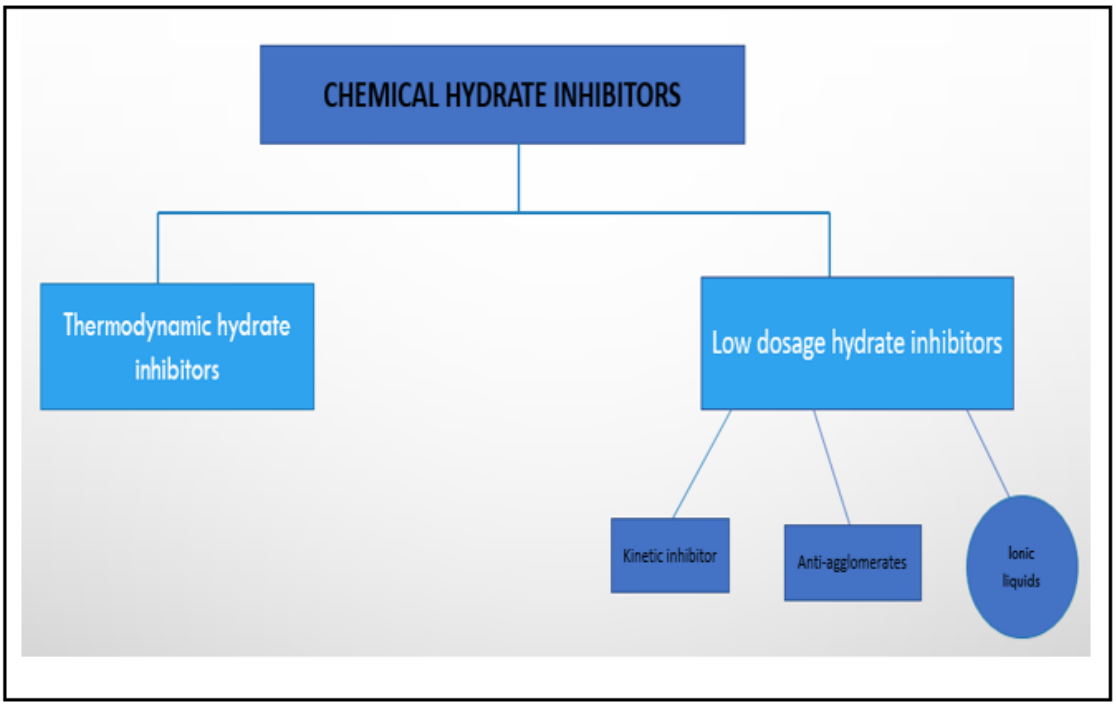

Figure 2-8: Shows several types of chemical hydrate inhibitors.

a) Thermodynamic Hydrate Inhibitors (THIs)

Thermodynamic hydrate inhibitors (THIs) are by far the most prevalent and widely used of all the substances that can be employed to prevent hydrate formation. The THIs shifts the thermodynamic stability to lower temperatures and higher pressures, which removes the strength of the hydrogen bond that is binding water particles together to create the structure of gas hydrate. Several different compounds, including alcohols, glycols, and salts, are used in the process of thermodynamic hydrate inhibition. (Najibi et al., 2009). It is more difficult for water to take part in the formation of hydrates when alcohols, glycols, and salts that have been dissolved in aqueous solution create a hydrogen bond with the water molecule.

THIs has many benefits that include the following: the ability to work with any kind of hydrocarbon; the possibility of recycling however, THIs also has several drawbacks such as

their use in high concentrations; their corrosive nature; the inflated cost of recycling thermodynamic inhibitors.

Low Dosage Hydrate Inhibitors

Kinetic Hydrate Inhibitors (KHIs) are a type of molecular polymer that is soluble in water. KHIs attach themselves to the surface of hydrates to slow down the nucleation and formation of gas bubbles. Subcooling is absolutely necessary for the efficiency of KHIs. They are most effective at lower concentrations, specifically between 0.5 and 1 weight percent of the whole solution.

The benefits of KHIs include being cost-efficient, being effective even at low dosages. KHIs have several drawbacks, including the fact that they are not biodegradable and that they are ineffective during shutdown.

AAs are most effective when present in concentrations of less than one weight percent (Igboanusi, 2011). They are not reliant on the amount of time that has passed or the subcooling degree. They do this to stop the formation of plugs, which is caused when hydrate crystals clump together.

In transporting gas and oil, gas hydrates should be avoided at all costs since they have the potentially disastrous consequence of plugging pipes. The petroleum sector must spend enormous sums of money to take precautions against the formation of gas hydrate in flow channels (Lederhos et al., 1996). Additives are also known as inhibitors. tending to stop (in the case of thermodynamic inhibitors) or slow down (in the case of kinetic inhibitors) the creation of such harmful hydrates (Cha et al., 2013).

Injecting thermodynamic inhibiters into a pipeline to modify the conditions under which hydrate formation takes place to higher pressures and lower temperatures is a popular solution to the issue of pipe blockage (Najibi et al., 2009). To perform their function as thermodynamic inhibitors, additives need to be able to disrupt the hydrogen bonds in the clathrate structure, which are responsible for holding water molecules together. Electrolytes, alcohols, and glycols are successful at achieving this as suggested by the list of additives given in Table 2- 8.

Table 2-1: Experimental hydrates reported in the literature

Systems	Inhibitors	T/ K	P/ MPa	Authors
CO_2	Methanol Ethylene glycol KCl $CaCl_2$	259,18 to 269,16	1,68 to 2,96	Najibi et al., 2013
C_3H_8	Propanone Sodium Chloride	264,7 to 276,9	0 to 0,514	Maekawa, 2010
H_2S CO_2	Methanol Ethylene gylcol Sodium Chloride	241,1 to 290,1	0,180 to 3,29	Mohammadi et al., 2012
CO_2	TMAB + MEG TEAB + MEG	274 to 281,9	2 to 3,5	Qasim et al., 2021
CH_4 CO_2	Methanol + $MgCl_2$ Ethylene gylcol + $MgCl_2$	263,74 to 283,56	0,98 to 8,02	Sami et al, .2013

Included among the newly developed inhibitors are amino acids and ionic liquids. (Lin et al., 2014; Shin et al., 2016). Amino acids are biologically organic substances that serve as proteins' building components. Essential components of amino acids are amine ($-NH_2$) and carboxylic acid (-COOH) functional groups. In addition, the distinctive side chain, which can range from a polar alkyl chain (hydrophobic) to a positively or negatively charged molecule (hydrophilic), characterizes the physical and chemical properties of compounds (Vyas et al., 2010). Amino acids can also be categorized according to the side chain group (R-group), as their physicochemical properties and interactions with water vary greatly (Maderia et., 2014). Figure 2.9 shows the general structure of amino acids.

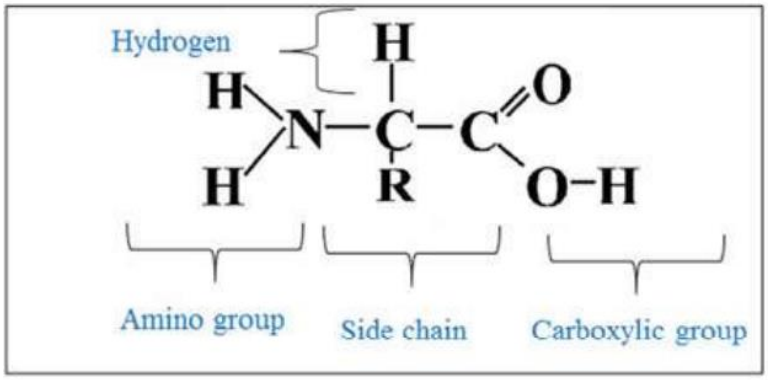

Figure 2-9: Basic structure of amino acids

In 2011, Sa et al. reported the hydrate—liquid—vapor equilibrium curve of CO_2 hydrates having three amino acids (glycine, alanine, and valine) at concentrations of 0.1 and 0.5 mol%. The results showed that all the investigated amino acids inhibit CO_2 hydrates significantly. The increasing order of amino acid inhibition was determined to be valine < alanine < glycine. The thermodynamic impact of inhibition increased as the hydrophobicity of amino acids increased. In 2013, Sa et al. investigated the natural hydrophobic amino acids as new KHIs. Lower hydrophobicity amino acids were reported to be effective KHIs for delaying nucleation and retarding growth, which breaks the hydrogen-bonded network of water, while higher hydrophobicity amino acids enhanced the local water structure.

Recent research by Bavoh et al. (2017) shows that amino acids can inhibit both CH_4 and CO_2 systems to a similar degree. For both CH_4 and CO_2, hydrates, the total inhibitory effect of 10 weight percent (wt%) of amino acids was reported as follows: arginine (1,03 K) serine (1,21 K) proline (1,44 K) alanine (1,64 K) glycine (1,83 K). Since glycine had the shortest side chain and arginine had the longest side chain among the examined amino acids, it was determined that the shorter side chain length of amino acids displayed more effective inhibition. However, the effects of amino acids on the thermodynamics of CH_4 and CO_2 are poorly documented.

The ILs possess distinct advantages over conventional organic solvents such as non-volatility, lower interfacial tensions, and non-flammability together with relatively less toxic nature (Ratti et al., 2014). Together with their tunable properties, ILs can form extended hydrogen bonds and are highly structured in the liquid state (Marsh et al., 2004). Attributed to the reasons mentioned above, ILs are attracting more significant interest in varied industrial applications. Some of the core areas are as catalysts and solvents in organic reactions, biomass conversions biological applications, in energy and fuels applications, as functional materials, in electrochemical applications (Xu et al., 2014). Moreover, ILs also considered as a potential alternative to the conventional hydrate inhibitors attributed to their aforementioned excellent physicochemical properties together with the ability to form efficient hydrogen bonding with water (Xiao et al, 2009).

ILs showed an ample potential to work as dual functional gas hydrate inhibitors, as they possess the ability to perform adequate hydrogen bonding with water molecules, which attributed to gas hydrate inhibition. For effective hydrate thermodynamic inhibitions, firstly, ILs must be hydrophilic; otherwise, if the IL is hydrophobic, it tends to exist in a distinct phase, therefore, unable to disrupt hydrogen bonding network of water molecules. Secondly, individual

functional groups such as oxygen O^- or hydroxyl OH^+ groups in the structure of the ILs create further intermolecular (hydrogen bonding) disruptions with water molecules, thus effectively prevent the gas hydrate formations.

the ILs show inhibition properties suitable for hydrate dissociation in pipelines. It may address the need for a prosperous solvent for flow assurance issues. Thus, ILs with extraordinary properties offer a unique opportunity to study its potential application as gas hydrate inhibitors Tariq et al, (2014) reviewed ILs extensively for dual functional gas hydrate inhibitors which have led to a certain structure-activity relationship of ILs for gas hydrate inhibition. They concluded that the efficiency of ILs as thermodynamic gas hydrate inhibitors decreases with increasing chain length of the cation. This phenomenon was observed as the increase in alkyl chain length increased the hydrophobicity of ILs. Moreover, the substitution of OH groups in the cation enhances the performance of gas hydrate inhibition. Since, the IL with OH-substituted cation can easily be incorporated into the hydrogen bonding network of water, thus making the gas hydrate formation difficult.

Lee et al., (2016) evaluated the pyrrolidinium-based ILs as kinetic hydrate inhibitors in the presence of the tetrafluoroborate ($BF4^-$) anions in synthetic natural gas system. The studied ILs were 1-hydroxyl-1-ethyl-1-methy] pyrrolidinium tetrafluoroborate ((HEMP) ($BF4^-$)), 1-butyl-1-methyl pyrrolidinium tetrafluoroborate ([BMP][BF4]), 1-hydroxyl-1-methy] pyrrolidinium tetrafluoroborate ((HMP)($BF4^-$), and 1-hexyl- 1-methyl pyrrolidinium tetrafluoroborate ((OMP)(BF_4)). The results revealed that ((HEMP) ($BF4^-$)), which contained the hydroxyl functional group in the cation, functioned as an auxiliary group which performed much better than the other studied ILs by delaying the induction time from 14 min (pure water) to 89 min at 3 wt% conditions

2.4 Gas hydrate equilibrium models

The calculation of the gas hydrate equilibrium, which is used to predict data regarding gas hydrates, can be carried out by hand or via computer calculations. The gas gravity method and the distribution coefficient method are both examples of equilibrium approaches that can be utilized in the process of estimating the conditions (P; T) under which gas hydrates form. The fact that less information is required for these models means that they have a disadvantage: when the temperature and pressure data of equilibrium can be predicted, the models can use less information. This method's inaccuracy can be attributed to the fact that it is nearly impossible to avoid predicting the conditions that were anticipated(Carroll, 2014).

2.4.1 Method based on gas gravity

This approach to estimate three-phase conditions was first proposed by Katz (1945). Figure 2-10 illustrates the gas gravity chart that is used to predict the conditions in which gas hydrates will dissociate.

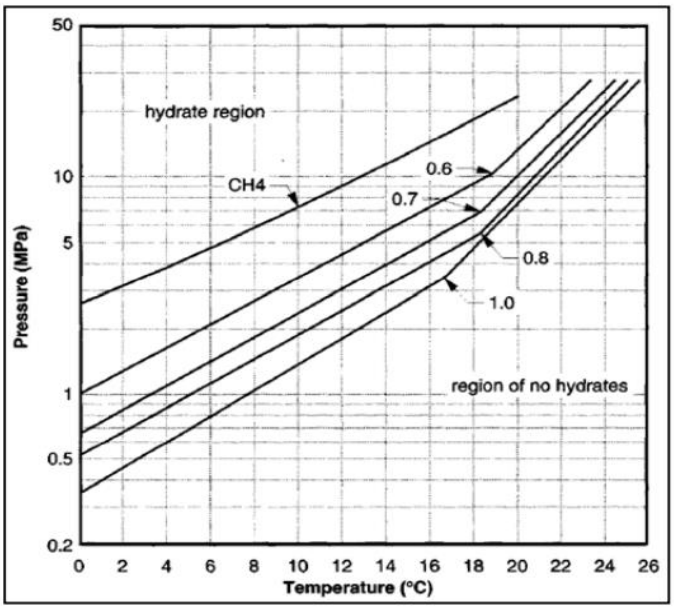

Figure 2-10: Displays a chart for predicting three-phase conditions based on the gas gravity (Sloan et al., 2008)

The chart of equilibrium formation can be used to determine the temperature or pressure required to compute equilibrium formation. The following equation describes the gravitational pull of gas:

$$G = \frac{M_{w\ of\ the\ gas}}{M_{w\ of\ the\ air}} \quad (2\text{-}1$$

Where, G stands for gravity, $M_{w\ of\ the\ gas}$ stands for molecular mass of the gas. $M_{w\ of\ the\ air}$ stands for molecular weight of air. $M_{w\ of\ the\ air} = 28{,}9966$. This technique is only applicable to gas lines that mostly consist of natural gas, with just a trace number of other gases that are incombustible. In cases where the specific gravity fell between 0.9 and 1, the gas hydrate approach was found to be erroneous (Sloan et al., 2008).

2.4.2 The distribution coefficient method (Kvsi – value)

In 1941, Wilcox et al. proposed this approach, which Carson and Katz examined in 1942. According to their findings, temperature and pressure alter the hydration composition. The K value chart for a certain gas must be predicted.

$$K_{vsi} = \frac{y_i}{x_i} \quad (2\text{-}2)$$

Where y_i and x_i presents mole fraction in the aqueous liquid and solid hydrate, respectively. Each hydrate-forming component of natural gas has its own K-value chart. In this case, too, the temperature and pressure must be known for this procedure to work.

2.4.3 The sour gas chart technique

For sour gas, the Kvsi-value and gas gravity were not proper measures (containing Hydrogen sulfide). In 1987, Baillie and Wichert developed the chart approach, which uses gas gravity to anticipate gas hydrate conditions. When hydrogen sulfide is between 10 and 50 mol% and propane is up to 10 mol%, this is the method to use. For mol% that is between 0.6 and 1 this is the ideal technique. The Baillie and Wichert's chart for sour gas is shown in Figure 2-11.

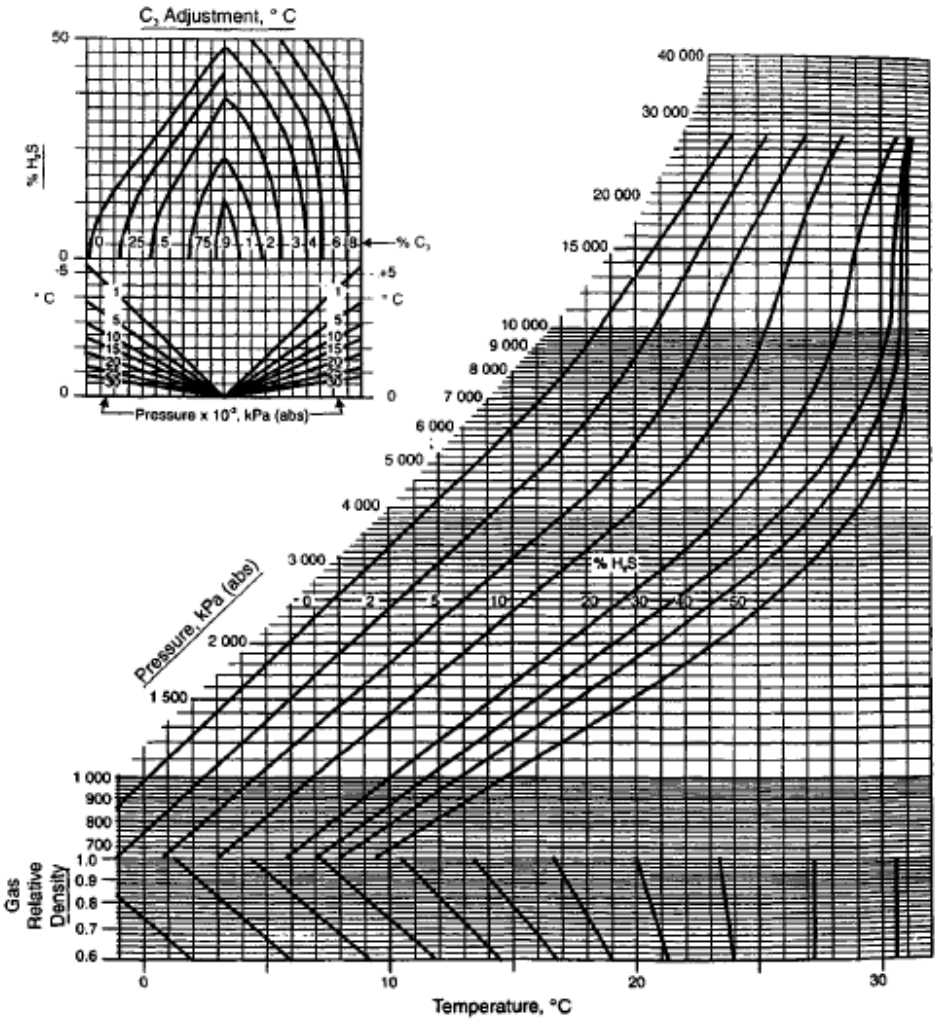

Figure 2-11: Baillie-Wichert chart for sour gas hydrate formation conditions estimation (Carroll, 2014)

2.4.4 Empirical Correlations

2.4.4.1 Makogon Correlation

Makogon (1981) was the first person to uncover the correlation that can be used to calculate the formation of hydrates given the circumstances (P; T) and the gas gravity. This association is helpful for determining the properties of paraffin hydrocarbon.

$$logP = \beta + 0.0497(t + kt^2) - 1 \quad (2\text{-}3)$$

Where β and k are a graphical correlation,

$$\beta = 2.681 - 3.811G + 1.679G^2 \quad (2\text{-}4)$$

$$k = -0.006 + 0.011G + 0.011G^2 \quad (2\text{-}5)$$

Where G is gas gravity

2.4.4.2 Towler and Mokhatab Correlation

Towler and Mokhatab made a discovery in 2005 regarding a correlation that might be used to calculate the temperature of hydrate formation given the pressure and gas gravity.$T = 13.47lnP + 34.27lnG - 1.675lnP\ x\ lnG - 20.35$ (2-6)

2.4.5 Computational Method

2.4.5.1 The Van der Waals-Platteeuw model

In the year 1959, Van der Waals-Platteuw presented a method for the system that forms hydrates. This method depended on a statistical model that focused on the hydrate and how it dealt with the adsorption of the gas phase to the solid phase. The following are some of the presumptions that were made when the Van der Waals-Platteeuw model was being developed (Sloan et al., 2008): There is only room for one gas molecule in each cavity; traditional statistical methods are reliable; there is very little guest-to-guest interaction; the hydrate lattice is distorted as a result of the presence of guest molecules.

The Van der Waals-Platteuw model can be stated in the following way:

$$\Delta\mu^H - \Delta\mu^\beta = RT \sum_i c_m \ln(1 - Y_i)$$
(2-7)

In equation 2-7 $\Delta\mu^H$ and $\Delta\mu^\beta$ each represent the water chemical potential for the solid phase and the unoccupied hydrate phase, respectively. c_m is a number of cavities Y_i is the probability function of cavity occupied by the guest molecule,

$$Y_i = \frac{c_i P}{1 + c_i P} \quad (2\text{-}8)$$

Where c_i denotes the function and cage that is being used by the guest molecules.

2.4.5.2 Parrish and Prausnitz

According to Van der Waals and Platteeuw, the following equation can be used to predict the Langmuir adsorption constants using the Lennard-Jones-Devonshire cell theory:

$$C = \frac{4}{kT}\int_0^{\infty} \exp\left[-\frac{w\,(r)}{kT}\right] r^2\, dr \qquad (2\text{-}9)$$

Where k denotes the Boltzmann's constant and T presents is temperature $w\,(r)$ presents the spherical core cell potential function to define the interaction between the water and guest molecule and *r* defines the distance between the cavity centre and guest molecule.

Kihara cell potential was employed by McKoy and Sinanoglou (1963) to predict hydrate dissociation conditions. They ran three different models through its paces to see which one could best predict hydration data. While Lennard-Jones-Devonshire works best for spherical core molecules, Kihara cell potential works best for non-spherical molecules, according to the researchers.

In later years, Parrish and Prausnits revised the Kihara cell potential equation to look like this:

$$V = 2z\varepsilon\left[\frac{\sigma^{12}}{R^{11}r}\left(\delta^{10} + \frac{\alpha}{R}\right) - \frac{\sigma^{6}}{R^{5}r}\left(\delta^{4} + \frac{\alpha}{R}\delta^{5}\right)\right]$$

(2-10)

Where

$$\delta^N = \mathrm{N}^{-1}[(1 - \mathrm{r(R)}^{-1} - \alpha(R^0)^{-N} - (1 + (R^0)^{-N}] \qquad (2\text{-}11)$$

In the equation that was just presented, the symbol for the core radius of interaction between molecules (water and gas) is denoted by the α . The symbol for the collision diameter which is distance at 0 potential is denoted by the . The symbol for the free cavity radius is denoted by the R^0. The symbol for the coordination number of cavity is denoted by the letter z . The symbol N equals 4, 5, 10, and 11, respectively.

2.4.5.3 The Klauda and Sandler Model

This methodology, which may be applied to both structure I and structure II hydrates, was proposed by Klauda and Sandler (2000).

$$f_w{}^H = f_w{}^\beta exp\left(-\frac{\mu_\beta - \mu_H}{RT}\right) \qquad (2\text{-}12)$$

$f_w{}^\beta$ is the fugacity of water.

2.5 Methods and equipment for measuring hydrate equilibria.

2.5.1 Methods for hydrates

To measure the gas hydrate phase equilibria, one can use either a direct (visible) or indirect (non-visual) method with a stationary apparatus. Both methods have their advantages and disadvantages. The isochoric approach (volume constant) is based on the non-visual method, in contrast to the isobaric method (constant pressure) and the isothermal method (constant temperature), which are both based on eye observation. One of the three parameters of temperature, pressure, and volume is held constant in each of these techniques (isothermal, isobaric, and isochoric), while the other two values fluctuate because of the formation and dissociation of gas hydrates (Ye and Liu, 2012). As was noted earlier, the visual approaches (isobaric and isothermal) are not proper for use in conditions below the freezing point of water because it is difficult to differentiate between the ice crystals and the gas hydrate clusters. These conditions make it impossible to use these methods (Schroeter et al., 1983). The isochoric approach is precise and does not call for the observation of the production or dissociation of gas hydrates. The considerable shift in the slope of the heating curves in the P-T diagram is used in this method to identify the hydrate dissociation conditions. This method is described in more detail below.

2.5.1.1 Method of searching using visual isothermal pressure

Temperature is maintained at a constant level during an isothermal pressure search experiment at the beginning of the experiment. To eliminate any contamination, the equilibrium cell is evacuated, and the pressure of the system is set above the expected zone of hydrate formation. To achieve equilibrium, the system must first be agitated and then allowed to cool to the desired temperature. When hydrate nucleation begins, the temperature at the hydrate interface rises as molecules move from the gas and liquid phases to the hydrate phase, releasing translational energy. However, agitation or conduction/convection are required to remove this energy from the system and transfer it to the bath and adjacent phases. The pressure in the system drops during hydrate formation because to gas encasing. A gas or liquid, such as mercury, is exchanged from an external reservoir to control the experiment's pressure. By removing fluids (gas or liquid) from the external reservoir, the pressure progressively decreases until all gas hydrate crystals have been removed. Only pure liquids or gases can be used in this operation. Hydrate at a constant temperature has a visible equilibrium pressure point at this location.

Experimentation on hydrate formation and dissociation should be conducted twice to prevent inaccuracies when employing the visual effect (Sloan and Koh, 2008).

Isothermal pressure search methods that don't require visual observation of hydrates have been adopted by several researchers (Makogon and Sloan, 1994; Makogon and Sloan, 1996; Mohammadi and Richon, 2010). As seen in Figure 2-12, this process necessitates a lot of trial and error. To begin the process of forming the hydrate, an increase in pressure is required. A little amount of gas is then expelled from the system, which results in hydrate dissociation. To determine the smallest difference between the hydrate lower formation and upper dissociation pressures at the specified temperature, this procedure is repeated.

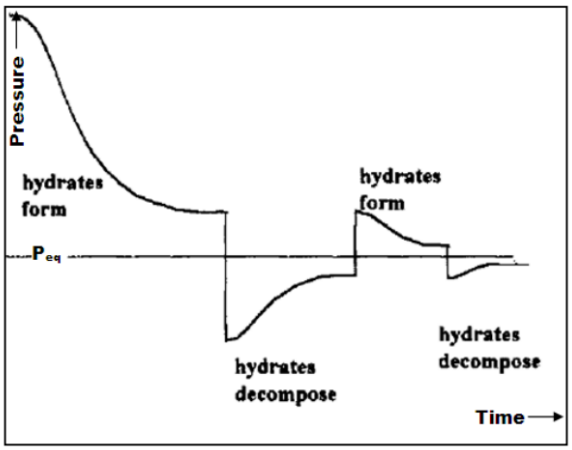

Figure 2-12: Schematic diagram of the non-visual isothermal pressure search procedure (Makogon and Sloan, 1994).

2.5.1.2 Isobaric pressure

Using this technique, the temperature is kept stable while the pressure is changed, which is accomplished most frequently by adjusting the volume. During the experiment, the level of pressure is brought to a level that is higher than the anticipated equilibrium point, but the temperature is held steady. As a direct consequence of this, the formation of the hydrate will take place under these conditions.After that, the pressure is gradually lowered until the hydrates are fully separated, at which point the process is finished. This process is repeated as many times as necessary until the difference in pressure between the formation and dissociation points falls within the acceptable range.

2.5.1.3 Isochoric pressure search method

The conventional process that was created in the laboratory of Professor Kobayashi serves as the foundation for the isochoric technique (Marshall et al., 1964). In most cases, the formation of hydrates takes place in the isochoric manner when the temperature of the system is lowered. In a cell with a constant volume, the rate of change in differential pressure is measured in relation to the concurrent rate of change in differential temperature. The P-T curve can be determined by monitoring the pressure as a function of the temperature for each cell loading. This makes it possible to determine the curve. Therefore, the slope of the isochoric P-T curve can be expressed as $\left(\frac{\partial P}{\partial T}\right)_v$.This can be done because the curve is isochoric. After that, the hydrate crystals are dissociated using a stepwise heating process.

According to Ohmura et al. (2004), the hydrate dissociation point can be located by finding the point at where the curves representing cooling and heating intersect. This intersection reveals a phase transition, which in turn reveals the location of the hydrate dissociation point. Figure 2-13 is a diagram that depicts a graphical illustration for the process of determining the point at which the hydrate dissociates. As a result, the hydrate phase boundary of a system can be identified by graphing multiple experimental dissociation data at varying pressures for a given load. This will result in the identification of the hydrate phase border.

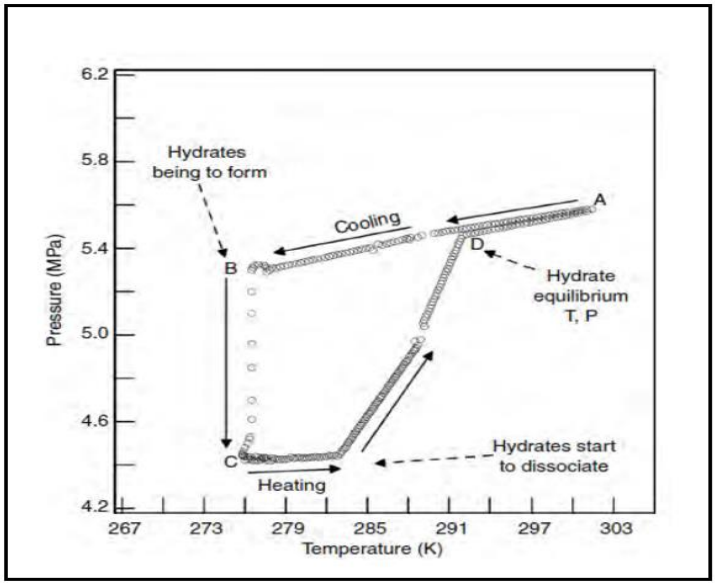

Figure 2-13: Shows the pressure isochoric search method's primary cooling and heating curves for the generation and dissociation of simple hydrates (Sloan and Koh, 2008).

2.5.2 Experimental Equipment

The following is a list of the significant parameters that need to be taken into consideration while developing an equipment for the measurement of gas hydrate phase equilibria:

1. The device needs to have vigorous agitation, and it can either use mechanical or magnetic agitators. This is necessary for the entire transformation of the water. Hammerschmidt made the observation in 1934 that agitation was necessary to begin the process of hydrate production and to decrease the gas hydrate metastability zone (Hammerschmidt, 1934). The amount of water molecules in the hydrate phase was reduced when the agitation of the neighbouring phases (gas, liquid, and hydrate phase) in an equilibrium cell was increased. In addition, water occlusion may be prevented, and the surface renewal of the gas and liquid phases at the interface can be made better thanks to the agitation of the cell. According to
Villard's research from 1896, the synthesis of nitrous oxide hydrate may take up to fifteen days if there is no agitation in the system (Sloan and Koh, 2008).

2. The point at which the hydrate finally dissociates is more reproducible than the curve that describes its production. Because of this, picking the point at which the hydrate dissociation is complete as the equilibrium data point is the most reliable option. To prevent the development of the metastable pressure, the hydrate must be heated up to the ultimate dissociation point in a manner that is both slow and in a step-by-step fashion. When expressed another way, this means that the occurrence of metastability is impossible if the rate of heating towards the point of final dissociation is kept low (Tohidi et al., 2001, Sloan and Koh, 2008). In the visual method, the point at which all crystal hydrates have dissociated is the hydrate equilibrium point. Alternatively, the point at which a notable change in the slope of the pressure versus temperature plot occurs is also considered to be the hydrate equilibrium point because this method is more accurate than the visual methods (Sloan and Koh, 2008).

3. When doing hydrate measurements in a cell with a constant volume, if the pressure suddenly drops or the temperature suddenly rises, this is an indication that hydrate is forming in the cell. The primary reason for the decrease in pressure that occurs during the formation of hydrates is that the gas is encased inside the cavities of the hydrates. The temperature rises throughout the process of hydrate nucleation because the production of hydrates is an exothermic reaction, and the translation energy of the encapsulated molecules in the hydrate phase is lower than that of those in the vapour and liquid phases (Sloan and Koh, 2008).

The equilibrium cell, which is often contained within a thermostatic bath, is the component of the hydrate apparatus that holds the highest significance.

5. A thermometer and a pressure transducer (or a Bourdon tube gauge) are placed inside the cell to measure the temperature and pressure during the process of hydrate formation and dissociation. These instruments are then placed outside of the cell.

6. The most critical component of the equilibrium cell in the visual approach, also known as the direct method, is a sight glass that allows one to observe the process of gas hydrate production and decomposition inside the equilibrium cell.

2.5.2.1 Hydrate equilibrium cell

The stirring autoclave is the primary component of this equipment, which also features openings for adding and removing components as per the design work of (Deaton and frost Jr, 1946). The pressure was determined using a pressure gauge, and the temperature was determined using a thermocouple. The diagram that was constructed can be seen in Figure 2-14. (Deaton and Frost Jr, 1946). Either the composition can be visually identified, or it can be attached to the GC machine to be analysed.

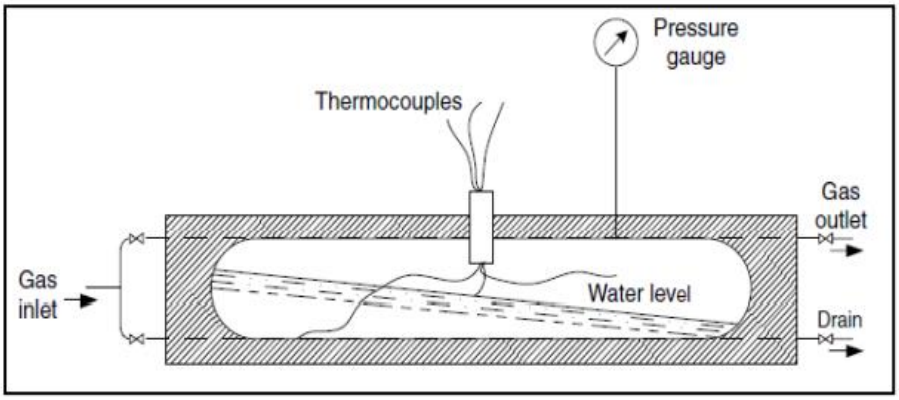

Figure 2-14: Static hydrate equilibrium cell design by Deaton and Frost, 1946 (Sloan and Koh, 2008).

2.5.2.2 Quartz Crystal Microbalance

The Quartz Crystal Microbalance is a tool for determining the conditions under which hydrates develop, and it is the method that is most chosen due to the short amount of time needed for experiments and the small sample sizes involved (Mohammadi et al., 2003). The QCM diagram

is represented here by Figure 2-15. (Sloan et al., 2008). The change in the resonance frequency of the QCM that occurs when an electric current is passed through is the basis for the measurements used to determine the hydrate stability zones.

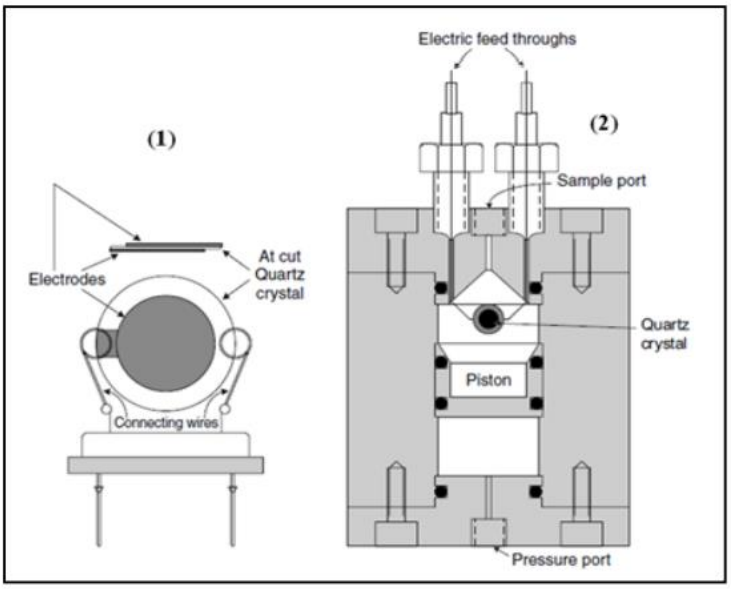

Figure 2-15: The schematic diagram of the QCM, (2) the QCM mounted with high pressure (Sloan and Koh, 2008).

A tiny disk of quartz is compressed between two electrodes within the QCM. When an electric current flows through the electrodes of this equipment, the quartz disk begins to oscillate at a particular resonance frequency. The frequency of the disk is depending on its crystal characteristics. During hydrate development, the quantity of hydrate mass adhered to the disk's surface varies. This change in mass can alter the resonance frequency. Changes in frequency and disk oscillations can therefore detect hydrate production and dissociation. The QCM device is extremely sensitive and can measure extremely minute amounts of mass, hence reducing the time required for investigations. In this apparatus, the time required to reach equilibrium at each temperature step is fifteen minutes, a significant reduction from the many hours required by conventional approaches. This equipment is capable of measuring phase data with pressures up to 6000 psi. A pressure transducer and a thermocouple were used to measure the system's temperature and pressure, respectively.

2.5.2.3 High-pressure differential scanning calorimeter

This technique was created by Dalmazzone et al.,(2003). Figure 2-16 illustrates the schematic diagram of HPDSC. HPDSC was developed to operate in an isobaric environment. It can

function at temperatures ranging from (230 to 393.1 K) and pressures up to 40 MPa Tumba et al., 2016.

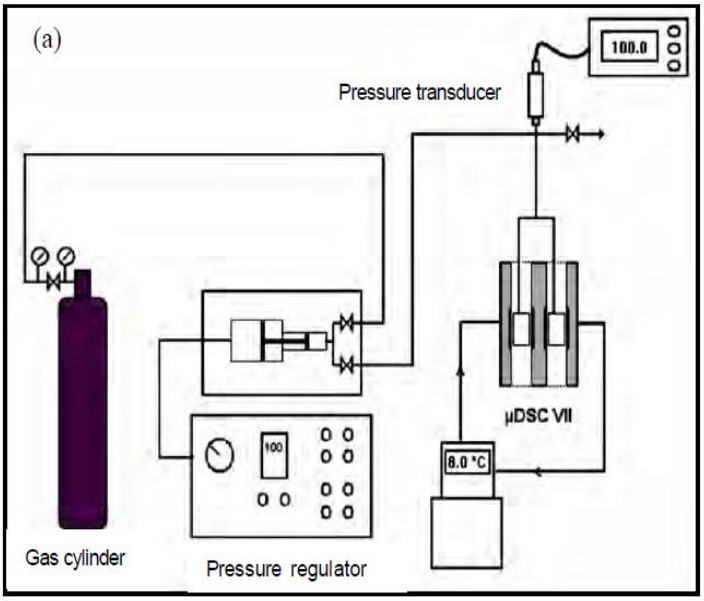

Figure 2-16: Schematic diagram for high-pressure differential scanning calorimeter (Deschamps and Dalmazzone, 2003)

2.5.2.4 Rocking cell

The apparatus developed by Deaton and Frost (Deaton and Frost Jr., 1946), rocking the cell was an option for effectively mixing the contents of the cell. This was essential for achieving high water-to-hydrate conversion rates and for minimizing the amount of time needed to get equilibrium data. Many other researchers, such as Najibi et al. (2010), Adisasmito et al. (1991), Holder et al. (1980), and Mohammadi et al. (2010), agreed with the concept and used it in their own studies (2005). The equipment for determining hydrate phase equilibria that is depicted in Figure 2-17 is an example of a conventional rocking cell.

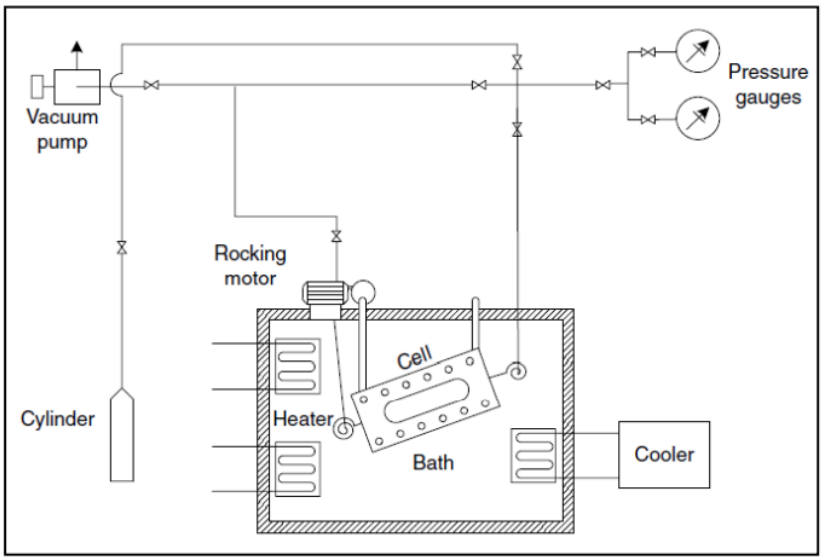

Figure 2-17: Rocking cell for hydrate equilibrium apparatus (Sloan and Koh, 2008).

2.5.2.5 Variable volume cell

Ngema et al.,(2014) proposed the use of a variable volume cell as a means of avoiding the limitations of the isochoric method (isothermal technique and time consumption). 10 centimetres cubed is the volume of the cell. The graphical representation of the schematic diagram can be found in figure 2-18. The pressure of 20 MPa and the temperature of 373.15 K were intended to be withstood by the cell during the manufacturing process.

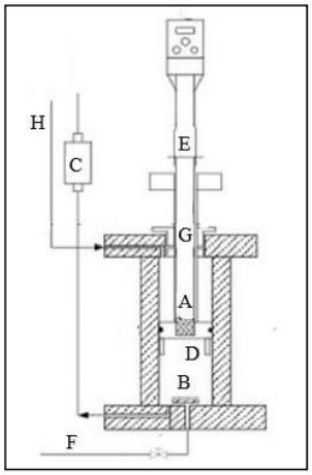

Figure 2-18: Schematic diagram of Transparent variable volume cell used by Ngema et al. (2014). A) neodymium magnet; B) magnetic stirrer bar; C) pressure transducer; D) impeller; E) overhead mechanical stirrer; F) drain and loading line; G) mechanical shaft; H) inlet for the hydraulic liquid

Chapter 3

3 Deep Eutectic Solvents (DESs)

This chapter discusses deep eutectic solvents in general and includes the general naming of Deep Eutectic Solvents (DESs); a brief history documenting the evolution of DESs categorization; and some notable attributes of DESs.

3.1 History and Definition

Deep eutectic solvents (DES) were found in 2001 by Abbott and his colleagues. Abbott and his colleagues defined DESs as the mixture of elements that are formed from simple halide salts and hydrogen bond donor (HBD). To create a blended mixture, the components must have the ability to interact with one another through the hydrogen intermolecular forces (Quraishi et al., 2017). When compared to other types of solvents, such as ionic liquids, DESs are thought to be more environmentally friendly alternatives to other types of solvents. DESs are distinguished by several qualities, including their low cost and absence of any negative impact on the environment (Zhang et al., 2012).

Because of their low cost, ease of storage, biodegradability, and reduced impact on the environment, these substances are referred to as "green solvents" (Yu et al., 2008; Ilgen et al., 2009 and Waever et al., 2010;). The eutectic point of a mixture is seen in Figure 3-1. This is the point at which the molar ratio of the two constituent chemicals yields the lowest melting point attainable. When two different components are combined, the result is a compound that has a lower melting point than either of the individual components. The interaction of the HBD with the anion of the salts improves the efficacy of the anion, which in turn decreases the attraction of the negatively charged ion to the positively charged ion. Therefore, the point at which the mixture melted was lowered (Carriazo et al., 2012).

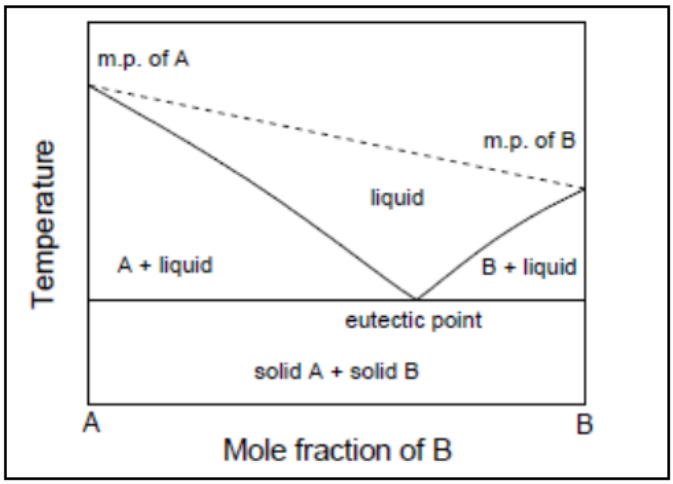

Figure 3-1: Schematic representation of the two components phase diagram

The formation of DES takes place through the reaction of organic salts with either simple halide salts or hydrogen bond donors. Choline chloride is the organic salt that is utilized the most. Abbot et al., (2004) and Smith et al (2014) describe general formula Cat^+X^-zY where Cat refers to the cation X^-, z refers to the anion of the halide, refers to the number of molecules of Y that interact with the anion, and R refers to the alkyl group.

DES can be broken down into one of four distinct groups. The overall methodology for DES categorization can be found in Table 3-1. They are constructed using MCl_x.

Table 2-1: General formula of DES types (Smith *et al*., 2014)

Type	General formula	Examples of terms
Type1	$Cat^+X^-zMCl_x$	M = Zn, Sn, Fe, Al, Ga,
Type 2	$Cat^+X^-zMCl_x.yH_2O$	M = Cr, Co, Cu, Ni, Fe
Type 3	Cat^+X^-zRZ	M = $CONH_2$, COOH, OH
Type 4	$MCl_x + RZ = MCl_{x-1}{}^+.RZ + MCl_{x-1}$	M = Al, Zn Z = $CONH_2$, OH

Type 1 DES's

Metal halides (such as SnCl2 and FeCl3) are combined with organic salts and quaternary ammonium salts in their composition (ChCl). When mixing metal halides with organic salt, the molar ratio that should be employed is 1: 2. There are distinct differences in the qualities and charge densities of each Type 1. (Bernasconi et al., 2017). The conductivity and viscosity of type 1 mixes are both affected by the size of the ions in the mixtures. When compared to aluminium ionic liquids, DESs, which are anhydrous zinc and iron salts, have bigger ions, which causes the conductivity to be lower while also increasing the viscosity of the liquid.

Type 2 DES's

The formation of type 2 takes place through the combination of organic salt (ChCl) with metal salt hydrate ($CoCl_{26}H_2O$). These are DESs that are not sensitive to dampness. The most common use for DESs of type 2 is in the industrial sector (Caja et al., 2000). The presence of water brings about a decrease in lattice energy, which in turn brings about a lower melting point. When compared to anhydrous salts, Endres et al. (2008) found that it is more likely for hydrates to create mixtures with QAS that are liquid under the conditions that are present in the environment.

Type 3 DES's

It is produced by reacting organic salts (ChCl) with substances that may donate hydrogen bonds, such as polycarbonic acids and urea (Smith et al., 2014). In certain type 3 mixes, the degree to which the freezing point is lowered is of an exceedingly high order (Abbot et al., 2004).

Type 4 DES's

The metal salt hydrate ($CRCl_{36}H_2O$) is combined with HBD to produce it (urea, ethylene glycol). Type 4 generates cationic metal complexes, which guarantees a high concentration of metal ions in the area immediately adjacent to the electrode surface (Abbott et al., 2014).

Most organic solvents are hazardous to handle, can be poisonous, and influence the surrounding environment. Some of the potentially dangerous solvents, such as volatile organic solvents that generated photochemical smog, were made illegal. Chlorofluorocarbons, which are responsible for the depletion of the ozone layer. (Clark, et al., 2002). Because of their low vapor pressure, DESs are relatively non-toxic and produce fewer emissions to be released into the atmosphere. Simple to manipulate, and it does not require any sort of purification. Because of this, it is now much simpler to manage greater quantities of DESs.

During their research, scientists examined characteristics such as density, viscosity, electric conductivity, and surface tension. They discovered that these characteristics are comparable to those of ionic liquids in many respects (Zhang et al., 2012). Choline chloride DESs were used in the manufacturing of analytical equipment, the electropolishing of steel, the lubricating of steel, the processing of metal oxides, and the drug solubilization procedure.

Synthesis of DESs

One of the benefits of DESs is how simple their synthesis is. Jacketed vessel and mechanical mixer are required components for the preparation of DESs. The components used include materials that are both environmentally benign and biodegradable (Abbot et al., 2003a; Hayyan et al., 2012).

As was mentioned before, the HBD has an interaction with an anion of the salts, which boosts the efficacy of the anion while simultaneously reducing its attraction to the cation. The temperature at which the combination freezes is brought down. It is common knowledge that DESs have a high depression temperature and can be found in liquid form at temperatures lower than 150 degrees Celsius(Abbot et al., 2004).

3.2 Properties of deep eutectic solvents

Properties of a substance that pertain to its physiochemistry and thermodynamics such as its density, viscosity, freezing point, or conductivity, are essential because they help determine the constraints placed on its use in industrial applications. Most organic solvents are hazardous and toxic, which means that they have a negative impact on the environment. Because they contribute to the depletion of the ozone layer, organic compounds are regarded as being hazardous to the environment (Anastas and Kirchhoff, 2002; Clark and Tavener, 2007). As a result of this, an effort has been made to replace OCs by investigating some potential alternative solvents that are safer for the environment and can be used in chemical processes. In this context, research has been done on various solvents, including water, supercritical fluids, inert liquids (ILs), and solvent-free processes (Clark and Tavener, 2007). However, although it is getting easier, finding suitable "green" solvents as an alternative to OCs is still difficult. For a solvent to be considered "green" regarding the environment, it must satisfy several criteria (Anastas and Kirchhoff, 2002), which are outlined in Table 3-2. These criteria are as follows:

Table 2-2: Considerations to be made when choosing a "green" solvent (Plechkova and Seddon, 2008)

Criteria	Reasons
Price	Ensure the stability of the chemical process; the solvent should be cost-effective
Grade	Technical grade solvents are preferred for purification to reduce energy consumption.
Availability	Bulk availability of the solvent is necessary to ensure its constant availability.
Recyclability	Solvent should be completely recycled in a chemical process using eco-friendly procedures.
Synthesis	The preparation of the solvent should be accomplished in a manner that conserves energy, and the synthetic reaction should be highly atom efficient.
Performance	Solvents must match or outperform presently used solvents to be eligible.
Flammability	Solvents must be non-combustible for safety.
Stability	In a chemical reaction, the solvent must be both chemically and thermally stable. To comply with all transport regulations, solvent storage must be feasible.
Renewability	Regarding carbon emissions, the solvent must be synthesized using renewable raw materials.
Biodegradability	The solvent must be biodegradable and produce no toxic metabolites.
Toxicity	To reduce the risk to nature or humans, solvents must exhibit negligible toxicity.

3.3 The DES's physicochemical characteristics

Thermophysical properties of materials are required for the design of both processes and process equipment. Inaccuracies in the estimation of properties may lead to inadequate design results with some undesirable financial consequences.

3.3.1 Freezing point

The hydrogen bond donor, the chemical composition, and the presence of organic salts are to blame for the lowering of freezing points. As a result, the ability for interaction between HBD and anion is of utmost significance. Strong attraction is the reason of the bigger freezing temperature divergence, while weak interactions between the components are the cause of the smaller freezing temperature deviation (Zhang et al., 2012). The low freezing point is a direct consequence of the high molar ratio of HBD. According to Zhang and co-workers (2012), DESs have a freezing point that is lower than 150 ^{o}C; however, the ones with a freezing point that is lower than 50 ^{o}C are the most ideal.

3.3.2 Density

The size, mass, and form of the molecules all play a role in determining how closely they can pack together, which in turn determines the density. Previous research published in the scientific literature has indicated that the density of DESs can range anywhere from 1.1 to 2.4 grams per cubic centimetre (Zhang et al., 2012; Carolin et al., 2012). The densities depend on temperature, molar ratio, pressure, and moisture content. The DES densities decreases whenever there is an increase in the length of the alkyl chains present in the components (Zhang et al., 2012; Florindo et al., 2014). In addition to this, it was discovered that the densities drop when the molar ratio of HBA to HBD goes up (Abbott et al., 2011).

3.3.3 Viscosity

Temperature, the molar ratio, and the amount of water in a substance all influence its viscosity. When the temperature is raised, the viscosity of a substance will, in most cases, decrease. Bernasconi et al. (2017) state that to study the link between temperature and viscosity, either the Arrhenius equation or the Vogel-Fulcher-Tammaann model is utilized. The abundance of HBD components promote sluggish movement of species, which, combined with the mixture of DES, leads to high viscosity (Zhang et al., 2012; Garca et al., 2015). High viscosity is caused by the combination of ion size and the Van der Waal force. The DESs that have a low viscosity are most desired in the chemical sector because they are easier to manage. On the other hand, the DESs that have a high viscosity result in higher pumping expenses.

3.3.4 Conductivity

The capacity of a material to carry an electric current is referred to as its conductivity. According to Ju et al. (2012), in general, the lower the resistance that something offers when it

comes to conducting electric current, the higher the value of conductivity that it possesses. Polymers, amino acids, ionic liquids and nanoparticles have shown good potential to replace the conventional inhibitors It defines the cohesive forces that are present between the molecules of the liquid. The molar ratio, temperature, and amount of water content are the three elements that influence the surface tension of DESs. Temperature and surface tension are related to one another, although in a roundabout way. (Zhang et al., 2012; Ventura et al., 2014).

3.4 The Law of Polarity

Reichardt was the one who initially proposed the concept of polarity, which can be defined as the capacity of a fluid to dissolve solutes. The polarity can be determined by starting with the wavelength of the maximum absorbance of the dye in different solvents at a temperature of 25 degrees Celsius and a pressure of 1 atmosphere. The value of Reichardt's dye, or ET, can be determined by solving the following equation:

$$\frac{E_T(30)}{kcalmol^{-1}} = \frac{h_{CU_{max}} N_A}{\lambda_{max}} = \frac{28591}{\lambda_{max}} \quad (3\text{-}1)$$

Where h is the constant of Planck, c is the speed of light, N_A is the number of Avogadros, and λ_{max} is the wavelength at which there is the greatest amount of absorption.

3.5 Possible applications of DESs in the industrial sector

Although research and uses of DESs are still in the initial stages of development, DESs are already being used in a wide variety of creative ways. It has been stated in the literature that DESs can have a variety of applications. The following are some examples of the applications of DESs: Biodiesel purification (Abbot et al., 2007; Shahbaz et al., 2010) Drug solubilization (Morrison et al., 2009) Transformation in the biological realm (Gutierrez et al., 2009) Carbon dioxide absorption (Li et al., 2008; Sui et al., 2009; Lu et al., 2015; Ali et al., 2014) Biotransformation (Krystof et al., 2013; Pöhnlein et al., 2015) Nanoparticles (Liao et al., 2008) Naphtha as a source for the extraction of aromatic hydrocarbons (Kareem et al., 2012) Chemistry of Electrons (Abbott et al., 2011) Biological material being dissolved in solvents (Helalat-Nezhad et al., 2015) putting an end to bacteria (Toennesen et al., 2016) Batteries based on redox flow (Bahadori et al., 2017) Solar cells that are dye-synthesized (Boisett et al., 2013; Jhong et al., 2009).

3.6 Molecular Dynamic Simulation

One of the computational tools that is utilized in the process of analysing the behaviour of different systems and chemicals on the molecular level is called molecular dynamic simulation. A simulation system can be established using the Materials Studio software (Bovia, 2019) to investigate the stability of carbon dioxide gas hydrates. This was accomplished through geometric optimization and the minimization of energy consumption. This approach provides new insights into the effects of factors like temperature, pressure, and inhibitors like deep eutectic solvents will have on hydrate formation/dissociation. To understand the structural, thermodynamic, and dynamic properties of systems, molecular dynamic simulations are necessary, as stated by Kondori et al. (2019). The equation of motion derived from Newton is used in computer simulations of molecular systems.

$$m_i \frac{\partial^2(u)\, r_i}{\partial t^2} = F_i\,, i = 1 \ldots \ldots N \tag{3-2}$$

where, m_i is mass of the particle and its acceleration, ai. The total energy of the N-molecule system is composed of kinetic K and potential u energies r_i.

$$H = K + U(r) \tag{3-3}$$

Where is K located:

$$K = \sum_{i=1}^{N} m_i \frac{v_i^2}{2} \tag{3-4}$$

This entails selecting the potential for a molecular dynamics simulation: potential energy as a function of inter-particle separation, that is $U(r_1, r_2, \ldots\ldots r_N)$ When the atoms are arranged in the manner that is specified, certain positions of the atoms will represent the potential energy of the system. This function has both translational and rotational components and is typically constructed from the relative positions of the atoms with respect to one another, as opposed to their absolute positions (Mayo et al. 1990). The relative positions are important because energy is a functional of the distances between particles.

Calculating the potential energy or force of intermolecular interaction is the most time-consuming and crucial aspect of any molecular simulation. The potential reflects the spherically averaged effects of all orders of many-body interactions, despite being a pairwise

additive potential, hence the three-body and higher order interactions are accounted for despite the potential only being explicitly stated in terms of the two-body interactions. The potential functions of molecular systems can be divided into three categories:

- The non-bonded interactions are computed using a neighbour list, which is a list of non-bonded atoms within a certain radius from which exclusions have been removed. Lennard-Jones or Buckingham, and Coulomb or modified Coulomb are unbonded.
- Bonded: bond stretching, angel-bending, improper dihedrals, and property dihedrals. These are computed using predetermined lists.
- Restraints: position restraints, angle restraints, distance restraints, orientation re-strains and dihedral restraint

The energy expression is the equation that describes the surface of a model's potential energy as a function of its atomic coordinates. Potential energy of a system can be expressed as the sum of valence (or bond) interactions, cross-term interactions, and nonbonded interactions:

$$E_{total} = E_{valence} + E_{crossterm} + E_{non-bonded} \quad (3\text{-}5)$$

The diagonal terms are bond stretching (E_{bond}), valence angle bending (E_{angle}), dihedral angle torsion ($E_{torsion}$) and out-of-plane ($E_{electrostatic}$) terms:

And $U\ (r)$ is summation of different energies:

$$U\ (r) = E_{stretch} + E_{bond} + E_{torsion} + E_{inversion} + E_{cross-term} + E_{LJ} + E_{HB} \quad (3\text{-}6)$$

Bond Stretching refers to the energy required to cause a change in the bond length in relation to its equilibrium value. A harmonic potential, which does not allow the breaking of bonds, can be used to approximate the energy level that is close to being in equilibrium (Peerlman et al., 1991). Vibration spectroscopy is a method that can be used to ascertain the constant of the stretching force. The formula below refers;

$$E_{bond} = \frac{1}{2} K_b (b - b_0\ )^2 \quad (3\text{-}7)$$

Where E_{bond} represents the amount of energy that is stored in the system's covalent bonds, each bond has a spring harmonic that has a specific constant force K_b , an actual length bond b , and an equilibrium bond b_0 . These are the distinguishing features of each bond.

The angle bending energy, or E angle, is a measure that describes the amount of energy required to deform the bond angles in relation to their equilibrium value. It is possible to get a good approximation of the energy near equilibrium by using harmonic potential. The value of this force constant can be ascertained using vibration spectroscopic research.

$$E_{angle} = \frac{1}{2} K_{\theta} (\theta - \theta_0)^2 \tag{3.8}$$

where E_{angle} denotes the valence angle energy that is produced whenever the angle between two covalent bonds θ shifts from its starting position θ_0 while the angle force K_{θ} constant remains the same.

Torsion is a phenomenon that results from the interaction of space and time and is responsible for the rotation of covalent bonds. An approximation of this term is something that can be accomplished with the assistance of several geometric functions.

$$E_{torsion} = \frac{1}{2} K_{\emptyset} \Big(1 + cos(n\emptyset - \emptyset_{\emptyset})\Big) \tag{3.9}$$

Where $K_{\emptyset}$ represents the torsional barrier, $\emptyset$ represents the actual torsion angle, n represents the periodicity, and $\emptyset_{\emptyset}$ represents the reference torsional angle.

Calculating the non-bonded interactions that take place between all the atoms in the simulated system is the activity that consumes the most time and uses the most resources. This is because it must consider all the atoms' possible positions and orientations. When using a pairwise model, the number of interactions that are not bonded, such as Van der Waals and electrostatic interactions, is proportional to the square of the number of atoms in the system that is being simulated. This is the case even when using an extremely small number of atoms to perform the simulation.

This is the case for both types of interparticle exchanges. It is preferable to avoid computing all the possible pair interactions to avoid exerting such a large amount of computational effort, and this can be accomplished by avoiding the practice of computing all the possible pair interactions. The introduction of a cut-off distance is done in such a way that it makes it possible to disregard the interactions between any two atoms that are separated by a distance that is greater than the cut-off distance.

This concept was conceived because of the observation that the strength of the van der Waals interactions, which are described by a Lennard-Jones potential, (Allen, 2004) decreases significantly with increasing distance between two atoms. It is possible to ignore the interactions of any two atoms that are separated by a distance that is greater than the cut-off distance. This method, however, is not appropriate for calculating electrostatic interactions because those interactions do not decay strongly as such distances. By making use of a tried-and-true approximation technique, one can separate the short-range and long-range components of the electrostatic interactions that are taking place in this scenario.

In accordance with the initial Coulomb potential equation, a direct calculation is performed to determine the short-range component. While the long-range one can be estimated through various methods such as the Ewald approach (Ewald 1921).

van der Waals and electrostatic (Coulombic) terms are responsible for the energy that is transferred during interactions between atoms that are not bonded to one another.

$$E_{non-bonded} = E_{vdW} + E_Q \quad (3\text{-}10)$$

The non-bonded interactions of atoms in the simulated system are composed of the Lennard-Jones (LJ, the fourth term), and the Coulombic or electrostatic (the last term) potentials, which are described by the last two terms in Eq. (3-6).

E_{vdW} - provides a description of the dispersive interaction that takes place between atoms, or, to put it another way, the interatomic forces. This term can be approximately calculated by using the 9-6 potential, which can be envisioned of as a function of the distance between the centres of the two atoms or molecules that are interacting.

$$E_{vdW} = \sum \frac{A_{ij}}{r_{ij}^{12}} - \frac{B_{ij}}{r_{ij}^{6}} \quad (3\text{-}11)$$

Where A_{ij} and B_{ij} are the coefficients for the repulsive and attractive terms, respectively, and $r_{ij}$is the distance between the two atoms in the system.

Hydrogen Bond term E_{HB} – This term is used to describe the energy that exists between atoms that have the capability of forming hydrogen bonds. When a hydrogen atom that is bonded to

a strongly electronegative atom is in the vicinity of another electronegative atom that has a lone pair of electrons, a weak type of force known as a hydrogen bond is formed. This force gives rise to a unique kind of dipole-dipole attraction It is approximated by using the 12-6 potential, which is similar to the Lennard Jones Potential, but in this case, the attractive interaction between atoms fades away more quickly.

$$E_{HB} = \frac{1}{\varepsilon}\frac{q_1 q_2}{r_{ij}} \tag{3-12}$$

Where q_1 and q_2 are the charges on the atoms involved in the interaction, is the dielectric constant, and r_{ij} is the distance between the atoms in question.

Cross Terms The vast majority of interaction terms, which we have just investigated, do not generally exist independently in biomolecules but instead influence one another. The cross term refers to all interactions that influence others. Interaction types known as "cross terms" include "stretch-stretch," "stretch-bend," "bend-bend," "bend-torsion," and "stretch torsion."

3.6.1 Methods for Temperature Control in Dynamic Simulation

In dynamic simulation, there are four techniques for regulating the temperature. Constant atom number, temperature, pressure (NPT), constant atom number, energy, volume (NVE), constant atom number, pressure, enthalpy (NPH), and constant atom number, temperature, volume (NVT). The NVT ensemble is used to reach equilibrium structure under a given systemic density, while the NPT ensemble is used to obtain the correct system density. As for NVT and NPT ensembles, MD simulation is beneficial for obtaining thermodynamic variables as well.

3.6.1.1 Thermostat

By default, a constant-energy ensemble is sampled in MD by solving the classical equations of motion for every atom in the simulated system. To compare simulation results with experimental data, which are typically obtained at constant temperature, it is preferable to sample a constant-temperature ensemble. Moreover, temperature control can be advantageous for studying temperature-dependent processes, enhancing conformational sampling, and preventing energy drift due to the accumulation of numerical errors. The stochastic coupling method (Andersen et al. 1986), the weak-coupling method (Berendsen et al., 1984), and the extended system method Nosé-Hoover can all be used to conduct simulations at constant temperature.

The temperature is maintained in the Andersen thermostat by coupling randomly selected particles to the heat bath via stochastic forces. Upon a collision event, the selected particles are assigned new velocities chosen from a Maxwell-Boltzmann distribution at the desired temperature. Because stochastic collisions disturb particle dynamics in an unrealistic manner, this thermostat is unsuitable for studying dynamic properties. In MD simulations, Berendsen and Nosé-Hover thermostat methods are used more frequently. In the Berendsen thermostat, the temperature is maintained by adjusting the particle velocities at each time step so that the system relaxes toward the desired temperature at a rate based on the Berendsen method. Variation in temperature for each step of the Berendsen method is given by;

$$\lambda = \sqrt{1 + \frac{\Delta t}{\tau}\left(\frac{T}{T_1} - 1\right)} \tag{3-13}$$

Where Δt is the step time, τ is the characteristic relaxation time, T is the target temperature (K) and T_1 is the instantaneous temperature (K)

When using the direct velocity scaling method, the velocities of all the atoms are altered. Because of the shift in velocities, the temperature at the target can either rise or fall to correspond with the value of the instantaneous temperature. The velocities have been scaled down in a uniform manner as:

$$\left(\frac{v_o}{v}\right)^2 = \frac{T}{T_i} \tag{3-14}$$

In the Nosé-Hoover method, the friction term is added into Newton's equation of motion

$$\bar{a}_i = \frac{\bar{F}_i}{m_i}\,\zeta\,.\,\bar{v}_i \tag{3-15}$$

$$\frac{d\zeta}{dt} = \frac{1}{Q}\left[\sum_{i=1}^{N} m_i \bar{v}_i{}^2 - 3NK_B\,T\right] \tag{3-16}$$

The friction coefficient $\zeta\ (t)$ flacuates in time just roughly at zero. Q is user-defined constant Andersen Method the velocity of randomly selected particles superseded by predefined collision period. The predefined collision period which is proportional to $N^{\frac{2}{3}}$ was implemented by material studio. When N is the atom number.

3.6.1.2 Barostat

Similar to how temperature can be maintained by coupling the simulated system to an external temperature source, pressure can be maintained by coupling the system to an external "pressure bath." Several distinct algorithms, such as the Berendsen barostat (Berendsen et. al. 1984), the extended-ensemble Parrinello-Rahman barostat (Parrinello et al., 1980), are all viable options for controlling the pressure. The Berendsen and Parrinello-Rahman barostats are discussed in this section because both of those barostats were used in the simulations that were included in this thesis. The atomic coordinates and the simulation box vectors are rescaled at each step in the Berendsen algorithm to bring the pressure closer to the target value.

$$\frac{dP}{dt} = \frac{P_{target} - P_{current}}{\tau_p} \quad (3\text{-}17)$$

Where τ_p is the time constant for the pressure coupling.

The simulation box volume is scaled at each time step by a factor

$$\gamma = 1 - \beta \frac{\Delta t}{\tau_p} \left(P_{target} - P_{current}\right) \quad (3\text{-}18)$$

Where whereas the atomic coordinates and the box vectors are scale by $\gamma^{1/3}$, β is the isothermal compressibility. Generally, the value of β is unknown but the sufficient to have a rough estimate of it for example $\beta = 4{,}6x10^{-10}Pa^{-1}$ for water at $300\ K$ (similar to the value of other most liquids) because it does not affect the average pressure. The equation of motion is modified as

$$\frac{dr}{dt} = v - \beta \frac{P_{target} - P_{current}}{3\tau_p} r \quad (3.19)$$

Notably, the Berendsen barostat is highly effective at relaxing the system to the desired pressure, but it does not produce the exact NPT ensemble. Therefore, it should be used early on in a production simulation to achieve the desired pressure. Therefore, it should be used early on in a production simulation to achieve the desired pressure.

Based on the Andersen barostat in which the system is coupled to the volume of the simulation box to simulate the action of a piston, the Parrinello-Rahman method was developed. The box vectors in this barostat are represented by the $3\ x\ 3$ matrix $H = \{h_1, h_2, h_3\}$,

where h_1, h_2, h_3 are the box's sides. The formula for calculating the volume of the box is $V = h_1 \, x \, h_2 \, x \, h_3$. The atomic coordinates are scaled according to the following equation in terms of a scaled variable, S , whose components (s_a, s_b, s_c) range from 0 to 1:

$$r = Hs = s_a h_1 + s_b h_2 + s_c h_3 \tag{3-20}$$

The equations of motion related to the scaled variable and the matrix H are obtained as:

$$\frac{d^2 s}{dt} = \frac{H^{-1} F}{m} - G^{-1} \frac{dG}{dt} \frac{ds}{dt} \tag{3-21}$$

Where $G = H^T H$

$$\frac{d^2 H}{dt} = V W^{-1} (H^{-1}) \left(P_{target} - P_{current} \right) \tag{3-22}$$

Where W^{-1} is a matrix parameter determining the coupling strength and its inverse is defined as:

$$W^{-1} = \frac{4\pi^2}{3} \frac{\beta}{\tau_P^2} \tag{3-23}$$

β isothermal compressibility, τ_p the time constant for the pressure coupling, L the largest box matrix element.

Chapter 4

4 Experimental Apparatus and Procedure

This chapter provides a description of each individual piece of apparatus that was used during this investigation. The gathering of precise experimental data on the gas hydrate equilibrium state is a crucial step in the process of designing a process that relies on hydrates. In addition, such information is necessary for the development and verification of predictive thermodynamic models. Reliable apparatus and an experimental method that is both precise and capable of being replicated are required to generate accurate data regarding the hydrate equilibrium. Accurate data cannot be generated without these two components. The static non-visual isochoric method, which is extensively discussed in Chapter 4, is a more reliable procedure with a higher level of accuracy than the isobaric and isothermal methods, which are based on visual observation to detect the gas hydrate formation and dissociation conditions. Isobaric and isothermal methods are used to detect the conditions under which gas hydrates form and dissociate. These methods were discussed in greater depth in Chapter 2,

The results of this investigation into the equilibrium of gas hydrates were obtained by employing a technique known as isochoric pressure search method as well as a static high-pressure equilibrium apparatus. The non-visual apparatus and the technique adopted here have several benefits when compared to the techniques described in the literature and discussed in Chapter 2. These benefits include a higher level of accuracy, stronger agitation, and an automated process. In addition to this, the fact that measurements can be carried out over the course of an entire night and that non-corrosive solutions such as deep eutectic solvent aqueous solutions can be used are both advantages in their own rights.

The apparatus for the experiment consists primarily of a high-pressure equilibrium cell that is housed within a temperature-controlled bath. A number of additional pieces of equipment, such as an agitator, a temperature probe, a pressure transducer, a vacuum pump, and a data acquisition system, are also utilized by this apparatus. The accuracy of these measuring devices as well as the constraints placed on their application are going to be covered in this chapter. In addition, particulars pertaining to the components, purities, and providers of the chemicals that were used are outlined in this section. Before beginning the experimental measurements that are going to be explained in the sections that follow, temperature and pressure calibrations, as well as a leak test, are going to be performed. These tests are going to be performed before

beginning the experimental measurements. This is done in order to obtain data that is as accurate as possible.

4.1 Chemicals

4.1.1 DESs

The salts and their formulas used in this study are presented in Table 4-1while the HBDs and their formulas are presented in Table 4-2

Table 4-1: Salts and their formulas used in this study

Chemical	Formula
Tetramethylammonium chloride	$C_4H_{12}NCl$
Tetrapropylammonium bromide	$C_{16}H_{36}BrN$

Table 4-2: HBDs and their formulas used in this study

Chemical	Formula
Glycerol	$C_3H_8O_3$
Ethylene glycol	$C_2H_{14}O_2$

The aforementioned chemicals were chosen because not only were they readily available but were also utilized in the research that was carried out by Nkosi et al.(2018). Sigma-Aldrich Chemicals was the company that provided the chemicals (New Germany, South Africa) at a minimum of 98 % purity.

4.1.2 The procedure for DES synthesis

The HBD compound and the ammonium salts were mixed with magnetic stirrer bar at temperatures ranging from $353\ to\ 393\ Kelvin$. The mixing ratio were as follows:

- DES-1 ($C_{12}H_{28}NBr + C_3H_8O$) 1: 2
- DES-2 ($C_4H_{12}NCl + C_3H_8O$) 1,001: 2
- DES-3 ($C_4H_{12}NCl + C_2H_6O_2$) 1,004: 2

The mixture was mixed until it was uniform in appearance and completely clear. To ensure the dependability and accuracy of the DES synthesis, the mixing could be extended for a period between four to eight hours until it forms a mixture that is perfectly homogenous.

Before being used, the DESs were put through an eight-hour heating process in an oven set at 373.15 K for the purpose of removing any moisture that may have been present.

4.1.3 Experimental apparatus

A newly developed high-pressure equilibrium cell, commissioned in this study, was used for the experimental hydrate measurements. The schematic diagram of the apparatus is presented in Figure 4-1 and a picture of the experimental setup is also shown in Figure 4-2

The experimental setup consisted of:

- A stainless-steel equilibrium cell (approximately $100\ cm^3$)
- Magnetic stirrer
- a liquid temperature bath ($500\ mm\ x\ 500\ mm\ x\ 380\ mm$)
- a programmable temperature controller
- two Pt100 temperature sensors
- a WIKA pressure sensor
- a 34972A LXI Agilent data acquisition unit
- temperature programmable circulator
- one Polyscience IP-35 cold finger
- vacuum pump

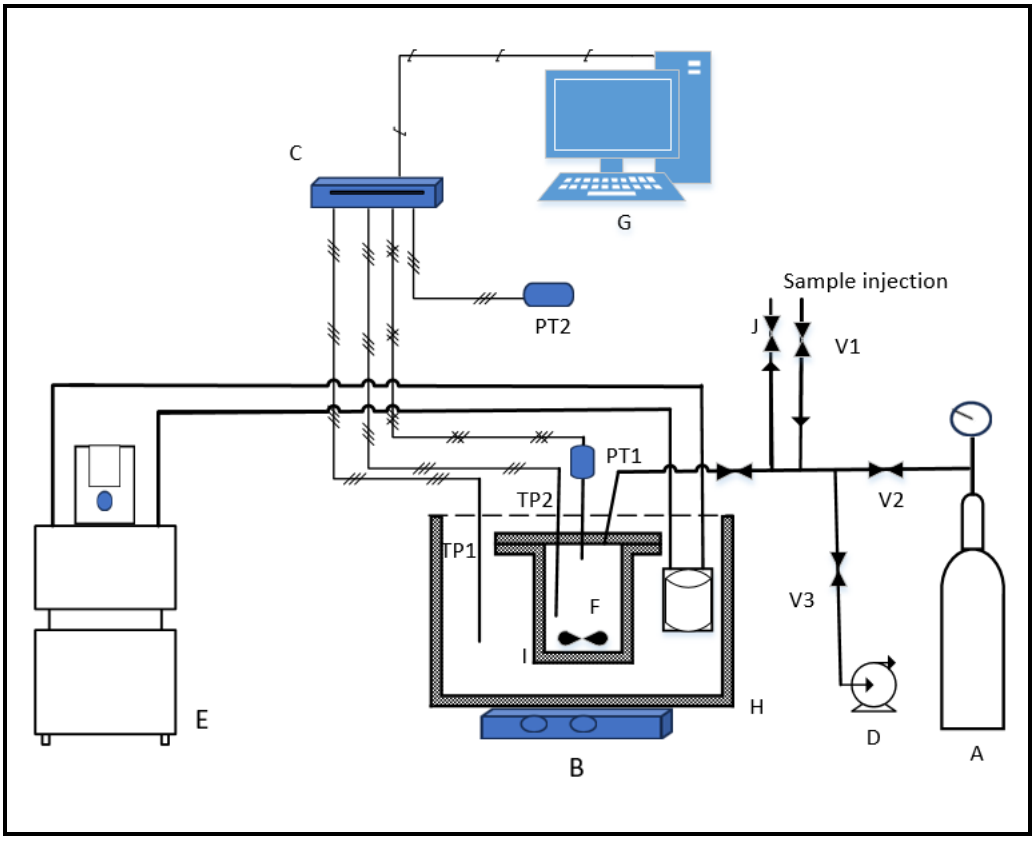

Figure 4-1: Schematic diagram for the high-pressure equilibrium apparatus: (A) gas cylinder; (B) magnet stir; (C) data acquisition system; (D) vacuum pump; (E,) LTC4 unit with built-in circulating bath; (F) neodymium magnet stir bar; (G) computer; (H) thermostated bath; (I) high-pressure equilibrium cell; (TP1, TP2) temperature probes (Pt-100); (J) relief valve; (V1−3) shut-off valves; (PT1,2) pressure transducers.

Figure 4-2: Photograph of the experimental setup.

4.1.3.1 The Equilibrium Cell

The equilibrium cell is made of 316 stainless steel because of its remarkable properties, which include mechanical strength and corrosion resistance; the cell has a volume of 100 cm^3 with an inner diameter of 52 mm, an outer diameter of 60 mm, and a height of 125 mm. The equilibrium cell has a volume of 100 $cm^3$and can withstand pressures of up to 100 bar. Four 14$inch$ diameter openings at the top of the cell serve as tubing for the pressure transducer, while the second opening serves as the cell's feed. Temperature sensors were installed in the third port (Pt-100s). The final opening served as the pressure relief line. Figure 4-3 is a diagrammatic representation of a cell, and Figure 4-4 is a photograph of the equilibrium cell used in this study. All equipment lines were fitted with Swagelok valves, as these valves withstand a pressure and temperature combination of 423,15 K and 10 MPa. Figure 4-5 depicts a top view of an equilibrium cell with an internal magnetic stirrer and a side view of the equilibrium cell with threaded grooves for closing the cell. Inserting an O-ring into the flange's groove aids in sealing the flange to the cell body. The images in Figure 4-6 depict the cell body and the top flange.

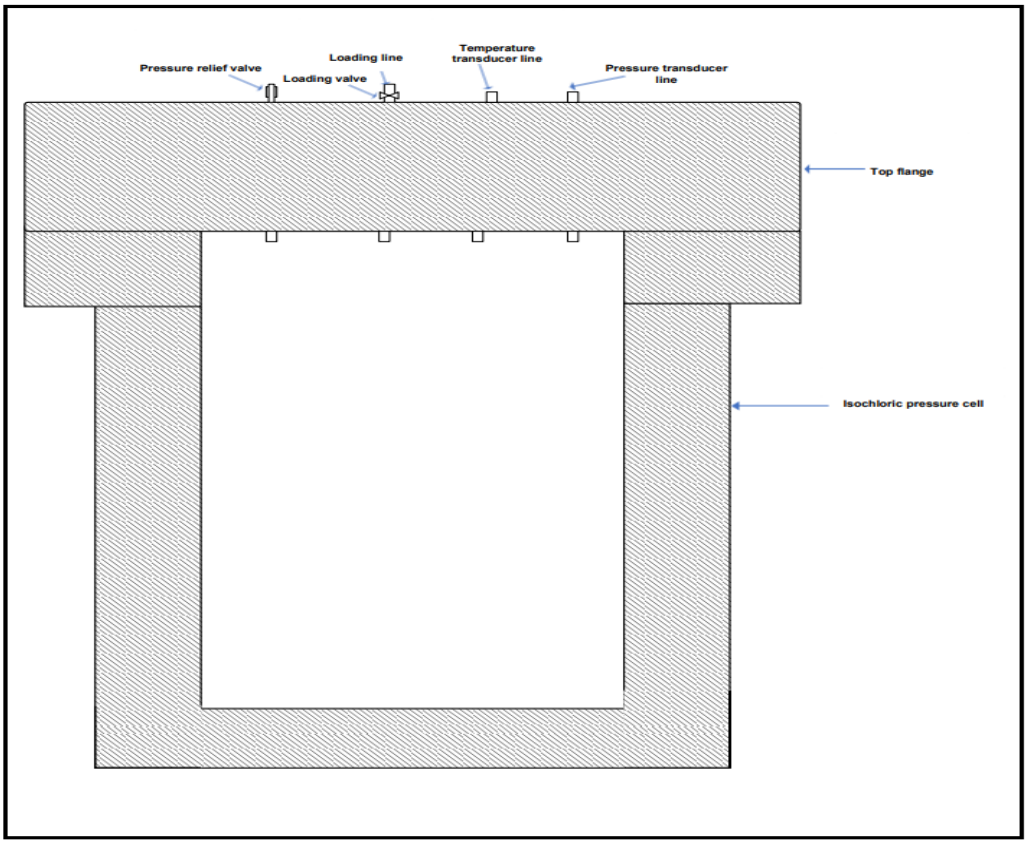

Figure 4-3: Schematic diagram of the equilibrium cell used in this study.

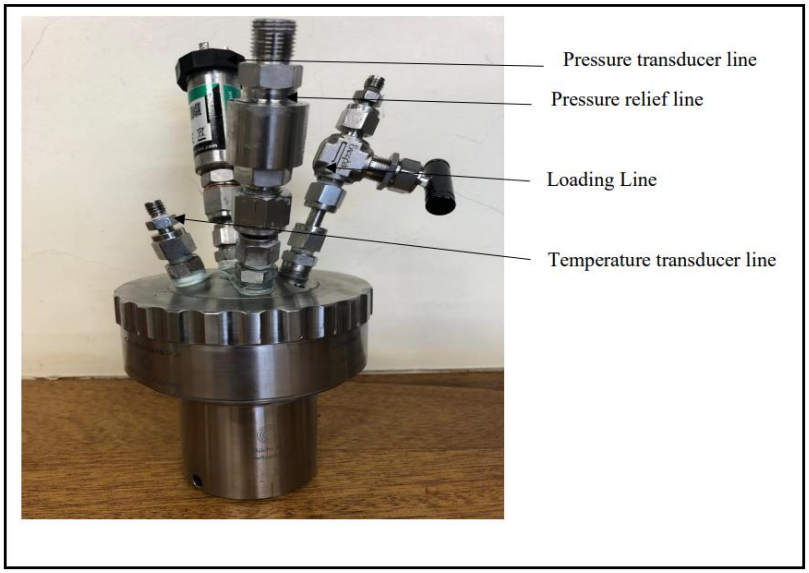

Figure 4-4: Photograph of equilibrium cell used in this study

Figure 4-5: The top view of the equilibrium cell with magnetic stirrer inside, the picture on sideview of the cell.

Figure 4-6: The top flange of the cell

4.1.3.2 Agitating device

Because the rate of gas hydrate formation is significantly increased by agitation of the system, a magnetic stirrer bar was used in this experiment. Within the cell, complete agitation of the phases is achieved at a speed of $600\ revolutions\ per\ minute\ (rpm)$. Mixing reduces time for gas hydrate formation/ dissociation.

4.1.3.3 The enclosure for the equilibrium cell

Figure 4-3 depicts the cell housing that was made from a Polystyrene foam, and the dimensions of the bath were 43 cm x 35 cm x 26 cm . Within the housing of the cell, water and glycerol were recirculated, and a programmable controller was used to maintain a temperature that was accurate to within $0.05\ K$. This study made use of a bath fluid that was a mixture of water and glycerol at a weight-percentage ratio of 50/50. This bath fluid is suitable for use in temperature ranges ranging from 228 to 397 K. The cell is submerged in the bath to prevent the heat from the surrounding environment from being transferred into the cell. To prevent heat loss or gain from the surrounding environment, the top surface of the water bath has polystyrene foam applied to it.

4.1.3.4 Liquid bath

The use of the liquid bath was necessary to guarantee that the temperature was kept constant. The height of the bath was 500 mm and its length and width both measured 500 mm each. In this study, the glycerol and water solution that made up the bath fluid were combined at a weight-to-weight ratio of $50/50$. The solution was pumped from the chiller into the equilibrium cell housing, where it was used to cool the cell.

4.1.3.5 Temperature controller

To bring the temperature of the bath up to the level that was desired using the model (Grant OptimaTM TX 150) programmable controller, a programmable low-temperature circulator, and an internal thermocouple were utilized. The temperature range that the controller can accommodate is between 243.15 and 323.15 K. This apparatus comes equipped with both an immersion circulator pump as well as an internal temperature probe. The temperature bath was able to keep the contents of the equilibrium cell at a constant temperature by either heating or cooling the mixture of glycerol and water that was contained within the temperature bath. This meant that the temperature bath kept the contents of the equilibrium cell at the same temperature.

During the process of hydrate formation and dissociation, the Squirrel View software was used to provide step-by-step heating and cooling programs as well as specific rates of heating and cooling.

4.1.3.6 Pressure controller

For measuring the cell pressure, a Wika pressure transducer was utilized. The accuracy of the pressure transducer was within a margin of error of $0{,}05\ percent$. A stable temperature was always preserved within the transducer. To get an accurate reading of the pressure inside the cell, a pressure transducer was attached to it. Using the 34972A LXI Agilent data acquisition system, the pressure and the time were both monitored, and the data was logged every two minutes.

4.1.3.7 Data acquisition system

During the experiment, a data acquisition unit was wired up to a computer to keep track of the pressure, temperature, and passage of time. Using Squirrel View, the readings were continuously logged at intervals of 2 seconds for a predetermined amount of time. Every bit

of data from the log was copied over to the computer and kept there. The data was exported to a spreadsheet in Microsoft Excel after the data acquisition unit had finished logging the data for the specified settings. This was done so that the data could be further analysed. To determine the hydrate dissociation point, the pressure values were plotted against temperature data.

4.1.4 The preparation of the isochoric cell

Preparing the apparatus for hydrate measurements is necessary to ensure the production of precise and trustworthy experimental results. The following tasks made up the preparation: cleaning the equilibrium cell and the adjourning lines; calibrating the temperature and pressure sensors; and ensuring that there are no leaks in the adjourning lines.

4.1.4.1 The process of isochoric cell cleaning

Before beginning any experimental measurements, the equilibrium cell was thoroughly cleaned. This was done with the goal of minimizing the risk of any cell contents becoming contaminated. At first, there was fifty millilitres of pure methanol loaded into the cell. The methanol was then allowed to agitate inside the cell at a speed of $600\ rpm$ for one hour to absorb any contaminant that might have been present on the cell wall. After that, the methanol was removed from the cell by draining it. The cell was then cleaned with acetone on two separate occasions. After the acetone had been drained from the cell, helium was utilized to flush any traces of acetone that may have been left behind. This was done to make sure that the cell was tidy and devoid of any moisture. After that, an Edwards vacuum pump was utilized to evacuate the cell to a pressure of $0.0002\ kPa$ for a period of thirty minutes. This was done to remove any air or other volatile matter that may have been present in the cell. Following the conclusion of this cleaning procedure, the cell was ready to undergo leak testing.

Since all the systems only contained deep eutectic solvent, ultrapure water, and the carbon dioxide gas, the procedure for cleaning the cell in between experiments needed to be less intensive. At the beginning of the process, the cell was emptied, and the top flange was taken off. After loading the cell with $50\ ml$ of ultrapure water, the contents of the cell were allowed to agitate for a period of five minutes. The agitation device and the stirring mechanism were both removed from the cell, and the water was drained out of the cell. The magnetic stirrer, the top flange, and the O-ring were all dried after being cleaned with water. In addition to this, the cell was disinfected with alcohol and allowed to dry before the O-ring and the top flange were reattached. The space was subsequently purged to a pressure of $0.0002\ kPa$ for a period of

five minutes. The chamber was then washed out with carbon dioxide gas three times. Before moving on to the next system of interest, this procedure in its entirety was repeated.

4.1.4.2 Leak test

Testing for leaks was done on the equilibrium cell to cut down on the number of errors that could have been brought on by a drop in pressure. In addition to being performed prior to hydrate measurements and calibrations, leak testing was also conducted after a line was disconnected or a fitting was replaced. During the first phase of the leak test, the cell was pressurized to a level equivalent to 10 MPa with helium, and the inlet valve leading into the cell was closed. SNOOPY was used to treat all the fittings and the surrounding area of the cell. The presence of bubbles in that fitting allowed for the location of the leak to be determined. When it was discovered that there was a leak, every fitting was either retightened or replaced. After that, the equilibrium cell was put into the liquid bath and left there for a while. To eliminate fluctuations in temperature and pressure, the temperature of the bath was maintained at a steady 298.15 K throughout the experiment. The experimental set-up was left at these conditions (10.0 MPa and 298.15 K) for the full 24 hours that the experiment lasted. This was done to ensure that there was no significant loss of pressure during the experiment. After ensuring that there were no leaks remaining, the calibrations were carried out.

4.1.5 Calibration of measuring devices

Evaluation of the precision of various measuring instruments is a crucial component of the calibration procedure. To generate trustworthy equilibrium data, it is essential to recalibrate the measuring instruments. This is done by comparing the temperature probes and pressure transducers to the reference instruments to get the level of accuracy that is needed.

4.1.5.1 Calibration of temperature probes

The accuracy of the two platinum pt-100s temperature probes were determined to be within 0.03 ^{o}C when compared to the WIKA CTH6500. The temperature probes and the reference temperature were both submerged in an oil bath made of temperature-controlling silicon. This was done to account for any hysteretic behaviour that might have occurred during the calibration process. The temperature of the bath was increased and decreased at constant intervals from 252,9 to 323,08 K. On the digital display, both the standard temperature and the actual temperature were displayed. After allowing the temperature readings to become stable, all the readings were recorded within 10 seconds of one another over the course of 5 minutes.

Calculations and records were made of the average values obtained from each measuring device. When plotted against the standard temperature values displayed by the two Pt-100 temperature probes, the reference probe's standard temperature values were examined. Using least squares regression, the calibration data were constrained to fit along a straight line. The results of the readings taken by the standard temperature probe plotted against the temperatures that were recorded. Figure 4-7 is an illustration of the calibration of the temperature probe (TP1), and Figure 4-8 is a representation of the deviation from the standard temperature.

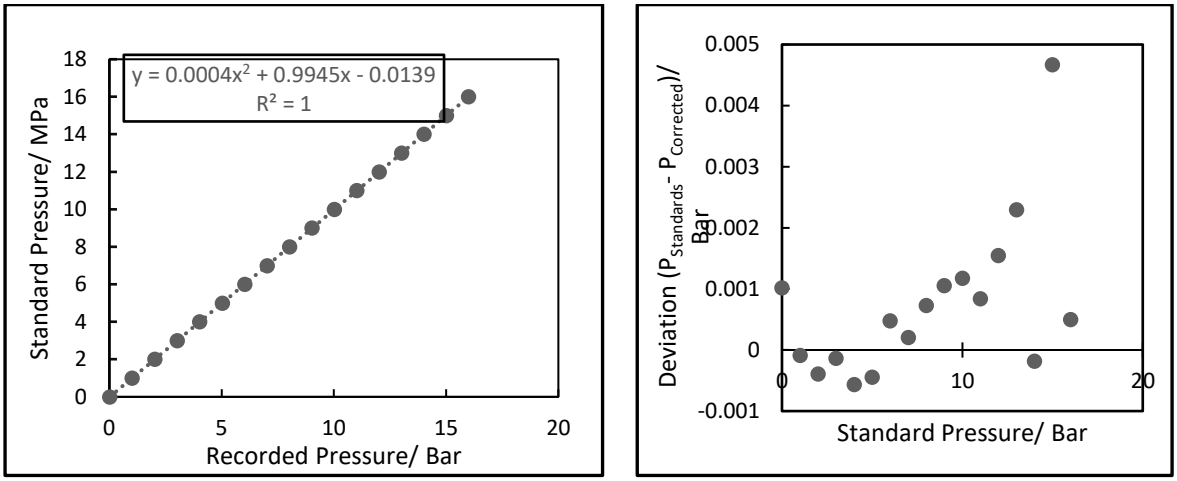

Figure 4-7: Calibration of temperature probe (TP1) and on the right is the deviation from the standard pressure

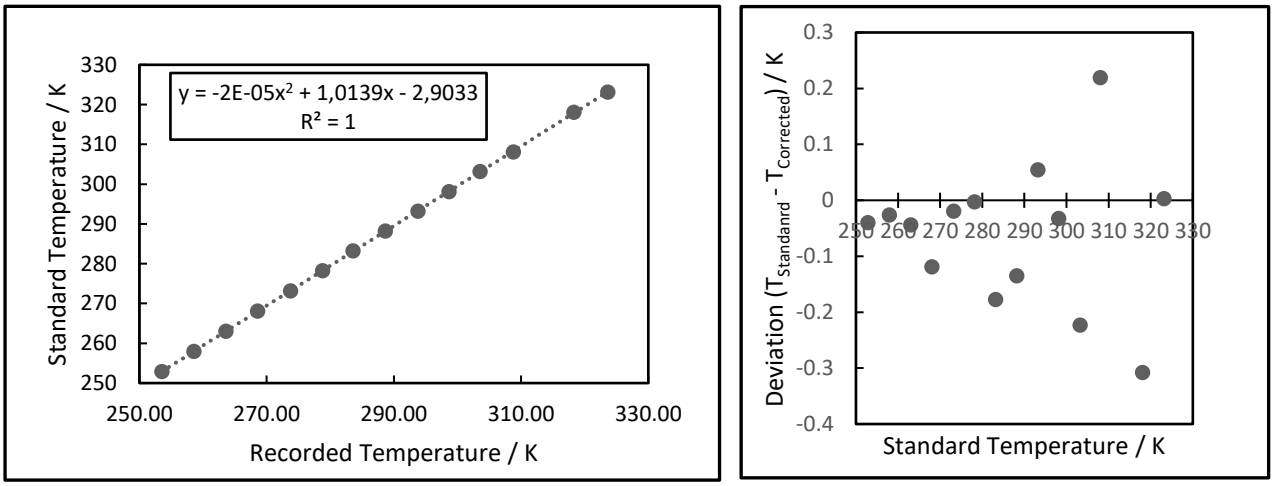

Figure 4-8: Calibration of temperature probe (TP2) and at the right is the deviation from the standard temperature.

4.1.5.2 Calibration of pressure probes

To calibrate the pressure transducers $(0\ to\ 50\ MPa\ and\ 0\ to\ 16\ MPa)$, a WIKA-supplied standard pressure transducer, model CPT 6000, was used. The standard pressure transduceris designed to operate effectively over a pressure range of 0 to 250 MPa. Both transducers were wired and connected to the equilibrium cell so that an accurate pressure reading could be obtained. The cell was pressurized with helium gas to the desired pressure, from low to high values and vice versa. This procedure was repeated multiple times for each pressure reading to identify hysteresis. On the digital display, both the standard pressure and the recorded pressure were simultaneously displayed. After allowing the pressure readings to stabilize, they were recorded within ten seconds of one another for five minutes. The average values obtained from each measuring instrument were calculated and recorded. Figure 4-9 depicts the relationship between a standard pressure transducer and a recorded pressure transducer as a second-order relationship. Figure 4-10 depicts the deviation between the standard pressure transducer and the recorded pressure transducer.

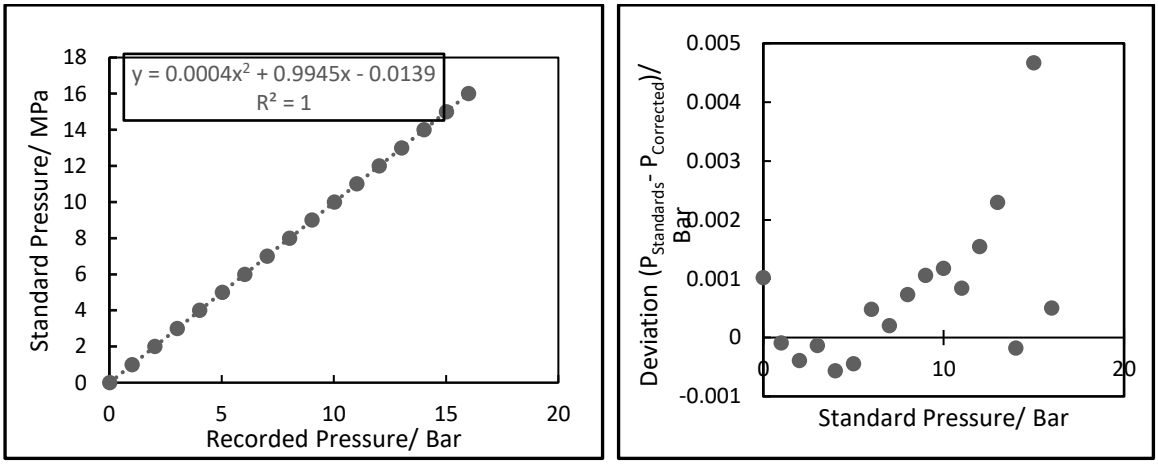

Figure 4-9: Calibration of pressure transducer (PP1) and on the right is the deviation from the standard pressure.

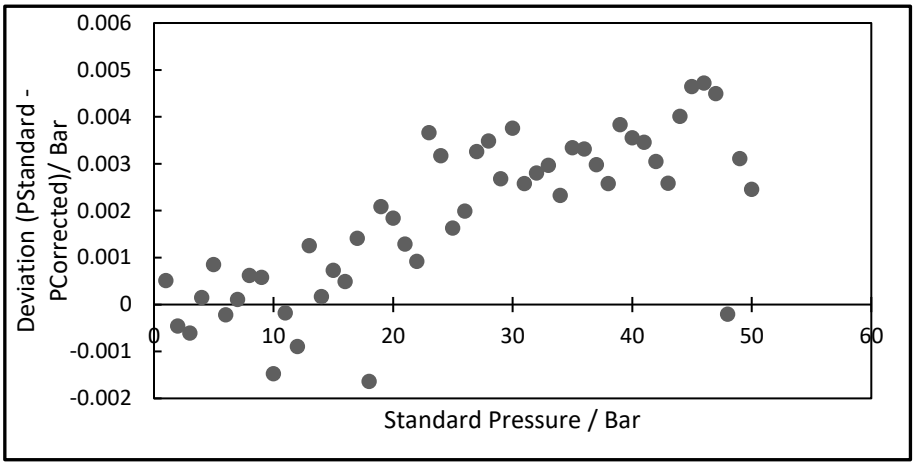

Figure 4-10: Calibration of the pressure transducer (PP2) and at the bottom is the deviation from the standard pressure.

4.2 Experimental procedure

4.2.1 Sample preparation

To obtain the desired weight percent, the aqueous solution was prepared in a beaker with a capacity of $50\ ml$ using an Rawag AS 220/C/2 digital mass balance. The uncertainty on the full scale of the mass balance was equal to or less than 0.0001 g. Before any measurements were conducted, the necessary quantities of deep eutectic and ultrapure water for each desired composition were calculated and determined. The mass of the emptied beaker was measured as well as the mass of the deep eutectic solvent. After that, using a syringe, the necessary quantity of water was added slowly to obtain the desired amount of total solution mass.

4.2.2 Hydrate dissociation point measurements

The dissociation points of hydrates were measured using the isochoric pressure search method, determined by measuring temperature and pressure. There is no need for visual observations or calculations, allowing for the accurate determination of hydrate equilibrium data. This experimental technique is also applicable across the entire temperature and pressure range necessary for hydrate formation. No volume adjustments are necessary. In addition, this method is suitable for automated experiment control (Smith, 2015). Compared to the isobaric and isothermal approaches, the isochoric method is deemed superior for investigating the phase behaviour of multicomponent systems. In this study, therefore, the isochoric method was combined with stepwise heating and effective mixing.

The first step of the experiment was the flushing the equilibrium cell with ultrapure water to eliminate any contamination that might already be there. After the cell had been thoroughly cleaned, the vacuum pump was utilized to evacuate all the air within the cell for a period of approximately half an hour. This step was taken to ensure that the cell did not contain any air, which would have had the potential to alter the composition of the solution that was going to be used in the experiment. To keep the cell in a vacuum state, the inlet valve of the cell was sealed off. After the aqueous solution had been prepared, 30 ml of it was poured into the cell. During the process of loading ultrapure water, the vacuum pump was reconnected to the cell to remove any air that could have gotten into the cell during the loading process. The cell was then cooled by being submerged in glycerol water solution. When the temperature was stable, the inlet valve on the carbon dioxide cylinder was opened so that the cell could be pressurized with the hydrate former (carbon dioxide) to the desired amount of pressure.

The magnetic stirrer was turned on and its speed was set to $500\ revolutions\ per\ minute$ (rpm). After the pressure in the system had stabilized and all the gas had been used up in the water, the temperature-controlled bath was brought to a level that was 263 K lower than the temperature at which hydrates dissociate. To facilitate the formation of the hydrate, the temperature was brought down gradually. During the process of cooling, a gradual decrease was observed, followed by an abrupt decrease in pressure caused by the encapsulation of the hydrate former. Once the hydrate has been formed in its entirety, the pressure and temperature will no longer continue to drop. To dissociate the hydrate, the system was heated at a slow rate, and the result was that the gas was released into the vapour space. As a result of the hydrate being broken apart, there was a rise in pressure within the system.

The point of dissociation was determined to be the point where the cooling curve and the hydrate dissociation curve intersected.

4.2.3 Shutdown procedure

After completing the hydrate measurements on each of the aqueous systems, the data logger was stopped and shutdown. The programmable temperature controller, the chiller unit, and the mechanical stirrer both had their switches turned off. After that, the level of the liquid bath was brought down, and the drain valve was opened to empty the cell. After that, the cleaning procedure described in section 4.4.2 was conducted in its entirety before moving on to the subsequent set of measurements.

4.3 Simulation Method

Molecular dynamics (MD) is a computer simulation method that is used in a variety of engineering and scientific fields to calculate the motion and equilibrium of each individual atom or molecule. MD simulations have become a powerful and widely used tool in recent years. It is helpful in acquiring knowledge concerning the structural and dynamical properties at the molecular level for a wide variety of systems, ranging from gas mixtures to straightforward liquids, and a useful tool for carrying out analyses and characterizations of systems subjected to varying levels of pressure as well as high and low temperatures. According to Kondori et al (2019) research, the only properties that are necessary to run simulations are intermolecular and atomic properties.

In this study, the building was done using Material Studio by Accelrys Inc. from San Diego, California. Carbon dioxide hydrates were thought to exist in either the absence of or presence of a deep eutectic solvent, depending on the system to produce the slab carbon dioxide hydrate. The procedures for MD simulation consisted of four primary steps, which are the sketching of the molecules that were involved, the creation of the simulation box, the simulation of the equilibrium and production phases, and finally the analysis of the trajectory output. The COMPASS, Ewald, and atom-based summation methods were used for the electrostatic interaction and the Van der Waals interaction, respectively. The MD simulations are conducted by making use of the Forcite modules. A periodic simulation system was established using

The Materials Studio software (Biovia, 2019) to investigate the stability of carbon dioxide gas hydrates. This was accomplished through geometric optimization and the minimization of energy consumption. Through the work that is being done now, new insights into the effects of factors like temperature, pressure, and inhibitors like deep eutectic solvents will be provided (tetramethylammonium chloride and glycerol; Tetrapropylammonium bromide and glycerol; and tetramethylammonium chloride and ethylene glycol). The first thing that needed to be done was to make a rough sketch of the molecules that contained all the atoms that were going to be used in this investigation.

The system's geometry was optimised using the forcite geometry optimisation. This calculation with Forcite makes it possible to conduct analyses of both straightforward properties like density variations and more complex properties like the dipole autocorrelation functional. The module containing the intelligent algorithm was chosen for the energy reduction process. Smart is a cascade as follows: the steepest descent, a quasi-Newton algorithm, and an adjusted basis set Newton-Raphson model were used. It used these methods in a cascading manner (Bovia, 2019). The convergence was adjusted to an extremely acceptable level, and the maximum number of iterations that could be performed was set to 2000. The goal of the minimization step was to reduce the amount of energy required to maintain the structure within the amorphous box. Additionally, this step was intended to correct the unrefined molecular structure which may have contained distorted bond angles and lengths as well as steric clashes between atoms.

After performing geometric optimization and energy minimization, there is still a possibility that the system's molecules will not reach a state of equilibrium. This is because the number of molecules involved in the association system is relatively low. Because of this, the energy and temperature of various associative systems are analysed to demonstrate that the motion of the molecules in the system eventually reaches a state of equilibrium. As a result, a simulation box was developed. The creation of the simulation box required two steps, namely the creation of the box and energy minimization.

A three-dimensional (3D) atomisation of the original structure was created using Material Studio. A 3D molecule structure was used in this simulation since it contains molecular mobility, which is necessary in MD modeling. Each molecule underwent geometry optimization to ensure molecular geometry stability for use in later simulation operations. The structure needed to be precise and close to the actual structure. X-ray single diffraction measurements can typically be used to determine the position of oxygen atoms in a gas hydrate structure (Kirchner et al., 2004). The Bernal-Fowler rule restricts how the hydrogen atoms in water molecules can be arranged (Bernal et al., 1933). This rule determines how the hydrogen atoms in water molecules are arranged. To guarantee the consistency of the molecular geometry that would be used in subsequent simulation steps, an optimization step for the geometry was performed on each of the molecules.

In the optimization procedure, forcite computing is used. Because Forcite computing is capable of performing dynamics simulations, energy optimization, and geometry optimization, it was used in this simulation. The unit cell of hydrate structure I was extended to form $3\,x\,3\,x\,3$ Supercell. The cells were built as cubic periodic cells with densities similar to the expected density under ambient circumstances using standard techniques included in the Amorphous Cell modelling package material studio. It was possible to get around the surface effect by using the cubic periodic boundary condition. The number of molecules that were put into the simulation determined how big the box was that it was played in.

Because the dimensions of the box and its fluctuations will be observed as the simulation is run, it is important that the simulation box size be selected appropriately. After the simulation box had been created, this model was run through a simulation to determine how to minimize the box's energy consumption.

For the energy minimization step, the Smart Minimize algorithm was chosen, and the convergence was adjusted to an ultrafine level while the maximum iteration was increased to $10{,}000$. The quality level is what determines the convergence thresholds between optimization cycles for things like maximum force, maximum stress, and maximum displacement. In addition, which of these criteria are evaluated is determined by the quality level. When all the thresholds that were specified are reached, the optimization process will end.

The goal of the minimization step was to reduce the amount of energy required to maintain the structure within the amorphous box. Additionally, this step was intended to correct the unrefined molecular structure, which may have contained distorted bond angles and lengths as well as steric clashes between atoms. Five simulations of the amorphous cell were run, and the frame were sampled every 1000 steps.

The following stage is the simulation of the equilibrium phase, which is done while maintaining a constant NVT (number of molecules, volume, and total temperature) ensemble. The simulation was run at a speed of $1000\ ps$ and the initial velocities were chosen at random for the purpose of the velocity initialization. This aided to relax the initial configurations. This gave the velocities values at random, based on a Gaussian distribution that was temperature dependent (Bovia, 2019). The number of time steps that were taken between each dynamic step was one fs, which is an extremely short amount of time and represents the bond stretching motion that occurs during C-H bond vibration (Jean, 2015). The equilibration step's primary objective was to establish that the system configuration had reached a stable state in terms of its overall energy. The following equation can be used to express the difference in temperature that occurs between each step of the Berendsen method (Berendsen et al, 1984).

$$\lambda = \sqrt{1 + \frac{\Delta t}{\tau_T}\left(\frac{T_0}{T} - 1\right)} \tag{4-1}$$

where T_0 refers to the bath temperature (target temperature in K); T stands for the instantaneous temperature (K); and τ_T and Δt represet a characteristic relaxation time and time step (ps), respectively. During the NPT simulations, the molecules in the system (the surface of the hydrate) were given the flexibility to move.

The use of NPT is required to adjust both the pressure and the temperature. Changing the volume of the system is how the pressure in the system is kept at the desired level. By adjusting the volume, the pressure that is exerted on the system can be controlled by the vectors of the simulation box as well as the positions of the particles. This technique is only utilized when dealing with periodic systems.

In the Berendsen method, the only thing that can change is the size of the simulation box; the shape is fixed. In the NPT method, the compressibility of the system (λ) and the relation time (τ_T) are both factored into the calculation of the scaling factor (). This is one of the advantages of using the NPT method. The following scaling factor (μ) is applied to each particle's x, y, and z coordinates before each step of the simulation so that they can be brought into proper proportion.

$$\mu = \left[1 + \frac{\Delta t}{\tau_P}\lambda(P_0 - P)\right]^{\frac{1}{3}} \quad (4\text{-}2)$$

P and P_0 resembes the target and instantaneous pressures, respectively. The units of compressibility and pressure are Pa^{-1} and Pa, respectively.

Initial simulations were run at $1000\ ps$ using the smart minimising method to minimize energy. This was done to reduce thermal noise in the structure and potential energy, which could cause the simulation to crash if molecules didn't touch well enough. The $5000\ ps$ production run was the second step. The molecular dynamic simulation of general equilibrium is made up of two parts. In the first part, simulation is used to let the system settle down and reach equilibrium. After that, a production run begins, and the data from that run is collected. Long-distance columbic and Van der Waals forces are computed using the Ewald summation method. The temperature was controlled by a Berendsen thermostat that was set to $0.2\ ps$ for the decay constant. A Berendsen barostat with a decay constant of $0.1\ ps$ was used to control the pressure (Berendsen et al, 1987). the trajectory output analysis was done on the sample structures. Figure 4-11 illustrate the stages involved in the molecular dynamic simulation of the dissociation of CO_2 gas hydrates.

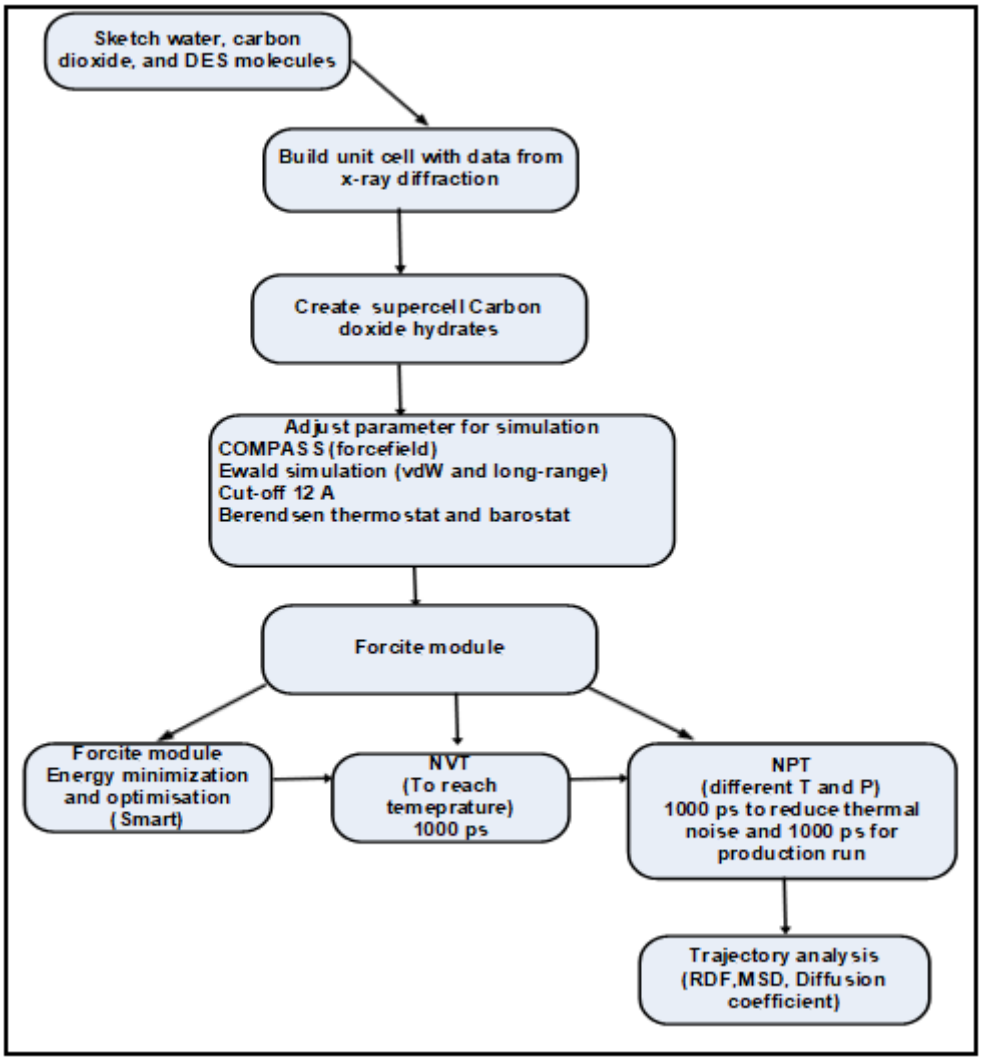

Figure 4-12: The stages involved in the molecular dynamic simulation of the dissociation of CO_2 gas hydrates.

Chapter 5

5 Results and Discussion

This purpose of this chapter is to present the key findings from the research conducted for this study. The outcomes are divided into two categories: experimental measurements and thermodynamic simulations. This study's primary objective was to examine the effect of an aqueous deep eutectic solvent as an inhibitor on hydrate phase equilibria. In the experimental measurement section, experimental hydrate dissociation data are reported for

- CO_2 + H_2O aqueous TPABr + glycerol solution,
- CO_2 + H_2O aqueous TMACl + glycerol solution, and
- CO_2 + H_2O aqueous TMACl + ethylene glycol solution.

In the section on thermodynamic simulation, measured hydrate phase equilibria for the system CO_2 + H_2O + DES solution was regressed using the methods described in Chapter 4.

5.1 Chemical used in this study

To compare the results with the data that was already available in the literature, it was necessary to measure the density of the investigated deep eutectic solvents. Densities were measured to evaluate the level of their purity. Table 5-1 provides an overview of the characteristics of DESs that were investigated for this study.

Table 5-1: Solvents and Densities used in this study.

Solvents	Densities (g/cm^3)
DES-1	1,098
DES-2	1,1632
DES-3	1,07219

Densities measured at $298K$

When determining the density of DESs, and Anton Paar density and sound velocity meter, model DSA 500M, was utilized. This model had an error of $0{,}0001\ g/cm^3$ when measuring density. The calibration of the apparatus was checked by determining the density of ultra-pure water. To assess how well the method worked, the sample was injected at least twice using the same procedure.

5.2 Experimental measurements of gas hydrate dissociation conditions

This study used the isochoric pressure search method at pressure and temperature ranges of $(1{,}9294 - 4{,}2538)\ MPa$ and $(276{,}9150 - 283{,}4638)\ K$ to obtain the clathrate hydrate dissociation pressure as a function of temperature for various deep eutectic solvents. The hydrates phase equilibria that were measured during this study are summarized in table 5-2.

Table 5-2: Hydrate phase equilibria measured in this study.

System	Temperature, K	Pressure, MPa	Concentration of the Inhibitor
$CO_2 + H_2O$	277,32 – 282,87	1,929 – 3,892	0
$CO_2 + H_2O$ + DES-1	276,92 – 283,67	1,924 – 3,971	0,05 0,10 0,25
$CO_2 + H_2O$ + DES-2	274,84 – 283,20	1,947 – 3,936	0,05 0,15 0,25
$CO_2 + H_2O$ + DES-3	278,05 – 283,47	2,168 – 4,254	0,05

5.3 Purity of Chemicals

The organic salts and HBDs that were used in this investigation were similar to those utilized in the investigation that was carried out by Nkosi et al. (2018). The purity of the chemicals used in hydrate measurements is outlined in Table 5-3 and Table 5-4, along with the suppliers of those chemicals. The laboratory that serves the Department of Chemistry at Mangosuthu University of Technology supplied the ultrapure Millipore Q water used in the experiments.

Table 5-3: Suppliers and purity of all Organic salts and HBDs used in this study.

Compounds	Supplier	Purity %
Tetrapropylammonium bromide	Sigma-Aldrich	≥ 99
Tetramethylammonium chloride	Sigma-Aldrich	≥ 99,9
Ethylene Glycol	Sigma-Aldrich	≥ 99,9
Glycerol	Sigma-Aldrich	≥ 99,5

ltrapure Millipore Q water; $15\ \mu S$*, at* $298\ K$

Table 5-4: Purity and supplier of the gas used in hydrate phase equilibrium measurements.

Gas	Supplier	Purity
Carbon dioxide	Afrox	99,9

5.4 FTIR

It is critical to investigate the functional groups that exist in a novel solvent, the mixture of different compounds, such as DESs, and the potential structural changes. FTIR is commonly used to investigate the interaction of distinct groups in order to analyze and identify materials (Yeu et al. 2012). As illustrated in Figure 5-1 a) - c), DES-1 and DES-2 have identical spectra, while DES-3 has somewhat different spectra due to the different HBA.

a)

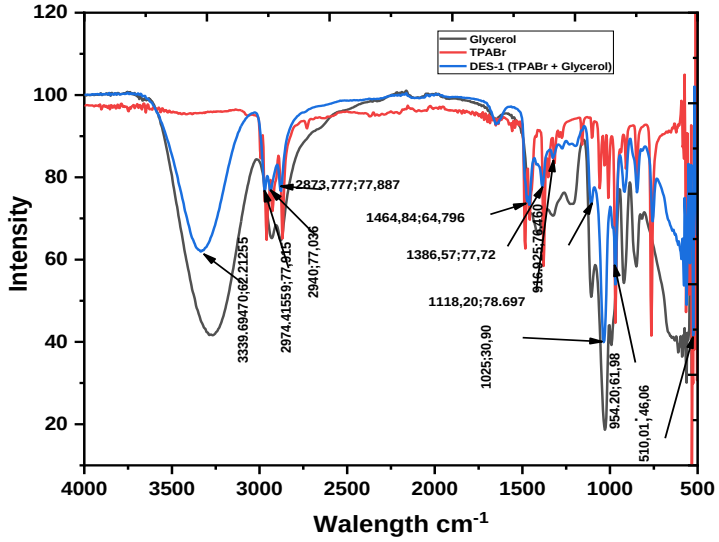

b)

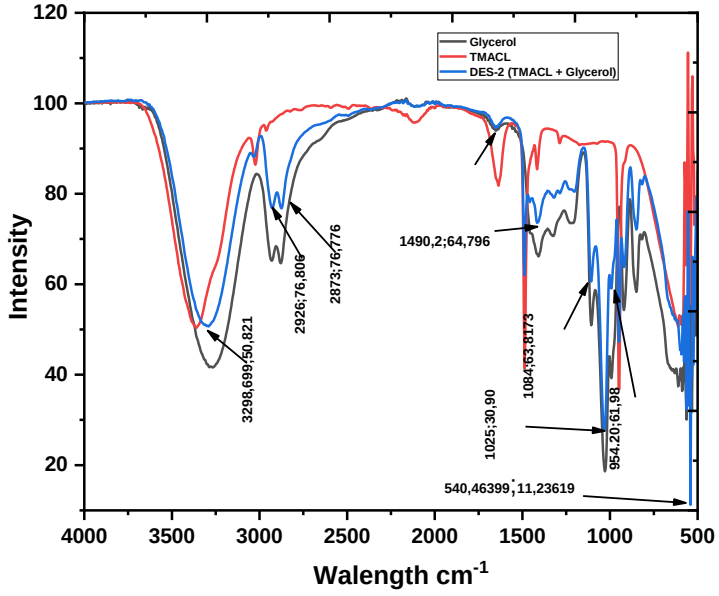

c)

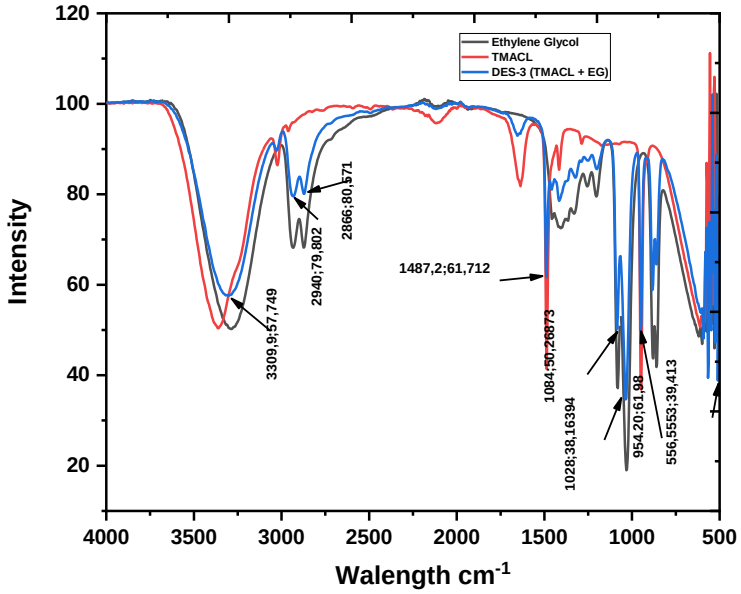

Figure 5-1: FTIR spectrum for DESs, with its HBD and HBA

The stretching bond between 3200-3600 cm^{-1} indicates the presence of water, where the presence of the O-H functional group is frequently indicated. Stuart et al., 2005; Luo et al., 2012. The N-H stretching is observed to overlap with the O-H between 3200-3600 cm^{-1}, Stuart (2005). the C-H appears to be between 2926-2840 cm^{-1} Stayanov et al. 2006 and Luo et al. 2012. There are no peaks in the 2800-1500 cm^{-1} range. Because of the molecular nature of the HBD, the absorbance spectra showed C-H bonding in the 600-1400 cm^{-1} region. Stuart (2005). The presence of Br and Cl was detected in the 600-1400 cm^{-1} range. Smith, 1998.

5.5 Test systems

There are many reports of experimental data that pertain to the conditions under which hydrates of carbon dioxide dissociate that can be found in published works by the scientific community. These systems were selected to check and ensure that the experimental procedure that was used in the current study was valid and reliable, as well as to check and ensure that the experimental apparatus that was used was reliable. The selection of these systems was based on the research conducted by Khan et al. (2017), Mannar et al. (2017), and Bavoh et al. (2017). During this research, measurements of the conditions under which hydrate dissociation occurs were conducted. The outcomes of those measurements are presented in Table 5-5 for carbon dioxide, along with data taken from the relevant body of prior research. The conditions for dissociation that were determined as part of this work are shown to be consistent with the data published in the past, as can be seen in Figures 5-2.

Table 5-5: Experimental results and literature data for the CO_2 + water system.

This work		Mannar et al., 2017		Bavoh et al., 2017		Khan at al., 2017	
P(MPa)	T(K)	P(MPa)	T(K)	P(MPa)	T(K)	P(MPa)	T(K)
1,76	276,35	1,87	276,65	1,81	276,65	1,85	277,40
1,96	277,46	2,48	279,15	2,48	279,15	2,58	279,60
2,32	278,67	3,00	280,77	3,05	280,77	2,95	280,40
2,94	280,93	3,32	281,50	3,41	281,50	3,51	282,45
3,37	281,40	3,78	282,70	3,95	282,70	3,95	283,00
3,82	282,78						

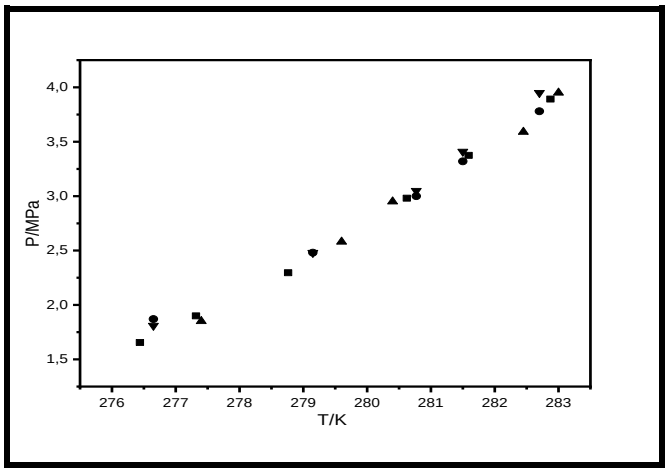

Figure 5-2: Experimental hydrate dissociation conditions and comparison with literature data for the carbon dioxide + water system; (●) Khan et al. 2017 (▲) Mannar et al. 2017; (▼) Bavoh et al. 2017. (■) This work.

5.6 Experimental results

Salts of Tetrapropylammonium bromide (TPABr) and tetramethylammonium chloride (TMACl), as well as glycerol and ethylene glycol HBD, have been proposed for use as hydrate inhibitors and promoters. These chemicals can effectively increase or decrease the equilibrium pressure and affect the formation rate. Conditions for the dissociation of hydrates have been measured and reported for the following systems:

- Carbon dioxide in the presence of DES-1, (TPABr and glycerol aqueous solutions).
- Carbon dioxide in the presence of DES-2 (TMACl and glycerol aqueous solutions).
- Carbon dioxide in the presence of DES-3 (TMACl and ethylene glycol aqueous solutions).

5.6.1 Data for the CO_2 + H_2O + DES-1 (Tetrapropylammonium Bromide TPABr + Glycerol) system.

The experimental phase equilibrium data for clathrate hydrate for the system consisting of CO_2, H_2O and DES 1 are reported in Table 5-6 and plotted in Figure 5-3

Table 5-6: Hydrate equilibrium data for the CO_2 + H_2O + DES-1 system.

Concentration	Pressure MPa	Temperature K
0	1,929	277,32
	2,296	278,76
	2,941	280,74
	3,370	281,59
	3,892	282,87
0,05	1,909	279,13
	2,491	280,67
	3,045	281,89
	3,422	282,66
	3,908	283,61
0,10	1,924	277,14
	2,009	277,68
	2,653	279,93
	2,954	280,66
	3,666	282,40
0,20	2,224	277,14
	2,009	277,68
	2,653	279,93
	2,954	280,66
	3,666	282,40

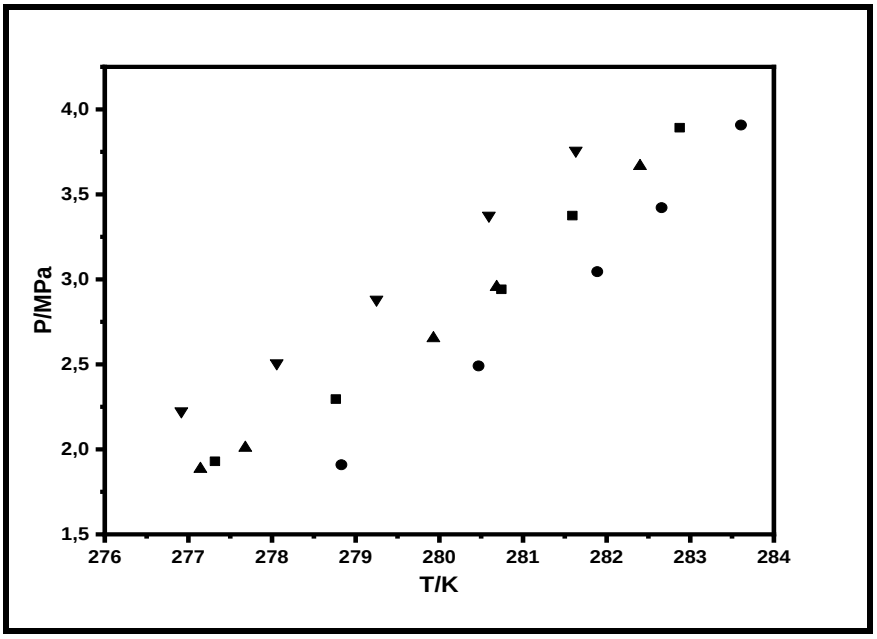

Figure 5-3: Hydrate dissociation data for the (CO_2 + DES-1 + H_2O) system with symbols represent experimental dissociation conditions; Pure water (■); 5 wt % (●); 10 wt %(▲) and 20 wt % (▼).

The data for hydrate dissociation were measured for the CO_2 + H_2O + DES-1 system at the concentration of 0,05; 0,10; and 0,20 for the DES-1 aqueous solution. The measured data on hydrate dissociation are presented in graph form in Figure 5-3, and they are summarized in Table 5-2. As can be seen in figure 5.3, the presence of DES-1 has both an inhibitory effect and a promotion effect on the formation of clathrate hydrate for the systems that are being considered. The conditions necessary for the formation of CO_2 hydrates are altered by DES-1 so that they become more moderate (lower pressure and lower temperature). The phase equilibrium temperature rises when the concentration of TPABr and glycerol in the aqueous solution is increased (from $conc = 0{,}05$ to $conc = 0{,}20$), while the equilibrium pressure falls. Additionally, it is important to note that TPABr and glycerol aqueous solution both promote gas hydrate formation at a concentration of 0,05. At lower pressures, the aqueous solution of DES-1 acts as a hydrate promoter, while at higher pressures, it acts as an inhibitor of hydrate formation. As can be seen, when the concentration is 0,10; the DES-1 either has no effects at all or has effects that are extremely mild. When the concentration of DES-1 is increased from 0,05 to 0,20; there is a corresponding increase in the inhibition effect. The higher the pressure, the more stable carbon dioxide becomes. As a result of the presence of the hydrate inhibitor based on the deep eutectic solvent, the conditions necessary for phase equilibrium shifted, moving from a higher temperature to a lower temperature while also moving from a lower pressure to a higher pressure.

5.6.2 Data for the CO_2 + H_2O + DES-2 (Tetramethylammonium chloride TMACl + Glycerol) system.

The experimental phase equilibrium data for clathrate hydrate for the system containing CO_2, H_2O and DES-2 are provided in Table 5-7 and plotted in Figure 5-4

Table 5-7: Hydrate phase equilibrium data for the CO_2 + H_2O + DES-2 system.

Concentration	Pressure MPa	Temperature K
0	1,929	277,32
	2,296	278,76
	2,941	280,74
	3,370	281,59
	3,892	282,87
0,05	2,091	278,82
	2,362	279,59
	3,059	281,40
	3,603	282,68
	3,936	283,20
0,10	2,278	276,69
	2,723	278,07
	3,326	279,48
	3,575	280,22
	3,913	280,85
0,20	1,947	274,64
	2,238	275,25
	2,988	276,79
	3,457	277,93
	3,967	279,17

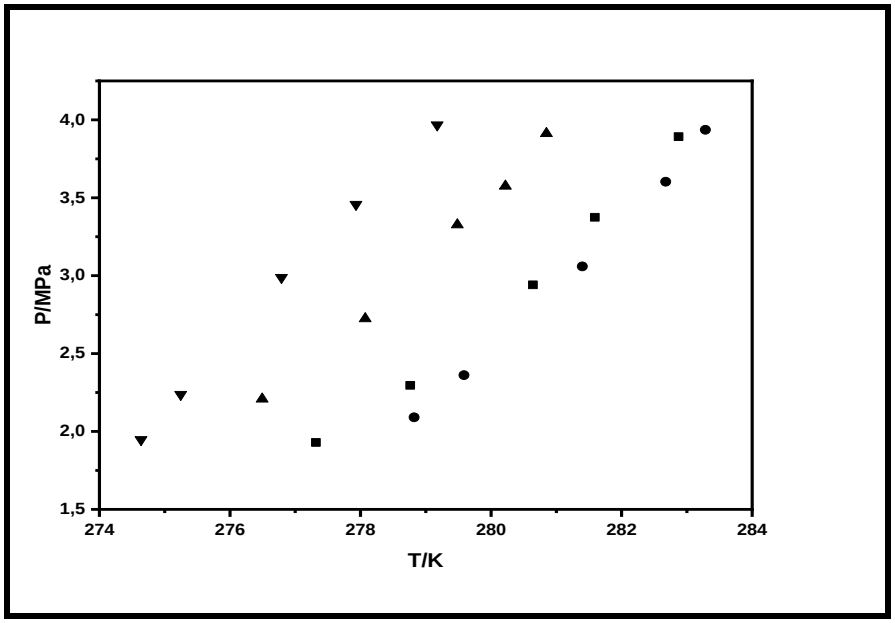

Figure 5-4: Hydrate equilibrium data of the (CO_2 + DES-2+ H_2O) system with symbols representing experimental dissociation conditions; Pure water (■); 0,05 (●); 0,10 (▲) and 0,20 (▼).

The data on the hydrate dissociation for the CO_2 + H_2O + DES-2 system was measured at the concentration of 0,05; 0,10; and 0,20 for the DES-2 aqueous solution. As can be seen in Table 5-7 and Figure 5-4, the clathrate hydrate dissociation conditions for the system of DES-2 behaved in a manner that was different from that of DES-1. The influence of 0,05 mol of DES-2 aqueous solution showed a promotion effect for DES-2 hydrate dissociation conditions. This effect was observed in conditions where the pressure was less than $1{,}92\ MPa$. When the concentration of DES-2 in the aqueous solution is increased to 0,10 and 0,20 DES-2 has an inhibition effect on CO_2 hydrates, the phase equilibrium temperature decreases while the equilibrium pressure increases. This occurs because the phase equilibrium temperature is directly proportional to the equilibrium pressure. In addition to this, the inherent stability of the hydrate is significantly improved. When the concentration of DES-2 is brought down to a concentration of 0,20 , however, the stability of the hydrate is decreased. One could conclude that a concentation of 0.20 produces the greatest inhibition effect of DES-2. In Figure 5.3, it is made abundantly clear that a decrease in the concentration of DES-2 from 0,20 to 0,05 mol results in an increase in the promotion effect of DES-2 on the formation of CO_2 hydrate. This is the case because an increase in the concentration of DES-2 results in an increase in the inhibition effect of DES-2.

5.6.3 CO_2 + H_2O + DES-3 (Tetramethylammonium chloride TMACl + Ethylene Glycol)

The experimental phase equilibrium data for clathrate hydrate for systems with CO_2, H_2O and DES-3 are tabulated in Table 5-8 and plotted in Figure 5-5

Table 5-8: Hydrate phase equilibrium data for the CO_2 + H_2O + DES-3 system.

Concentration	Pressure MPa	Temperature K
	1,929	277,32
	2,296	278,76
0	2,941	280,74
	3,370	281,59
	3,892	282,87
	2,278	277,25
	2,691	278,95
0,05	3,375	280,89
	3,975	282,14
	4,294	282,67

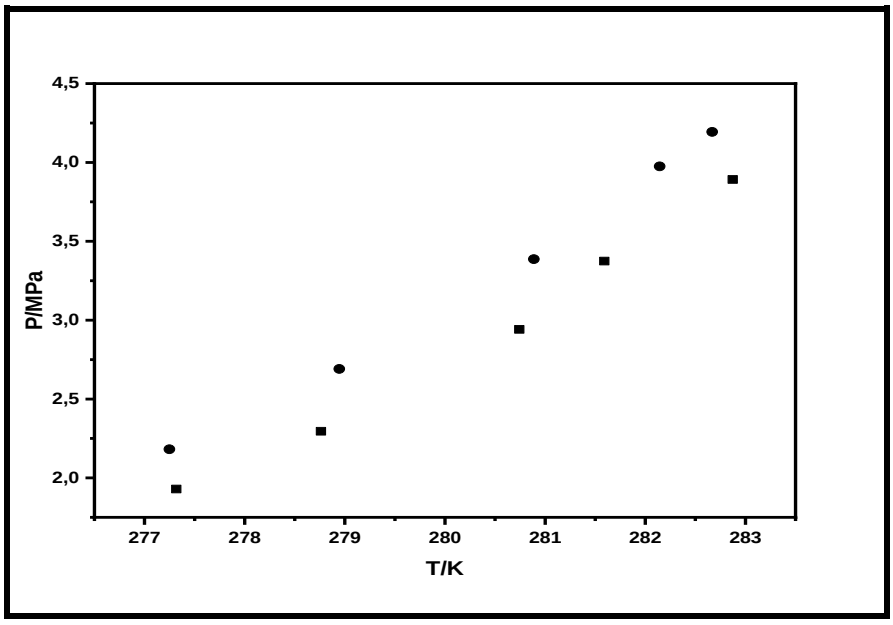

Figure 5-5: Hydrate equilibrium data for the (CO_2 + DES-3 + H_2O) system with symbols representing experimental dissociation conditions**;** pure water (■) and 0,05 (●).

A concentration of 0.05 for DES-3 in an aqueous solution was used to collect data on the dissociation of hydrates in a system that also contained CO_2 and H_2O. The clathrate hydrate dissociation conditions for the system were observed to exhibit a behavior that was distinguishable from that of DES-1 and DES-2. As can be seen in Table 5-8 and Figure 5-5, the presence of a concentration 0,05 of aqueous DES-3 solution had an inhibiting effect on the conditions of DES-3 hydrate dissociation when the pressure was higher than 2,27 MPa. The temperature of the phase equilibrium will decrease whenever there is an increase in the pressure within the phase equilibrium. In addition to this, the inherent stability of the hydrate is significantly improved.

Previous literature (Khan et al. 2017a; and Tuariq et al 2014) has demonstrated that the behavior is more dependent on their individual side chain attributes (hydropathy, side chain alkyl, length polarity, functional group, etc.), solubility, concentration, examined concentration, interaction between the guest molecule and hydrogen bond, and electrostatic force of attraction with water molecules. Because of their hydrogen bonding capabilities and electrostatic interactions, DESs reduce the affinity coefficient of water in the system,

As a result, it would inhibit the rearranging of water molecules to form hydrates and thus delay phase relaxation to hydrate structures.The presence of the hydroxyl group, which is regarded as the best anion for hygrogen bonding, explains for the high inhibition effect of DES-2 (TMACl + Glycerol) over DES-3 (TMACl + Ethylene Glycol) and DES-1 (TPABr + Glycerol).

Glycerol has three hydroxyl groups, whereas ethylene glycol only has two. The inclusion of three OH^- groups in DES-2 boosts its hydrogen bonding capabilities, causing increased disruption in water activity in hydrate formation and effective hydrate inhibition. Furthermore, because of its smaller alkyl chain, tetramethylammonium (TMA^+) cation is less hydrophobic, which contributes to its inhibitory strength. TMACl is composed of tetramethylammonium (TMA^+) cation and chloride (Cl^-) anion, which might explain the phenomenon. the halide anions, Cl^- is one of the finest at establishing hydrogen bonds with water.

The relatively longer alkyl chain in the Tetrapropylammonium (TPA^+) cation, TPABr + ethylene glycol inhibited the least of the DES investigated. TPA+'s longer alkyl chain increases its hydrophobicity, making it less miscible with water than shorter alkyl chain cations like TMA+. the presence of OH anion improved TPABr inhibition. TMACl has a higher inhibitory strength than TMAOH due to the combination of the lowest feasible alkyl chain and the hydrogen bonding affinity of the Cl^-. TBAOH inhibited the least of the AILs tested, owing to the comparatively long alkyl chain in the tetra butyl ammonium (TBA+) cation.

TBA+'s longer alkyl chain enhances its hydrophobicity, which makes it less miscible with water than shorter alkyl chain cations like TMA+. The presence of OH anion, on the other hand, enhanced TBAOH inhibition.

Figures 5-3 to figure 5-5 show dissociation data that reveals some interesting findings. All the DES evaluated were found to be capable of slightly shifting the CO_2 hydrate dissociation curves toward higher pressure and lower temperature regions. This behavior supports that the interactions between the chemical components of the DES and water result in inhibiting effects. These effective inhibitory effects are like those observed in the literature for alcohols, glycols, additives, and electrolytes. Figure 5-6 compares the investigated DESs + CO_2 + H_2O system to other types of studied ILs in the literature.

Table 5-9: Hydrate phase equilibrium data of aqueous AILs compared to DES for CO2 hydrates at different concentrations.

Pure water		DES wt 5%	
3,892	282,87	3,936	283,60
3,375	281,39	3,603	282,98
2,941	280,74	3,059	281,96
2,296	278,76	2,362	279,99
1,923	277,32	2,091	278,68
DES wt 10%		(EMPIP)(Br) wt 10%	
3,953	280,85	3,95	281,20
3,675	280,22	3,50	280,20
3,426	279,48	2,90	278,80
2,823	278,07	2,38	277,20
2,278	276,39	1,83	275,80
TBAOH wt 10%		TMAOH wt 5%	
4,95	285,00	4,07	282,00
4,05	283,60	3,54	280,60
3,10	281,30	3,00	279,00
1,95	277,60	2,50	277,80
		1,84	275,30
Lysine 5%		DES wt 20%	
4,10	281,80	3,967	279,17
3,00	279,65	3,457	277,93
2,50	278,34	2,988	276,79
2,00	276,20	2,238	275,25
		1,947	274,64
wt 5% TMAB + MEG			
3.5	282.3		
3	281.3		
2.5	277. 7		
2	275		

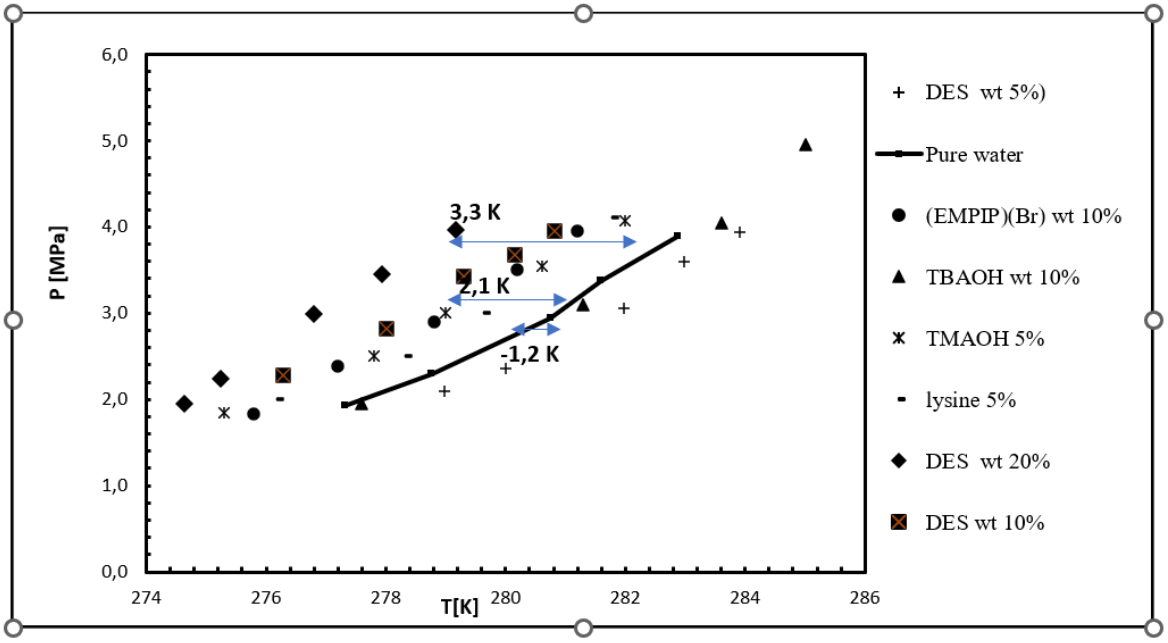

Figure 5-6: Average suppression temperature (ΔŦ) of carbon dioxide gas hydrates in the presence of 10 wt% aqueous solutions.

The inhibition performance of DES-2 concentrations of 10 wt %, and 5 wt % was compared with Ionic Liquid of), N-ethyl-N-methylpiperidinium bromide ([EMPip] [Br]), Tetramethylammonium hydroxide (TMAOH), Tetraethylammonium hydroxide (TEAOH), and Amino acids (Cha et al. 2016, Khan et 2017a, Khan et 2017b and Bavoh et al 2019). The inhibitory strength of DES-2 conc 10 wt % is found to be slightly better than that of the examined ILs. TEAOH was found to be promoting gas hydrate at the concentration of 10 wt %. It should also be recognized that the challenges indicated in Table 5-10 exist.

The thermodynamic inhibition performance of DES-2+ CO_2 + H_2O systems was compared to other AILs at the studied concentrations, as shown in Table 5-8 and Figure 5-6. The average suppression temperature (Ŧ) was obtained in this experimental study to assess the inhibitory performance of tetramethylammonium chloride + glycerol DES-CO_2 hydrate formation at compositions of 5, 10, and 20 wt % in the temperature and pressure ranges of 274 to 284 K and 2 to 4 MPa respectively.

$$Ŧ = \frac{\sum \Delta T}{n} = \frac{\sum_{i=1}^{n}\left(T_{0,pi} - T_{1,pi}\right)}{n}$$

Where, $T_{0,pi}$ and $T_{1,pi}$ are the equilibrium temperatures of CO_2 in water and DES aqueous solution, respectively. Dissociation temperatures should be obtained at the same pi and n is the number of pressure points analyzed.

the DES-2 + CO_2 + H_2O system outperforms the other systems in terms of thermodynamic inhibition, achieving average suppression temperatures of 2,1 K and 3,3 K at a DES composition of 10 wt % and 20 wt % respectively. Comparatively the 10 wt % TBAOH + CO_2 + H_2O system had a value of -1,2 K (hydrate promotion effect). TMAOH + CO_2 + H_2O systems achieved an average suppression temperature of 1,1 K and 1,6 K at 5 and 10 wt % TMAOH respectively Khan et al, 2017a. An (EMPIP)(Br) + CO_2 + H_2O system achieved an average suppression temperature of 1,8 K at a composition of 10 wt % (EMPIP)(Br) Cha et al., 2016.

It is still challenging to discover acceptable "green" solvents to replace OCs. Several requirements must be satisfied for a solvent to be called "green" in terms of the environment Anastas et al., 2002. DES are said to be environmentally favorable (solvents, inhibitors, etc.). Furthermore, they are less expensive than conventional hydrate and ionic liquid inhibitors and are biodegradable. As a result, these considerations should be considered in future decision-making for the specified processes. (Abbot et al., 2002 and Smith et al., 2014) the challenges with other inhibitors are indicated in Table 2.

Table 5-10: Challenges for different classes of inhibitors/ promoters for gas hydrates.

Class of Inhibitors/ Promoter	Challenge
Alcohols and Glycols	Required in high concentration Lighter alcohols are volatile Low efficiency
Polymers	Costly, except PVP Adsorb on hydrate itself Sensitive to low temperature
Amino acids	Oxidative and thermal degradation Low clouding point
Ionic Liquids	Costly Low solubility Low efficiency
Nanoparticles	Complex synthesis Stability and sedimentation

DES are said to be environmentally favorable (solvents, inhibitors, etc.). Furthermore, they are less expensive than conventional hydrate and ionic liquid inhibitors and are biodegradable. As a result, these considerations should be considered in future decision-making for the specified processes.

5.7 MD simulation results

This section has the MD results and a technical analysis of the work's findings. In terms of radial distribution function (RDF) and the structural and dynamic features of carbon dioxide hydrates are examined.

5.7.1 Radial distribution function

This section analyzes the radial distribution function (RDF) g (r) at various temperatures, pressures, and densities. The probability of finding the atom at r from the atom is RDF, g (r), which can be expressed as follows:

$$g_{\alpha\beta}(r) = \frac{V}{N_\alpha N_\beta}\left(\sum_{i=1}^{N_\alpha} \frac{n_i\beta(r)}{4\pi r^2 \Delta r}\right) \quad (5\text{-}1)$$

Where V is the volume of simulation box, N_α and N_β reperents total number of particles of atom α and atom β at the spherical distance of r.

The RDF can serve as an indication for determining the stability of hydrates in addition to providing valuable information regarding the crystal microstructure of hydrates. According to Konnert et al. (1986), the RDF plot displays several distinct peaks such as the location and the height which are reflective of the properties of hydrate structure.

There is a peak at 1,77Å, for DES3, 1,79Å for DES1 and DES2 which depicts strong hydrogen bonding; there is also a peak at 3,21Å for DES1 and DES2 and 3,25Å for DES3 which depicts strong O-O bonds. This information is displayed in figure 5-7to figure 5-9, which shows the results of an analysis of RDF. It can be seen from the fact that water fluids in DES-1, DES-2, and DES-3 have the same structure which is the indication that the deep eutectic solvents do not have a significant impact on the distance between the molecules of the fluids.

a.

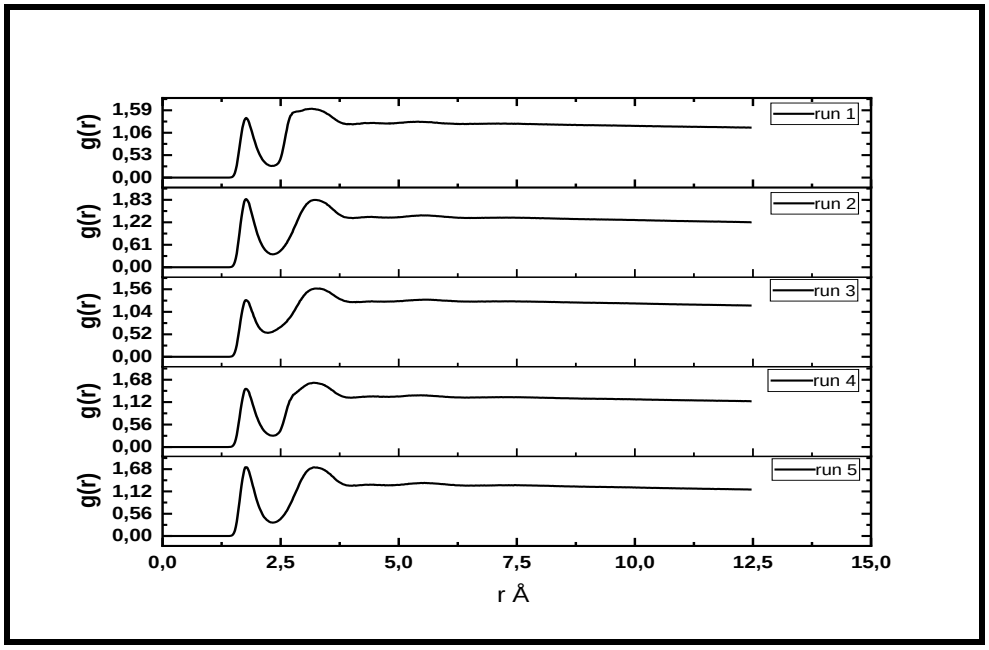
g(r)
1,59
1,06
0,53
0,00
run 1
g(r)
1,83
1,22
0,61
0,00
run 2
g(r)
1,56
1,04
0,52
0,00
run 3
g(r)
1,68
1,12
0,56
0,00
run 4
g(r)
1,68
1,12
0,56
0,00
run 5
0,0
2,5
5,0
7,5
10,0
12,5
15,0
r Å

b.

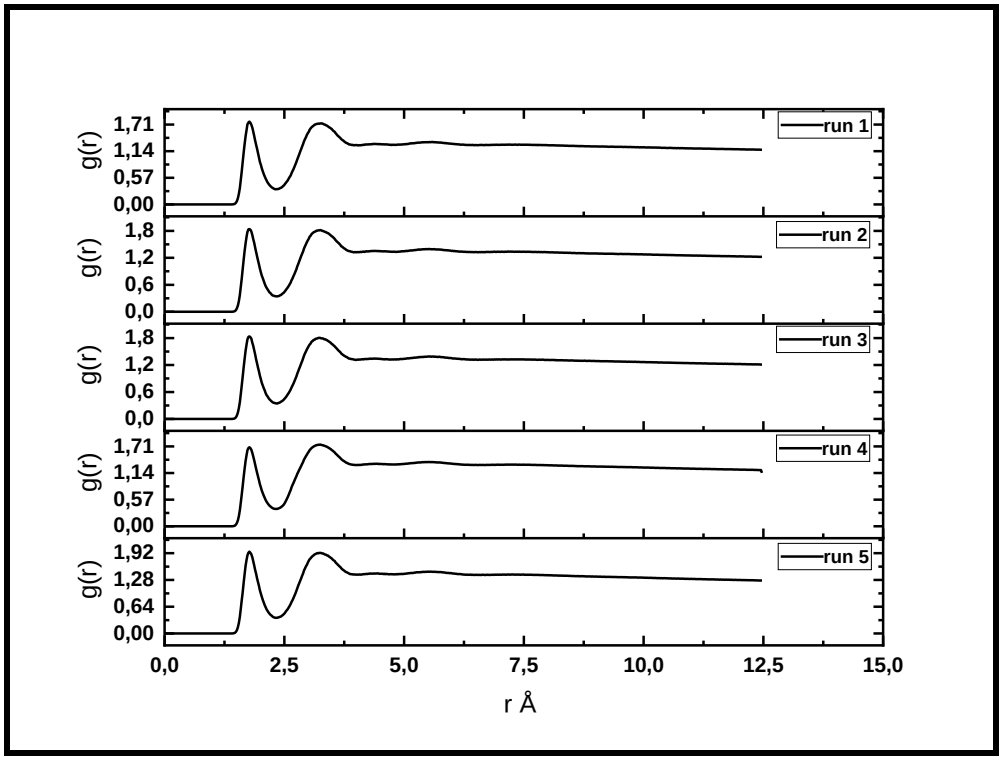
g(r)
1,71
1,14
0,57
0,00
run 1
g(r)
1,8
1,2
0,6
0,0
run 2
g(r)
1,8
1,2
0,6
0,0
run 3
g(r)
1,71
1,14
0,57
0,00
run 4
g(r)
1,92
1,28
0,64
0,00
run 5
0,0
2,5
5,0
7,5
10,0
12,5
15,0
r Å

c.

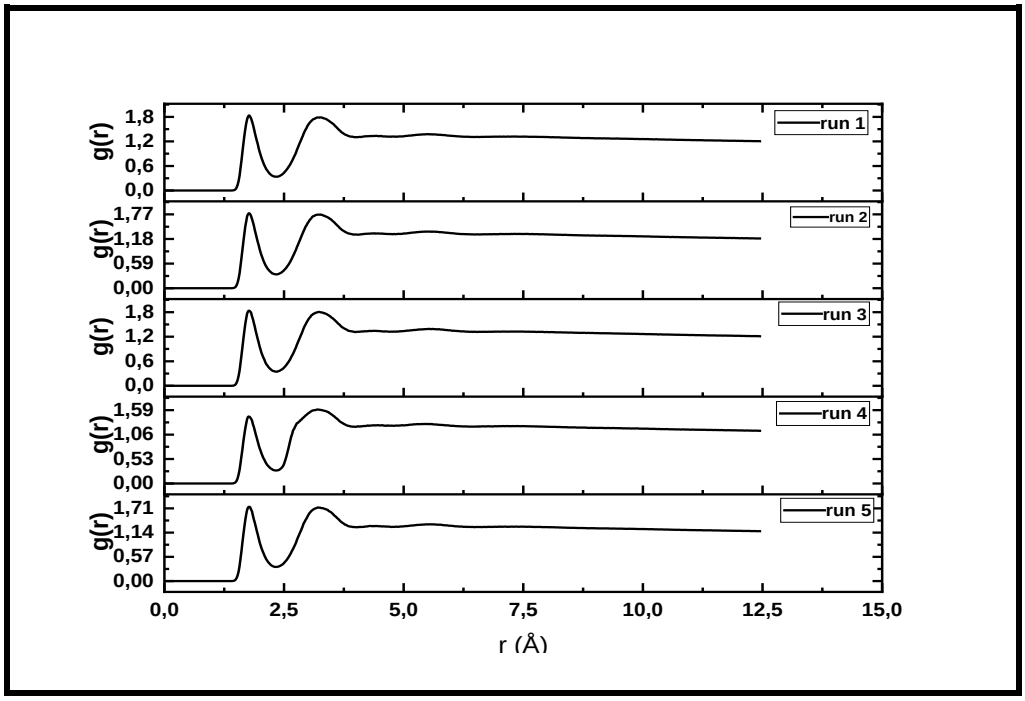

Figure 5-7: RDF plots of DES-1 a. 5 wt %, b. 10 wt % and c. 20 wt % at different temperatures and pressures.

d.

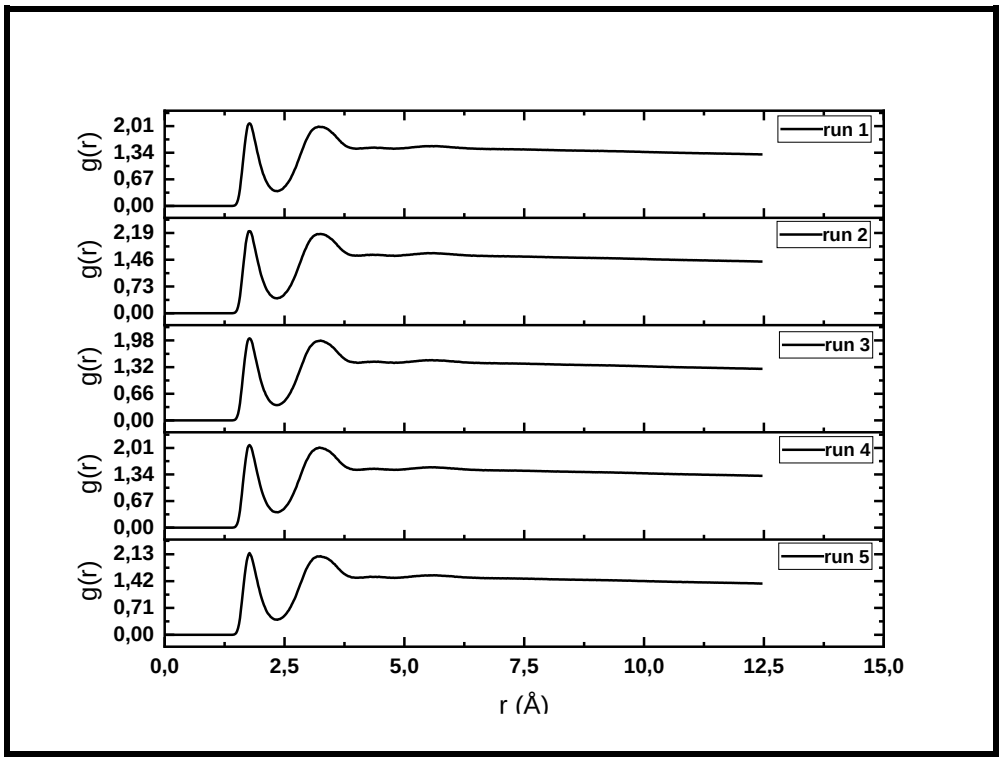

e.

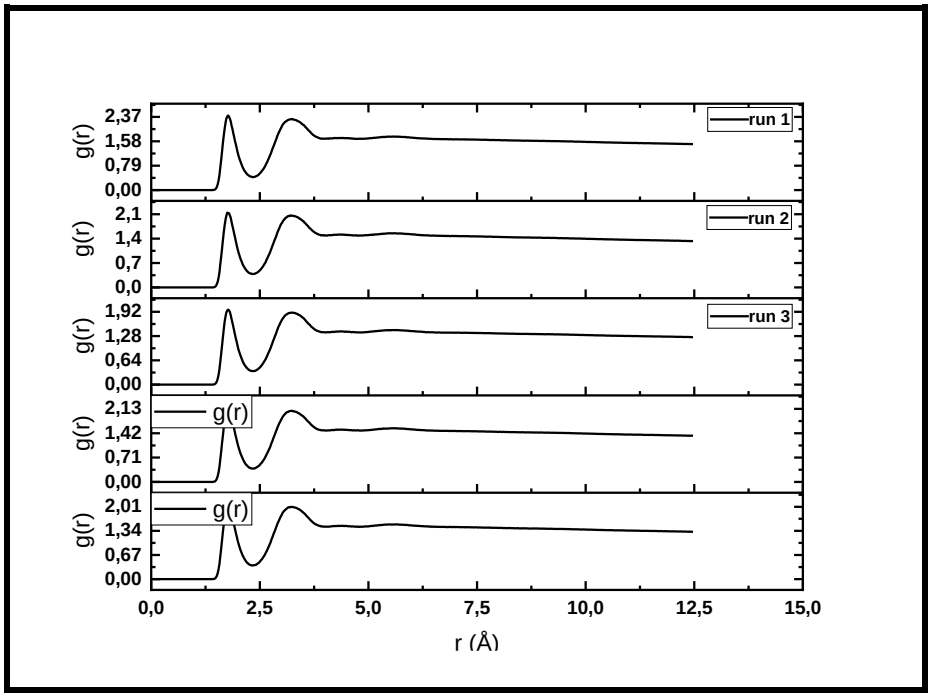

f.

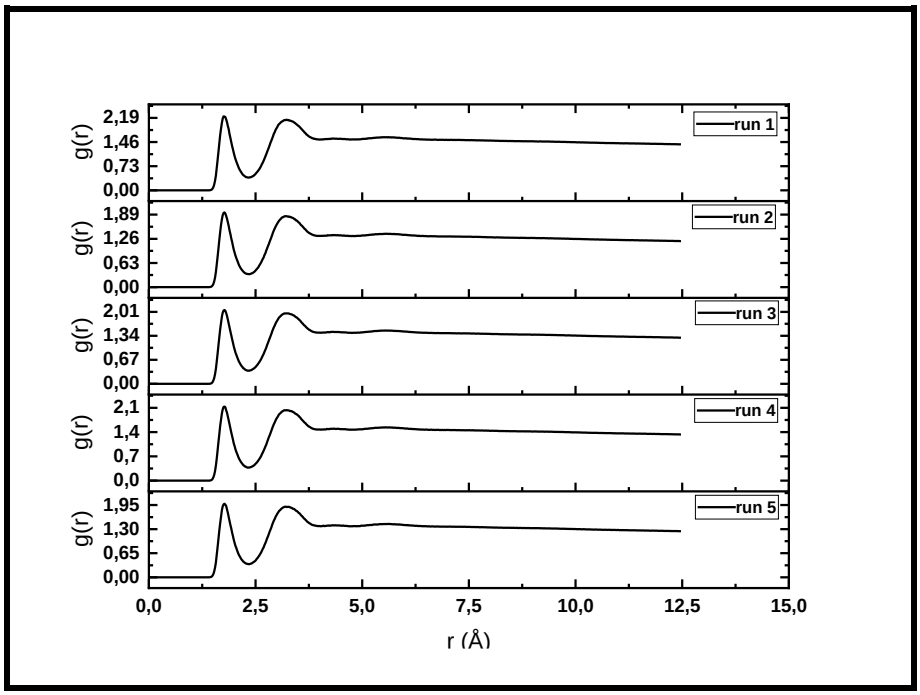

Figure 5-8: RDF plots of DES-2 a. 5 wt %, b. 10 wt % and c. 20 wt % at different temperatures and pressures.

g.

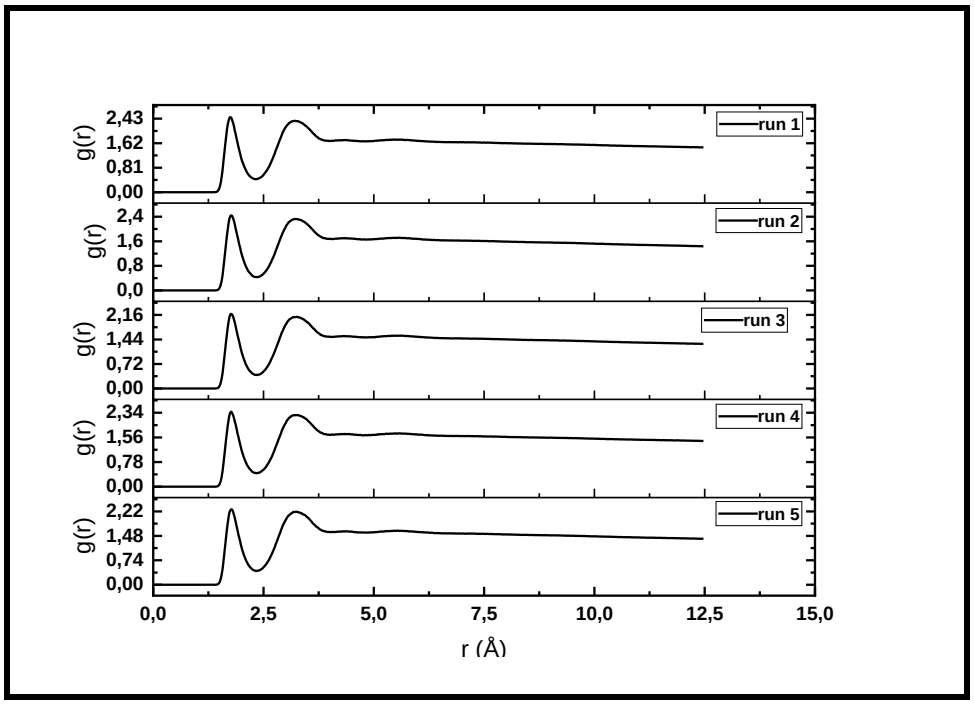

Figure 5-8: RDF plots of DES-3 g. 5 wt %, at different temperatures and pressures

The host-host RDF has the potential to be a powerful method for determining the crystal structure of hydrates. In a crystalline solid with a long maximum, the RDF plots have an unlimited number of sharp peaks due to the periodic arrangement of the system; these peaks correspond to the coordination of the nearest and next-nearest trajectory, and their distances apart and heights reveal the lattice structure's distinctive features Konnert et al., 1986. This contrasts with the short-range disarray and long-range disarray of a gas or liquid. Short-range disarray allows us to pinpoint the closest coordination shells to any given molecule in a liquid (or amorphous solid). However, as the distance r increases, the clearly defined positional relationships fade away gradually due to missing the long-range disarray. It is equally likely to find another molecule at any distance r from a given molecule in real gases, and the g(r) has no discernible shape (Reshadi et al., 2018). These conditions prove that the clathrate-hydrates modeled in this study maintain their crystalline phase throughout the simulation process.

6 Conclusion and Recommendations

6.1 Conclusion

The aim of this research was to conduct thermodynamic studies on the phase equilibria of gas hydrates to determine their potential use as enviromentally CO_2 hydrate inhibitors. An isochoric pressure search method was used to measure the phase equilibrium data because it does not require neither visual observation nor volume changes for the determination of hydrate equilibrium data.

Formation of gas hydrates in gas pipelines was historically a disadvantage for gas transportation. Hence, intensive research was carried to chemically inhibit its growth, without altering the operating conditions. Alcohols and glycols found commercial application. Polymers, amino acids, ionic liquids, and nanoparticles have shown good potential to replace the conventional inhibitors. However, many problems (like large dosage amounts for desired effect) instigated research for new options. Moreover, its potential to permanently encage several harmful and toxic gases has created a new class of hydrates.

DESs are the class of chemicals used for inhibition of hydrate formation have been tested for inhibiting/ promoting the hydrate formation with success. However, full-scale commercialization is not ascertained at this stage of development and requires extensive experimentation and theory development. The work provides a comprehensive overview of the prevailing inhibitors/ promoters, but also narrow down the gap for their commercial utilization.

The experimental set up and procedures were successfully validated from the comparison between new measurements and those reported in the literature in relation to the dissociation conditions of carbon dioxide hydrates dissociation data, equilibrium conditions in the hydrate stability region were measured and successfully compared to literature data, serving as proof of the reliability of the experimental data reported in the present study.

The other objective was to investigate the stability and dissociation of CO_2 gas hydrate by employing MD simulation within the Forcite module of the material studio software. The effects of temperature and pressure are taken into consideration. The study of carbon dioxide gas hydrate was accomplished in this work through the utilization of molecular dynamics simulations with the application of the COMPASS force field. Under a variety of P-T

conditions, the thermodynamic properties and equilibrium cell parameters of the systems that were successfully investigated were examined and analysed.

The average thermodynamics properties of the hydrates were evaluated, and the sharp peak of RDFs plots was analysed, as part of a set of NPT molecular simulations that were carried out with the intention of clarifying the effects of DES on the thermodynamics stability of carbon dioxide gas hydrates. As a result, one can reach the conclusion that the obtained RDFs reflect the characteristic configurations of the hydrate crystal structure, which can be used as an indicator of the stability of the hydrate.

6.2 Recommendations

Since there is no study in the literature which involves DES in gas hydrates it can be recommended that further phase equilibria studies can be done to establish the impact of different deep eutectic solvents on various gas hydrates

It is also recommended that further molecular dynamic work can be done to observe interactions between guest - host molecules in gas hydrates focusing on factors affecting hydrate formation by water molecules around the guest molecules.

As with any potential industrial scale process, the industrial efficiency and recovery systems of the DES needs to be investigated.

References

Abbott, A. 2011. *The electrodeposition of composite materials using deep eutectic solvents.* University of Leicester.

Abbott, A. P., Boothby, D., Capper, G., Davies, D. L. & Rasheed, R. K. 2004. Deep Eutectic Solvents Carboxylic Acids: Versatile Alternatives to Ionic Liquids. *Journal of the American Chemical Society,* 126**,** 9142Formed between Choline Chloride and -9147

Aissaoui, T., Alnashef, I. M. & Benguerba, Y. 2016. Dehydration of natural gas using choline chloride based deep eutectic solvents: COSMO-RS prediction. *Journal of Natural Gas Science and Engineering,* 30**,** 571-577.

Anastas, P. T. & Kirchhoff, M. M. 2002. Origins, current status, and future challenges of green chemistry. *Accounts of chemical research,* 35**,** 686-694.

Arjmandi, M., Chapoy, A. & Tohidi, B. 2007. Equilibrium data of hydrogen, methane, nitrogen, carbon dioxide, and natural gas in semi-clathrate hydrates of tetra butyl ammonium bromide. *Journal of chemical & engineering data,* 52**,** 2153-2158.

Adiasmito, S., Frank, R. J. & Sloan JR, E. D. 1991. Hydrate of carbon dioxide and methane mixture, *Journal of Chemical and Engineering Data,* 36.

Allen, M. P. 2004. Introduction to molecular dynamics simulation. *Computational soft matter: from synthetic polymers to proteins,* 23**,** 1-28.

Bavoh, C. B., Partoon, B., Lal, B., Gonfa, G., Khor, S. F. & Sharif, A. M. 2017. Inhibiton effect of amino acids on carbon dioxide hydrate. *Chemical Engineering Science,* 171**,** 331-339.

Bavoh, C. B., Lal, B., Osei, H., Sabil, K. M. & Mukhtar, H. 2019. A review on the role of amino acids in gas Hydrate inhibition, CO2 capture and sequestration, and natural gas storage. *Journal of Natural Gas Science and Engineering,* 64**,** 52-71

Berendsen, H. J., Postma, J. V., Van Gunsteren, W. F., Dinola, A. & Haak, J. R. 1984. Molecular dynamics with coupling to an external bath. *The Journal of chemical physics,* 81**,** 3684-3690.

Bernal, J. D. & Fowler, R. H. 1933. A theory of water and ionic solution, with particular reference to hydrogen and hydroxyl ions. *The Journal of Chemical Physics,* 1**,** 515-548.

Bernasconi, r., Panzeri, g., Accogli, a., Liberale, f., Nobili, l. & Magagnin, l. 2017. electrodeposition from deep eutectic solvents. *progress and developments in ionic liquids.* Intech.

Biovia, D. S. 2020. Materials Studio. 2020. *Dassault Systèmes: San Diego.*

Bjelić, A., Hočevar, B., Grilc, M., Novak, U. & Likozar, B. 2022. A review of sustainable lignocellulose biorefining applying (natural) deep eutectic solvents (DESs) for separations, catalysis, and enzymatic biotransformation processes. *Reviews in Chemical Engineering,* 38**,** 243-272.

Carriazo, D., Gutiérrez, M. C., Ferrer, M. L. & Del Monte, F. 2010. Resorcinol-Based Deep Eutectic Solvents as Both Carbonaceous Precursors and Templating Agents in the Synthesis of Hierarchical Porous Carbon Monoliths. *Chemistry of Materials,* 22**,** 6146-6152.

Carroll, J. 2020. *Natural gas hydrates: a guide for engineers*, Gulf Professional Publishing.

Cha, J.-H., Ha, C., Kang, S.-P., Kang, J. W. & Kim, K.-S. 2016. Thermodynamic inhibition of CO2 hydrate in the presence of morpholinium and piperidinium ionic liquids. *Fluid phase equilibria,* 413**,** 75-79.

Chandran, D., Khalid, M., Walvekar, R., Mubarak, N. M., Dharaskar, S., Wong, W. Y. & Clark, J. H. & Tavener, S. J. 2007. Alternative solvents: shades of green. *Organic process research & development,* 11**,** 149-155.

Chapoy, A., Haghighi, H., Burgass, R. & Tohidi, B. 2010. Gas hydrates in low water content gases:Experimental measurements and modelling using the CPA equation of state. *Fluid Phase Equilibria,* 296**,** 9-14.

Clark, J. H. & Tavener, S. J. 2007. Alternative solvents: shades of green. *Organic process research & development,* 11**,** 149-155.

Elgibaly, A. A. & Elkamel, A. M. 1998. A new correlation for predicting hydrate formation conditions for various gas mixtures and inhibitors. *Fluid Phase Equilibria,* 152**,** 23-42.

Ewald, P. P. 1921. Ewald summation. *Ann. Phys,* 369**,** 1-2.2.

Eslamimanesh, A., Gharagheizi, F., Illbeigi, M., Mohammadi, A. H., Fazlali, A. & Richon, D. 2012. Phase equilibrium modeling of clathrate hydrates of methane, carbon dioxide, nitrogen, and hydrogen+ water soluble organic promoters using Support Vector Machine algorithm. *Fluid Phase Equilibria,* 316**,** 34-45.

Garcia, G., Aparicio, S., Ullah, R. & Atilhan, M. 2015. Deep eutectic solvents: physicochemical properties and gas separation applications. *Energy & Fuels,* 29**,** 2616-2644.

Giavarini, C. & Hester, K. 2011. *Gas hydrates: Immense energy potential and environmental challenges*, Springer Science & Business Media.

Gupta, T. C. S. M. 2018. Deep eutectic solvents for extraction-desulphurization: A review. *Journal of Molecular Liquids*.

Gutiérrez, M. A. C., Ferrer, M. A. L., Mateo, C. R. & Del Monte, F. 2009. Freeze-drying of aqueous solutions of deep eutectic solvents: a suitable approach to deep eutectic suspensions of self-assembled structures. *Langmuir,* 25**,** 5509-5515.

Hayyan, M., Aissaoui, T., Hashim, M. A., Alsaadi, M. A. & Hayyan, A. 2015. Triethylene glycol based deep eutectic solvents and their physical properties. *Journal of the Taiwan Institute of Chemical Engineers,* 50**,** 24-30.

Hong, H., Pooladi-Darvish, M. & Bishnoi, P. 2003. Analytical modelling of gas production from hydrates in porous media. *Journal of Canadian Petroleum Technology,* 42**,** 45-56.

Hoover, W. G. 1985. Canonical dynamics: Equilibrium phase-space distributions. *Physical review A*, 31**,** 1695.

Hou, Y., GU, Y., Zhang, S., Yang, F., Ding, H. & Shan, Y. 2008. Novel binary eutectic mixtures based on imidazole. *Journal of Molecular Liquids,* 143**,** 154-15

Katz, D. L. 1945. Prediction of conditions for hydrate formation in natural gases. *Transactions of the AIME,* 160**,** 140-149.

Kareem, M. A., Mjalli, F. S., Hashim, M. A. & Alnashef, I. M. 2012. Liquid–liquid equilibria for the ternary system (phosphonium based deep eutectic solvent–benzene–hexane) at different temperatures: A new solvent introduced. *Fluid Phase Equilibria,* 314**,** 52-59.

Khan, M. S., Partoon, B., Bavoh, C. B., Lal, B. & Mellon, N. B. 2017. Influence of tetramethylammonium hydroxide on methane and carbon dioxide gas hydrate phase equilibrium conditions. *Fluid Phase Equilibria,* 440**,** 1-8.

Khan, M. S., Bavoh, C. B., Partoon, B., Lal, B., Bustam, M. A. & Shariff, A. M. 2017. Thermodynamic effect of ammonium based ionic liquids on CO_2 hydrates phase boundary. *Journal of molecular liquids,* 238**,** 533-539.

Khan, M. N., Warrier, P., Peters, C. J. & Koh, C. A. 2018. Advancements in hydrate phase equilibria and modeling of gas hydrates systems. *Fluid Phase Equilibria,* 463**,** 48-61.

Kelland, M. A. 2006. History of the development of low dosage hydrate inhibitors. *Energy & fuels, 20,* 825-847.

Kim, S. M., Lee, J. D., Lee, H. J., Lee, E. K. & Kim, Y. 2011. Gas hydrate formation method to capture the carbon dioxide for pre-combustion process in IGCC plant. *International journal of hydrogen energy,* 36**,** 1115-1121.

Kirchner, M. T., Boese, R., Billups, W. E. & Norman, L. R. 2004. Gas hydrate single-crystal structure analyses. *Journal of the American Chemical Society,* 126**,** 9407-9412.

Konnert, J., Karle, J. & D'Antonio, P. 1986. Radial distribution function analysis. *ASM Handbook.,* 10**,** 393-401.

Kondori, J., James, L. & Zendehboudi, S. 2020. Molecular scale modeling approach to evaluate stability and dissociation of methane and carbon dioxide hydrates. *Journal of Molecular Liquids,* 297**,** 111503.

Kurnia, K. A., Quental, M. V., Santos, L. M., Freire, M. G. & Coutinho, J. A. 2015. Mutual solubilities between water and non-aromatic sulfonium-, ammonium-and phosphonium-hydrophobic ionic liquids. *Physical Chemistry Chemical Physics,* 17**,** 4569-4577.

Lederhos, J., Long, J., Sum, A., Christiansen, R. & Sloan JR, E. 1996. Effective kinetic inhibitors for natural gas hydrates. *Chemical Engineering Science,* 51**,** 1221-1229.

Liao, H. G., Jiang, Y. X., Zhou, Z. Y., Chen, S. P. & Sun, S. G. 2008. Shape-controlled synthesis of gold nanoparticles in deep eutectic solvents for studies of structure–functionality relationships in electrocatalysis. *Angewandte Chemie International Edition,* 47**,** 9100-9103.

Lim, D., Park, S., RO, H., Lee, J.-W., Kang, H., Kwon, M. & Lee, H. Thermodynamic and kinetic effect of a dual-function inhibitor on gas hydrate formation. The Twenty-fourth International Ocean and Polar Engineering Conference, 2014. OnePetro.

Linga, P., Kumar, R. & Englezos, P. 2007. Gas hydrate formation from hydrogen/carbon dioxide and nitrogen/carbon dioxide gas mixtures. *Chemical engineering science,* 62**,** 4268-4276

Liu, W., Hu, J., Li, X., Sun, Z., Sun, F. & Chu, H. 2018. Assessment of hydrate blockage risk in long-distance natural gas transmission pipelines. *Journal of Natural Gas Science and Engineering,* 60**,** 256-270.

Luo, J., Conrad, O., Vankelecom, I F J., 2012. Physicochemical properties of phosiphonium-based and ammonium-based protic ionic liquids. *Journal of Material Chemicals,* 20574-20579.

Maekawa, T. 2010. Equilibrium conditions of clathrate hydrates formed from propane and aqueous solutions of propanone and sodium chloride. *Journal of Chemical & Engineering Data,* 55**,** 3645-3648.

Madeira, P. P., Bessa, A., Álvares-Ribeiro, L., Raquel Aires-Barros, M., Rodrigues, A. E., Uversky, V. N. & Zaslavsky, B. Y. 2014. Amino acid/water interactions study: a new amino acid scale. *Journal of Biomolecular Structure and Dynamics,* 32**,** 959-968.

Makogon, I. U. R. F. 1981. *Hydrates of natural gas,* PennWell Books Tulsa, Oklahoma.

Makogon, T. Y. & Sloan, E. D. J. 1994. Phase equilibrium for methane hydrate from 190 to 262 K. *Journal of Chemical and Engineering Data,* 39**,** 351-353.

Mannar, N., Bavoh, C. B., Baharudin, A. H., Lal, B. & Mellon, N. B. 2017. Thermophysical properties of aqueous lysine and its inhibition influence on methane and carbon dioxide hydrate phase boundary condition. *Fluid Phase Equilibria,* 454**,** 57-63.

Marsh, K. N., Boxall, J. A. & Lichtenthaler, R. 2004. Room temperature ionic liquids and their mixtures—a review. *Fluid phase equilibria,* 219**,** 93-98.

Mbous, Y. P., Hayyan, M., Hayyan, A., Wong, W. F., Hashim, M. A. & Looi, C. Y. 2017. Applications of deep eutectic solvents in biotechnology and bioengineering—promises and challenges. *Biotechnology advances,* 35**,** 105-134.

Mohammadi, A. H. & Richon, D. 2010. Ice− clathrate hydrate− gas phase equilibria for air, oxygen, nitrogen, carbon monoxide, methane, or ethane+ water system. *Industrial & engineering chemistry research,* 49**,** 3976-3979.

Mohammadi, A. H., Chapoy, A., Tohidi, B. & Richon, D. 2004. A semiempirical approach for estimating the water content of natural gases. *Industrial & engineering chemistry research,* 43**,** 7137-7147.

Mohammadi, A. H. & Richon, D. 2012. Phase equilibria of hydrogen sulfide and carbon dioxide simple hydrates in the presence of methanol, (methanol+ NaCl) and (ethylene glycol+ NaCl) aqueous solutions. *The Journal of Chemical Thermodynamics,* 44**,** 26-30.

Morrison, H. G., Sun, C. C. & Neervannan, S. 2009. Characterization of thermal behaviour of deep eutectic solvents and their potential as drug solubilization vehicles. *International journal of pharmaceutics,* 378**,** 136-139.

Najibi, H., Chapoy, A., Haghighi, H. & Tohidi, B. 2009. Experimental determination and prediction of methane hydrate stability in alcohols and electrolyte solutions. *Fluid Phase Equilibria,* 275**,** 127-131.

Najibi, H., Kamali, Z. & Mohammadi, A. H. 2013. Phase equilibria of carbon dioxide clathrate hydrates in the presence of methanol/ethylene glycol+ single salt aqueous solutions: experimental measurement and prediction. *Fluid Phase Equilibria,* 342**,** 71-74.

Ngema, P. T., Petticrew, C., Naidoo, P., Mohammadi, A. H. & Ramjugernath, D. 2014. Experimental measurements and thermodynamic modeling of the dissociation conditions of clathrate hydrates for (refrigerant+ NaCl+ water) systems. *Journal of Chemical & Engineering Data,* 59**,** 466-475.

Nkosi, N., Tumba, K. & Ramsuroop, S. 2018. Measurements of activity coefficient at infinite dilution for organic solutes in tetramethylammonium chloride+ ethylene glycol deep eutectic solvent using gas-liquid chromatography. *Fluid Phase Equilibria,* 462**,** 31-37.

Nkosi, N., Tumba, K. & Ramsuroop, S. 2018. Tetramethylammonium chloride+ glycerol deep eutectic solvent as separation agent for organic liquid mixtures: Assessment from experimental limiting activity coefficients. *Fluid Phase Equilibria,* 473**,** 98-105.

Nkosi, N., Nkazi, D. & Tumba, K. 2022. Experimental Hydrate Phase Equilibrium Data Relevant to Bitter Melon, Pineapple, and Grape Juice Concentration. *ACS omega,* 7**,** 34741-34751.

Parrinello, M. & Rahman, A. 1980. Crystal structure and pair potentials: A molecular-dynamics study. *Physical review letters,* 45**,** 1196.

Pearlman, D. A. & Kollman, P. A. 1991. The overlooked bond-stretching contribution in free energy perturbation calculations. *The Journal of chemical physics,* 94**,** 4532-4545.

Plechkova, N. V. & Seddon, K. R. 2008. Applications of ionic liquids in the chemical industry. *Chemical Society Reviews,* 37**,** 123-150.

Qasim, A., Heurtas, J., Khan, M. S., Lal, B., Shariff, A. M., Cezac, P., Foo, K. S. & Sundramoorthy, J. D. 2021. Thermodynamic modeling of electrolytic solutions of ionic liquids for gas hydrates inhibition applications. *Journal of Advanced Research in Fluid Mechanics and Thermal Sciences,* 81**,** 110-123.

Qasim, A., Khan, M. S., Lal, B. & Shariff, A. M. 2019. Phase equilibrium measurement and modeling approach to quaternary ammonium salts with and without monoethylene glycol for carbon dioxide hydrates. *Journal of molecular liquids,* 282**,** 106-114.

Quraishi, K. S., BUSTAM, M. A., Krishnan, S., Khan, M. I., Wilfred, C. D. & Lévêque, J.-M. 2017. Thermokinetics of alkyl methylpyrrolidinium [NTf 2] ionic liquids: Effect of alkyl chain on thermal stability. *Journal of Thermal Analysis and Calorimetry,* 129**,** 261-270.

Ratti, R. 2014. Ionic liquids: synthesis and applications in catalysis. *Adv. Chem,* 2014**,** 1-16.

Reshadi, P., Modarress, H., Dabir, B. & Amjad-iranagh, S. 2018. Molecular dynamics simulation for studying the stability of structure H clathrate-hydrates of argon and large guest molecules. *Journal of Dispersion Science and Technology,* 39**,** 1572-1581.

Sa, J.-H., Lee, B. R., Park, D.-H., Han, K., Chun, H. D. & Lee, K.-H. 2011. Amino acids as natural inhibitors for hydrate formation in CO2 sequestration. *Environmental science & technology,* 45**,** 5885-5891.

Sa, J.-H., Kwak, G.-H., Lee, B. R., Park, D.-H., Han, K. & Lee, K.-H. 2013. Hydrophobic amino acids as a new class of kinetic inhibitors for gas hydrate formation. *Scientific reports,* 3**,** 1-7.

Saberi, A., Alamdari, A., Shariati, A. & Mohammadi, A. H. 2018. Experimental measurement and thermodynamic modeling of equilibrium condition for natural gas hydrate in MEG aqueous solution. *Fluid Phase Equilibria,* 459**,** 110-118.

Sami, N. A., Das, K., Sangwai, J. S. & Balasubramanian, N. 2013. Phase equilibria of methane and carbon dioxide clathrate hydrates in the presence of (methanol+ MgCl2) and (ethylene glycol+ MgCl2) aqueous solutions. *The Journal of Chemical Thermodynamics,* 65**,** 198-203

Shahbaz, K., Mjalli, F., Hashim, M. & Alnashef, I. 2011. Using deep eutectic solvents based on methyl triphenyl phosphonium bromide for the removal of glycerol from palm-oil-based biodiesel. *Energy & Fuels,* 25**,** 2671-2678.

Shin, B. S., Kim, E. S., Kwak, S. K., Lim, J. S., Kim, K.-S. & Kang, J. W. 2014. Thermodynamic inhibition effects of ionic liquids on the formation of condensed carbon dioxide hydrate. *Fluid Phase Equilibria,* 382**,** 270-278.

Sivabalan, V., Walid, B., Madec, Y., Qasim, A. & Lal, B. 2020. Corrosion inhibition study on glycerol as simultaneous gas hydrate and corrosion inhibitor in gas pipelines. *Malaysian J Anal Sci,* 24**,** 62-69

Sloan JR, E. D. 2003. Fundamental principles and applications of natural gas hydrates. *Nature,* 426**,** 353.

Sloan JR, E. D. & Koh, C. A. 2008. *Clathrate hydrates of natural gases,* CRC press.

Smith, E. L., Abbott, A. P. & Ryder, K. S. 2014. Deep eutectic solvents (DESs) and their applications. *Chemical reviews,* 114**,** 11060-11082.

Smith, B. C., 1998. Infrared Spectral Interpretation: A systematic approach. *CRC Press,* 1998**.**

Soper, A. 2000. The radial distribution functions of water and ice from 220 to 673 K and at pressures up to 400 MPa. *Chemical Physics,* 258**,** 121-137.

Soper, A. K. 2013. The radial distribution functions of water as derived from radiation total scattering experiments: Is there anything we can say for sure? *International Scholarly Research Notices,* 2013.

Stephen, L. & Mayo, B. D. D. 1990. A generic force field for molecular simulation. *J Phy Chem,* 94**,** 889728909.

Stoyanov, E.S. Kim, C. K., Reed, C. A., 2006. An infrared *v*NH scale for weakly basic anions Implications for single-molecule acidity and superacidity. *Journal of American Chemical Society,* 128**,** 8600-8508.

Stuart, B. H., 2005., Spetral Analysis, Infrared Spectroscopy: Fundamentals and applications. *John Wiley and Sons,* 45-70**.**

Sun, Q. & Kang, Y. T. 2016. Review on CO2 hydrate formation/dissociation and its cold energy application. *Renewable and Sustainable Energy Reviews,* 62**,** 478-494.

Takeuchi, F., Ohmura, R. & Yasuoka, K. 2009. Statistical-thermodynamics modeling of clathrate-hydrate-forming systems suitable as working media of a hydrate-based refrigeration system. *International Journal of Thermophysics,* 30**,** 1838.

Tang, C., Zhou, X., Li, D., Zhao, X. & Liang, D. 2018. In situ Raman investigation on mixed CH 4-C 3 H 8 hydrate dissociation in the presence of polyvinylpyrrolidone. *Fuel,* 214**,** 505-511.

Tariq, M., Rooney, D., Othman, E., Aparicio, S., Atilhan, M. & Khraisheh, M. 2014. Gas hydrate inhibition: a review of the role of ionic liquids. *Industrial & Engineering Chemistry Research,* 53**,** 17855-17868.

Tohidi, B., Burgass, R., Danesh, A., Østergaard, K. & Todd, A. 2000. Improving the accuracy of gas hydrate dissociation point measurements. *Annals of the New York Academy of Sciences,* 912**,** 924-931.

Tsimpanogiannis, I. N., Diamantonis, N. I., Economou, I. G., Papadimitriou, N. I. & Stubos, A. K. 2014. Influence of combining rules on the cavity occupancy of clathrate hydrates using van der Waals–Platteeuw-theory-based modelling. *Chemical Engineering Research and Design,* 92**,** 2992-3007.

Vyas, N. & Ojha, A. K. 2010. Interaction of alanine with small water clusters; Ala– (H2O) n (n= 1, 2 and 3): A density functional study. *Journal of Molecular Structure: THEOCHEM,* 940**,** 95-102.

Weaver, K. D., Kim, H. J., Sun, J., Macfarlane, D. R. & Elliott, G. D. 2010. Cyto-toxicity and biocompatibility of a family of choline phosphate ionic liquids designed for pharmaceutical applications. *Green Chemistry,* 12**,** 507-513.

Wen, Q., Chen, J.-X., Tang, Y.-L., Wang, J. & Yang, Z. 2015. Assessing the toxicity and biodegradability of deep eutectic solvents. *Chemosphere,* 132**,** 63-69.

Wu, M., Wang, S. & Liu, H. 2007. A study on inhibitors for the prevention of hydrate formation in gas transmission pipeline. *Journal of Natural Gas Chemistry,* 16**,** 81-85.

Xiao, C. & Adidharma, H. 2009. Dual function inhibitors for methane hydrate. *Chemical Engineering Science,* 64**,** 1522-1527.

Xu, D., Yang, Q., Su, B., Bao, Z., Ren, Q. & Xing, H. 2014. Enhancing the basicity of ionic liquids by tuning the cation–anion interaction strength and via the anion-tethered strategy. *The Journal of Physical Chemistry B,* 118**,** 1071-1079.

Yin, Z., Khurana, M., Tan, H. K. & Linga, P. 2018. A review of gas hydrate growth kinetic models. *Chemical Engineering Journal,* 342**,** 9-29.

Yu, Y., Lu, X., Zhou, Q., Dong, K., Yao, H. & Zhang, S. 2008. Biodegradable naphthenic acid ionic liquids: synthesis, characterization, and quantitative structure–biodegradation relationship. *Chemistry–A European Journal,* 14**,** 11174-11182.

Zhang, C., Ding, Y., Zhang, L., Wang, X., Zhao, Y., Zhang, X. & YU, G. 2017. A Sustainable Redox-Flow Battery with an Aluminum-Based, Deep-Eutectic-Solvent Anolyte. *Angewandte Chemie International Edition,* 56**,** 7454-7459.

Zhang, Q., Vigier, K. D. O., Royer, S. & Jerome, F. 2012. Deep eutectic solvents: syntheses, properties, and applications. *Chemical Society Reviews,* 41**,** 7108-7146.